The Scientific World Journal

Cooperative Control and Its Engineering Applications in Power Systems

Guest Editors: Jinde Cao, Taiyou Yong, Guanghui Wen, Wenwu Yu, Xinghuo Yu, and Abdulaziz Alofi

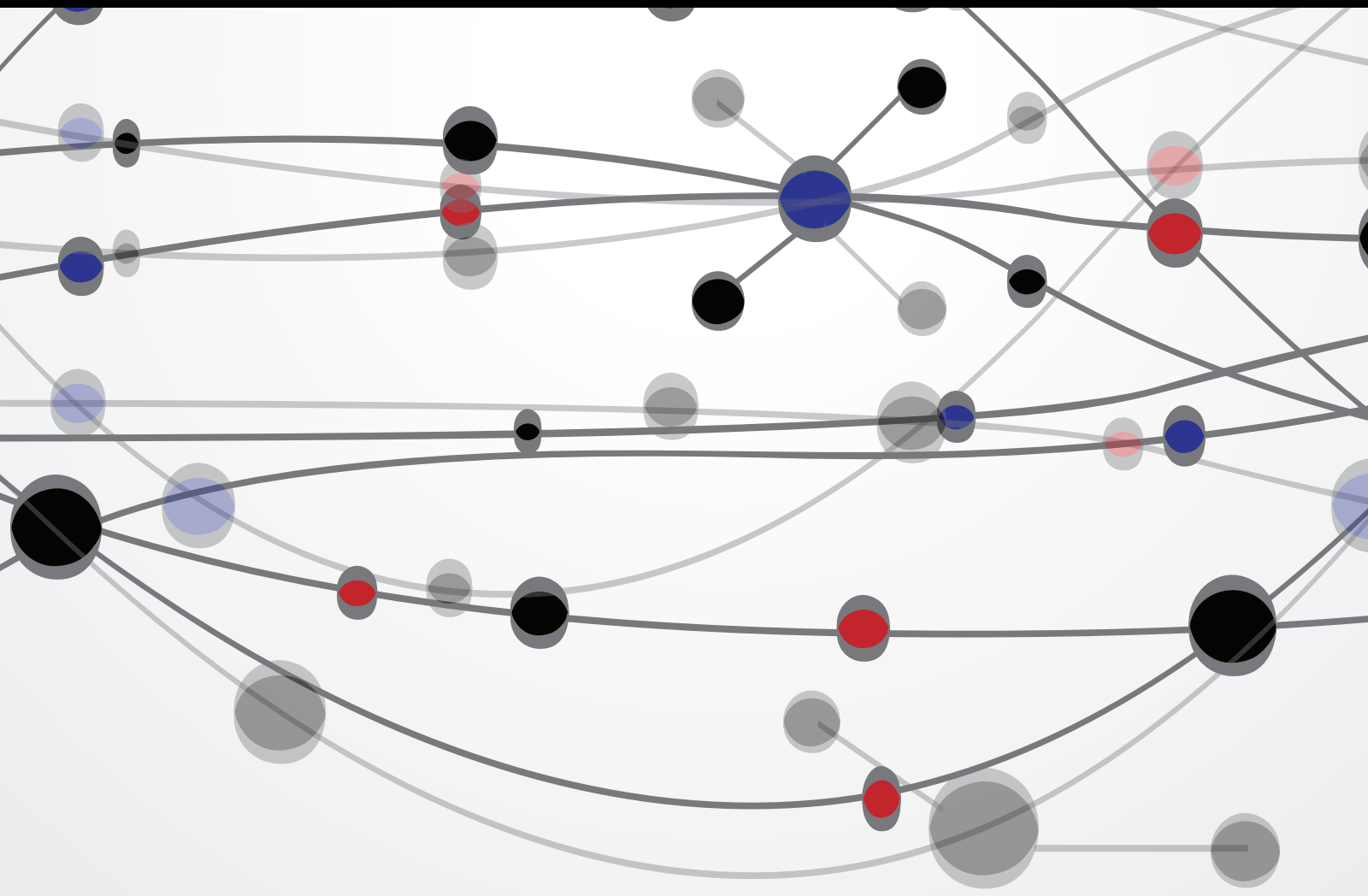

Cooperative Control and Its Engineering Applications in Power Systems

The Scientific World Journal

Cooperative Control and Its Engineering Applications in Power Systems

Guest Editors: Jinde Cao, Taiyou Yong, Guanghui Wen, Wenwu Yu, Xinghuo Yu, and Abdulaziz Alofi

Copyright © 2014 Hindawi Publishing Corporation. All rights reserved.

This is a special issue published in "The Scientific World Journal." All articles are open access articles distributed under the Creative Commons Attribution License, which permits unrestricted use, distribution, and reproduction in any medium, provided the original work is properly cited.

Contents

Cooperative Control and Its Engineering Applications in Power Systems, Jinde Cao, Taiyou Yong, Guanghui Wen, Wenwu Yu, Xinghuo Yu, and Abdulaziz Alofi
Volume 2014, Article ID 795389, 1 page

A Simple Attitude Control of Quadrotor Helicopter Based on Ziegler-Nichols Rules for Tuning PD Parameters, ZeFang He and Long Zhao
Volume 2014, Article ID 280180, 13 pages

Distributed Cooperative Regulation for Multiagent Systems and Its Applications to Power Systems: A Survey, Jianqiang Hu, Yaping Li, Taiyou Yong, Jinde Cao, Jie Yu, and Wenbo Mao
Volume 2014, Article ID 139028, 12 pages

Consensus Tracking for Multiagent Systems with Nonlinear Dynamics, Runsha Dong
Volume 2014, Article ID 130643, 10 pages

A Novel Memristive Multilayer Feedforward Small-World Neural Network with Its Applications in PID Control, Zhekang Dong, Shukai Duan, Xiaofang Hu, Lidan Wang, and Hai Li
Volume 2014, Article ID 394828, 12 pages

Performance Analysis of Autonomous Microgrid Subsequent to Symmetrical and Unsymmetrical Fault Triggered Condition, Chitra Natesan, Senthil Kumar Ajithan, Shobana Mani, Priyadharshini Palani, and Prabaakaran Kandhasamy
Volume 2014, Article ID 715963, 8 pages

Observer Design for a Core Circadian Rhythm Network, Yuhuan Zhang
Volume 2014, Article ID 476912, 8 pages

Synchronization Control for Stochastic Neural Networks with Mixed Time-Varying Delays, Qing Zhu, Aiguo Song, Shumin Fei, Yuequan Yang, and Zhiqiang Cao
Volume 2014, Article ID 840185, 10 pages

Hindawi Publishing Corporation
The Scientific World Journal
Volume 2014, Article ID 795389, 1 page
http://dx.doi.org/10.1155/2014/795389

Editorial

Cooperative Control and Its Engineering Applications in Power Systems

Jinde Cao,[1,2] Taiyou Yong,[3] Guanghui Wen,[1] Wenwu Yu,[1,4] Xinghuo Yu,[4] and Abdulaziz Alofi[2]

[1] *Research Center for Complex Systems and Network Sciences and Department of Mathematics, Southeast University, Nanjing 210096, China*
[2] *Department of Mathematics, Faculty of Science, King Abdulaziz University, Jeddah 21589, Saudi Arabia*
[3] *China Electric Power Research Institute, Nanjing 210003, China*
[4] *School of Electrical and Computer Engineering, RMIT University, Melbourne, VIC 3001, Australia*

Correspondence should be addressed to Jinde Cao; jdcao@seu.edu.cn

Received 23 November 2014; Accepted 23 November 2014; Published 30 December 2014

Copyright © 2014 Jinde Cao et al. This is an open access article distributed under the Creative Commons Attribution License, which permits unrestricted use, distribution, and reproduction in any medium, provided the original work is properly cited.

In the past few years, distributed cooperative control of multiagent systems has received much attention from various scientific fields due to its wide engineering applications. A multiagent system typically contains numerous nodes and lots of links among these individual nodes. It is thus difficult or practically impossible to design a centralized controller to control all the nodes. Within this context, control of large, multiagent systems is achieved by designing some distributed controllers where only some local information is involved. One changeling issue in solving the cooperative control problem of multiagent systems is that neighboring agents may communicate with each other in a constrained communication environment. Distributed cooperative control of multiagent systems has definite meaning in analyzing and designing modern power systems. It has been known that recent trends in the modernization of power systems require communication networks that support the inclusion of new devices, for example, smart meters, and intelligent electronic devices, to reduce operation and maintenance costs, and integrate distributed renewable energy sources. In this case, the centralized analysis and control techniques for power systems are inapplicable.

The main aims of this special issue are to present analysis methods for cooperative control of multiagent systems and discuss their potential applications in modern power systems. Call for papers has been carefully prepared by the guest editors and posted on the journal's web page, which has received much attention from researchers in different scientific communities. We have received 15 papers in related research fields. All manuscripts submitted to this special issue went through a thorough peer-refereeing process. Based on the anonymous reviewers' reports, 7 original research articles are finally accepted.

We hope that the papers published in this special issue will be useful to researchers in the fields of distributed cooperative control and power systems. We also hope that the published papers will arouse further research in the topics presented as well as in the other related topics.

Acknowledgments

We would like to sincerely thank all of the authors for their contributions and the reviewers for their effort and time for providing valuable comments and feedback. Our special thanks are due to the editorial board members of this journal owing to their great support and help for this special issue. This project was funded by the Deanship of Scientific Research (DSR), King Abdulaziz University. The authors, therefore, acknowledge with thanks DSR technical and financial support.

Jinde Cao
Taiyou Yong
Guanghui Wen
Wenwu Yu
Xinghuo Yu
Abdulaziz Alofi

Hindawi Publishing Corporation
The Scientific World Journal
Volume 2014, Article ID 280180, 13 pages
http://dx.doi.org/10.1155/2014/280180

Research Article

A Simple Attitude Control of Quadrotor Helicopter Based on Ziegler-Nichols Rules for Tuning PD Parameters

ZeFang He[1,2] and Long Zhao[1,2]

[1] *Science and Technology on Aircraft Control Laboratory, Beihang University, Beijing 100191, China*
[2] *Digital Navigation Center, Beihang University, Beijing 100191, China*

Correspondence should be addressed to Long Zhao; flylong@buaa.edu.cn

Received 25 August 2014; Accepted 10 October 2014; Published 29 December 2014

Academic Editor: Wenwu Yu

Copyright © 2014 Z. He and L. Zhao. This is an open access article distributed under the Creative Commons Attribution License, which permits unrestricted use, distribution, and reproduction in any medium, provided the original work is properly cited.

An attitude control strategy based on Ziegler-Nichols rules for tuning PD (proportional-derivative) parameters of quadrotor helicopters is presented to solve the problem that quadrotor tends to be instable. This problem is caused by the narrow definition domain of attitude angles of quadrotor helicopters. The proposed controller is nonlinear and consists of a linear part and a nonlinear part. The linear part is a PD controller with PD parameters tuned by Ziegler-Nichols rules and acts on the quadrotor decoupled linear system after feedback linearization; the nonlinear part is a feedback linearization item which converts a nonlinear system into a linear system. It can be seen from the simulation results that the attitude controller proposed in this paper is highly robust, and its control effect is better than the other two nonlinear controllers. The nonlinear parts of the other two nonlinear controllers are the same as the attitude controller proposed in this paper. The linear part involves a PID (proportional-integral-derivative) controller with the PID controller parameters tuned by Ziegler-Nichols rules and a PD controller with the PD controller parameters tuned by GA (genetic algorithms). Moreover, this attitude controller is simple and easy to implement.

1. Introduction

Unmanned helicopters have been widely applied in military and commercial fields [1, 2]. Unmanned four-rotor helicopters (quadrotor helicopters) are mostly used for search and rescue, surveillance, reconnaissance, data acquisition, and so forth. Their potential applications include border patrol, widefire monitoring, traffic monitoring, mineral exploration, and transportation [3–5]. Compared to conventional helicopters, quadrotor helicopters show many advantages. Quadrotor helicopters have hovering and VTOL (vertical takeoff and landing) capabilities which are also the characteristic of conventional helicopters. In other words, they have large maneuverability, do not require large takeoff and landing site, and can execute special tasks in dangerous and inaccessible environments. Furthermore, conventional helicopters are structurally complex, expensive, and hard to control, while quadrotor helicopters are mechanically simple, demand low manufacturing and operational costs, and are easy to control. Therefore, quadrotor helicopters draw intensive attention, and relevant technologies have also been an important research topic in recent years [6]. Quadrotor helicopter control is a challenging problem because a quadrotor helicopter is a complex system with high nonlinearities, strong couplings, and underactuation [7]. Therefore, the research for the control system of quadrotor helicopters has been widely conducted.

The methods for establishing a nonlinear model of quadrotor helicopters include white box modeling, black box modeling, and grey box modeling. Grey box modeling is commonly used in quadrotor modeling papers. The procedure for modeling quadrotor by the grey box modeling method is as follows: firstly, system model is written with the method of mechanism modeling; secondly, because some of the parameters in the model are unknown, they need to be derived by identification methods. There are two main mechanism modeling methods: Newton-Euler formalism and Lagrange-Euler formalism. In [8], a nonlinear model

was proposed by representing the quadrotor helicopters kinematics and dynamics characteristics based on Newton-Euler formalism. In [9], the same methodology was used to obtain the motion equations and the rotor dynamics were considered as well during the model establishment. The authors who established the quadrotor helicopters model using the Newton-Euler formalism in [9] described the quadrotor helicopters' dynamics by the Lagrange-Euler formalism in [10]. In this paper, quadrotor helicopter motion equations were obtained by the Newton-Euler formalism without considering the rotor dynamics during the model establishment.

The system equations were rewritten in state space for the controller design. The quadrotor motion can be split into two motions: the angular rotation motion and the linear translation motion. From the system equations, it can be seen that the rotational motion is independent of the translational motion, while the translational motion depends on the rotational motion. The quadrotor control structure is usually divided into internal and external loops according to the characteristics of the system model. The former is used to control attitude and the latter to control position. According to the control strategy which internal and external loop controls take, the quadrotor control can be divided into inner-outer loop control and full control. In inner-outer loop control methods, internal and external loops use different control strategies while, in full control methods, the same control strategy is used by internal and external loops. Different control methods which were recently tested on quadrotor helicopters are as follows: classic PID control [11], all kinds of improved methods of PID [6, 12], H_∞ control [4], predictive control [4], backstepping control [5, 7, 9], sliding mode control [9], LQR control [10], dynamic surface control [13], adaptive control [14, 15], neural network control [16], fuzzy control [17, 18], and the integrated method combined each other's advantages such as integral sliding mode control [3], integral backstepping control [19], fuzzy integral sliding mode control based on backstepping [20], and robust adaptive control [21–23]. Despite that the development of control methods has experienced the classical control, modern control, and intelligent control which largely improve the control effect, the classic PID control is still the most common and practical one in engineering controller design [24] because of its simplicity of control principle. An important step in the PID controller design is to tune PID controller parameters. Engineers generally use empirical methods to derive adjustable parameter, but it is time-consuming and thus inefficient. As such, a variety of intelligent PID parameter tuning methods have been proposed and studied in the literature. However, as with intelligent control methods, the parameter tuning methods are too complicated to be mastered by engineering technicians despite the good effect. The Ziegler-Nichols rules for tuning the PID controller, which were proposed by Ziegler and Nichols in 1942, have been widely recognized and used as described in [25] because it is simple and practical. In addition, the feedback linearization method [26] is also a very good method to decouple and linearize quadrotor models. In view of the advantages of the Ziegler-Nichols rules for tuning the PID controller and the feedback linearization method, the quadrotor attitude control strategy adopted in this paper is depicted as follows. The PD controller tuned by Ziegler-Nichols rules is firstly applied to the linearized model of quadrotor after the feedback linearization. Further, the nonlinear controller consisting of the PD control and feedback linearization item is applied to the quadrotor controlled object. The PD controller with PD parameters tuned by Ziegler-Nichols rules is first applied to quadrotor Helicopter in this paper.

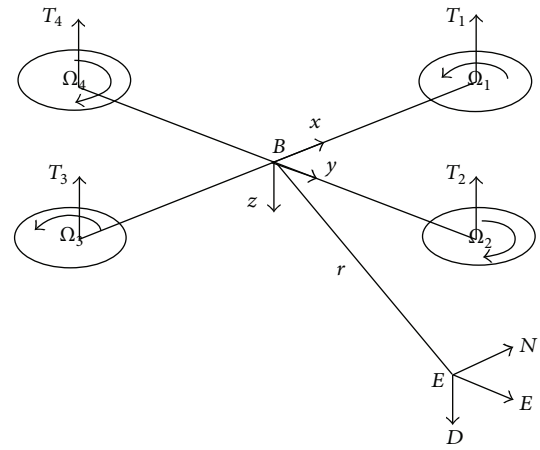

Figure 1: The structure of a quadrotor helicopter.

The remainder of the paper is organized as follows: the quadrotor helicopter model is described in Section 2. The control strategy is proposed in Section 3. In Section 4, the controller design principle is presented and contains feedback linearization, Ziegler-Nichols ruler for adjusting parameters, the controller parameter choice, and final form. Simulation results are reported in Section 5. Finally, the major conclusions of the paper are exposed in Section 6.

2. Quadrotor Model

A quadrotor helicopter uses four rotors as the direct power of flight. Four rotors with the same structure and radius are symmetrically located on the four edges of a cross formed by two arms and located on a plane at the same height. Rotor 1 and rotor 3 rotate in the counterclockwise direction and rotor 2 and rotor 4 rotate in the clockwise direction. Four motors were symmetrically installed on the stent ends of the quadrotor; flight control computer and external equipment were installed in the space of the stent middle. The structure of a quadrotor helicopter is shown in Figure 1, where B represents the body coordinate system and G represents the ground coordinate system.

The attitude and location of a quadrotor helicopter can be controlled to desired values by changing four motor speeds (which results in the changes of four rotor speeds and corresponding lift). The following several kinds of force and moment can be performed on the quadrotor helicopter: the lifts caused by rotors rotation, the pitching moment and rolling moment caused by the difference of four rotors lift, the

gravity, the gyroscopic effect, and aerodynamic torque effect, that is, yawing moment. The gyroscopic effect only appears in the lightweight construction quadrotor helicopter. Yawing moment is caused by unbalanced four rotors rotational speeds. The gyroscopic effect and yawing moment are in essence caused by the reaction torques. The reaction torques are caused by the rotor rotation; its direction is exactly opposite of the rotor rotation direction. Yaw moment can be cancelled when two rotors rotate in the opposite direction. The gyroscopic effect and aerodynamic torque effect are offset when the quadrotor hovers.

The space motion of the rigid body aircraft can be divided into two parts: the centre of mass movement and movement around the centre of mass. Six degrees of freedom are required in describing any time space motion. They are three barycenter movements and three angular motions, namely, three translation and three rotation motions along three axes. The control for six degrees of freedom motions can be implemented by adjusting the rotational speeds of different motors. Basic motions include forward and backward movements, lateral movement, vertical motion, roll motion, and pitch and yaw motions. The yaw motion of the quadrotor helicopter can be realised by a reactive torque produced by the rotor. The size of the reactive torque is relative to the rotor speed. When the four rotor speeds are the same, the reactive torques will offset by each other and quadrotor will remain still, whereas if the four rotor speeds are not absolutely same, the reactive torques will not be absolutely offset, and the quadrotor will start to rotate. The rotation of the quadrotor should be eliminated during the other motions of the quadrotor to ensure the stability of motions. That the four rotor speeds synchronously increase and decrease is also required in the vertical movement. When the quadrotor helicopter flies in the pitch and roll motion mode, horizontal motion along x- and y-axes will be triggered. In order to obtain the subduction motion and forward movement, the speed of the rear rotor must be increased and the speed of the front rotor must be decreased; on the contrary, nose-up pitch movement and backward movement can be produced. Similarly, the roll movement and lateral movement can be obtained by controlling the left rotor and right rotor.

Because of four inputs and six state outputs in a quadrotor, the quadrotor is considered an underactuated complex system. In order to control it, some assumptions are made in the process of quadrotor modeling as follows: quadrotor is a rigid body; the structure is symmetric; the centre of gravity and the origin of body coordinate system are coincident and ground effect is ignored.

The causes of the lift, gravity, and aerodynamic torque acting on a quadrotor differ from each other. Thus, it is very important to choose the appropriate coordinate system to exactly describe the quadrotor space motion state. For example, it is more convenient to describe the gravity of the aircraft in the ground coordinate frame and to describe the lift acting on the quadrotor; the body coordinate frame is more suitable. Therefore, when establishing a quadrotor motion model, reasonably choosing different coordinate frames is one of the important links to define and describe various motion parameters of the quadrotor.

Given an aircraft, the positive x direction in the body coordinate frame is usually defined as the moving direction, the positive y direction as the right side of the moving direction, and the positive z direction as the vertical downward direction; this is also termed forward-right-downward coordinate frame [26].

Because the fly altitude of quadrotor helicopters is limited in the atmosphere, the "flat earth hypothesis" can be adopted to consider the ground coordinate frame as an inertial coordinate frame to simplify the modeling complexity. In order to facilitate navigation and way-point tracking, the axis directions of the ground coordinate frame are chosen as north-east-down navigation frame directions, namely, that the X_g axis points to the north, the Y_g axis points to the east, and the Z_g axis is perpendicular to the ground and points to the center of the earth.

The procedure of the Newton-Euler formalism modeling is to project lift forces acting on the aircraft to the ground coordinate frame and analyze the linear motion of the aircraft with Newton's second law in the inertial coordinate system and the angular motion of the aircraft with the law of moment of momentum in the body coordinate system.

2.1. Kinematics Model. The transformation matrix between two rectangular coordinate systems is orthogonal. $R(x,\phi)$, $R(y,\theta)$, and $R(z,\psi)$ denote rotation matrices produced by the ground coordinate frame rotating roll angle ϕ, pitch angle θ, and yaw angle ψ around x-, y-, and z-axes, respectively, and the expressions are as follows:

$$R(x,\phi) = \begin{bmatrix} 1 & 0 & 0 \\ 0 & \cos\phi & \sin\phi \\ 0 & -\sin\phi & \cos\phi \end{bmatrix},$$

$$R(y,\theta) = \begin{bmatrix} \cos\theta & 0 & -\sin\theta \\ 0 & 1 & 0 \\ \sin\theta & 0 & \cos\theta \end{bmatrix}, \quad (1)$$

$$R(z,\psi) = \begin{bmatrix} \cos\psi & \sin\psi & 0 \\ -\sin\psi & \cos\psi & 0 \\ 0 & 0 & 1 \end{bmatrix}.$$

The rotation matrix from the ground coordinate system to the body coordinate system is the product of formulae (1), which denote rotation around the z-axis followed by rotation around y-axis and finally followed by rotation around x-axis; namely,

$$R_{E\to B} = R(x,\phi)\,R(y,\theta)\,R(z,\psi). \quad (2)$$

Therefore, the transformation matrix from the ground coordinate system to the body coordinate system is given by

$$R_{B\to E} = R_{E\to B}^{T}. \quad (3)$$

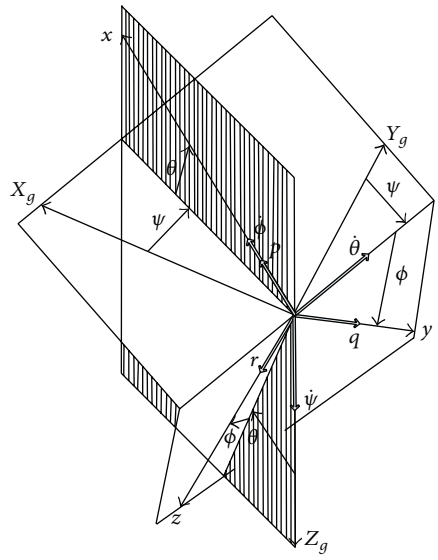

FIGURE 2: The relationships between angular velocity components and the attitude angle change rate.

The specific expression is given by

$$R_{B\to E} = \begin{bmatrix} c_\theta c_\psi & s_\phi s_\theta c_\psi - c_\phi s_\psi & c_\phi s_\theta c_\psi + s_\phi s_\psi \\ c_\theta s_\psi & s_\phi s_\theta s_\psi + c_\phi c_\psi & c_\phi s_\theta s_\psi - s_\phi c_\psi \\ -s_\theta & s_\phi c_\theta & c_\phi c_\theta \end{bmatrix}, \quad (4)$$

where $c_\cdot = \cos(\cdot)$ and $s_\cdot = \sin(\cdot)$.

The angular velocity components p, q, and r are the projection values on the body coordinate system of rotation angular velocity ω which denotes the rotation from the ground coordinate system to the body coordinate system. The relationships between angular velocity components and the attitude angle change rates are shown in Figure 2.

The transformation matrix from $[\dot{\phi}\ \ \dot{\theta}\ \ \dot{\psi}]^T$ to $[p\ \ q\ \ r]^T$ is given by

$$\begin{bmatrix} p \\ q \\ r \end{bmatrix} = R_r \begin{bmatrix} \dot{\phi} \\ \dot{\theta} \\ \dot{\psi} \end{bmatrix}, \quad (5)$$

where

$$R_r = \begin{bmatrix} 1 & 0 & -\sin\theta \\ 0 & \cos\phi & \sin\phi\cos\theta \\ 0 & -\sin\phi & \cos\phi\cos\theta \end{bmatrix}. \quad (6)$$

Around hovering position, R_r is assumed as a unit matrix [26].

2.2. Dynamic Model. The dynamics model is composed of the rotational and translational motions. The rotational motion is fully actuated, while the translational motion is underactuated. In the body coordinate system, the rotational motion equations are derived according to the law of momentum theorem and gyroscopic effect of quadrotor, and they are given by

$$J\dot{\omega} + \omega \times J\omega + \omega \times \begin{bmatrix} 0 & 0 & J_r\Omega_r \end{bmatrix} = M_B, \quad (7)$$

where J is the inertia matrix of quadrotor which is diagonal under the hypothesis of structure symmetry and the elements I_x, I_y, and I_z are, respectively, inertia matrices of x-, y-, and z-axes. The last item on the left side of (7) represents the gyroscopic effect which is caused by the inertia of the rotors J_r and relative speed $\Omega_r = -\Omega_1 + \Omega_2 - \Omega_3 + \Omega_4$, where Ω_i ($i = 1, 2, 3, 4$) represents the ith rotor speed. The aerodynamic force and moment produced by the ith rotor are directly proportional to the square of the rotor speed. The relationships are given by

$$\begin{aligned} F_i &= b\Omega_i^2, \\ M_i &= d\Omega_i^2, \end{aligned} \quad (8)$$

where b and d are the aerodynamic force and moment constants, respectively. The moments acting on the quadrotor in the body coordinate system are given by

$$M_B = \begin{bmatrix} l \cdot b\left(-\Omega_2^2 + \Omega_4^2\right) \\ l \cdot b\left(\Omega_1^2 - \Omega_3^2\right) \\ d\left(\Omega_1^2 - \Omega_2^2 + \Omega_3^2 - \Omega_4^2\right) \end{bmatrix}, \quad (9)$$

where l is the moment arm which represents the distance from the axis of a rotor to the center of quadrotor.

The translational motion equations are obtained in the ground coordinate system by the method of Newton's second law:

$$m\ddot{r} = \begin{bmatrix} 0 & 0 & mg \end{bmatrix}^T + RF_B, \quad (10)$$

where $r = [x\ \ y\ \ z]^T$ is the position of quadrotor in the ground coordinate system, m is the mass of quadrotor, g is the acceleration of gravity, and F_B is the total lift force acting on quadrotor in the body coordinate system; namely,

$$F_B = \begin{bmatrix} 0 \\ 0 \\ -b\left(\Omega_1^2 + \Omega_2^2 + \Omega_3^2 + \Omega_4^2\right) \end{bmatrix}. \quad (11)$$

2.3. The Motion Equations of Quadrotor. Synthesizing the kinematics and dynamics models of quadrotor, the motion equations of quadrotor can be derived as follows:

$$\begin{aligned} \ddot{\phi} &= \dot{\theta}\dot{\psi}\left(\frac{I_y - I_z}{I_x}\right) - \frac{J_r}{I_x}\dot{\theta}\Omega_r + \frac{L}{I_x}U_2, \\ \ddot{\theta} &= \dot{\phi}\dot{\psi}\left(\frac{I_z - I_x}{I_y}\right) + \frac{J_r}{I_y}\dot{\phi}\Omega_r + \frac{L}{I_y}U_3, \\ \ddot{\psi} &= \dot{\phi}\dot{\theta}\left(\frac{I_x - I_y}{I_z}\right) + \frac{1}{I_z}U_4, \\ \ddot{x} &= -\frac{U_1}{m}\left(\cos\phi\sin\theta\cos\psi + \sin\phi\sin\psi\right), \\ \ddot{y} &= -\frac{U_1}{m}\left(\cos\phi\sin\theta\sin\psi - \sin\phi\cos\psi\right), \\ \ddot{z} &= g - \frac{U_1}{m}\left(\cos\phi\cos\theta\right), \end{aligned} \quad (12)$$

where U_1, U_2, U_3, and U_4 are the control input variables, which can be calculated by $U_1 = b(\Omega_1^2 + \Omega_2^2 + \Omega_3^2 + \Omega_4^2)$, $U_2 = b(-\Omega_2^2 + \Omega_4^2)$, $U_3 = b(\Omega_1^2 - \Omega_3^2)$, and $U_4 = d(\Omega_1^2 - \Omega_2^2 + \Omega_3^2 - \Omega_4^2)$, respectively.

3. Control Strategy

The state space model adopted by the control system is $\dot{X} = f(X,U)$, where X is the state vector and U is the control input vector. The state vector is chosen as $X = [x\ y\ z\ \dot{x}\ \dot{y}\ \dot{z}\ \phi\ \theta\ \psi\ \dot{\phi}\ \dot{\theta}\ \dot{\psi}]^T$. In the design of controller, the state variables are chosen as $x_1 = x, x_2 = y, x_3 = z$, $x_4 = \dot{x}_1 = \dot{x}$, $x_5 = \dot{x}_2 = \dot{y}$, $x_6 = \dot{x}_3 = \dot{z}$, $x_7 = \phi$, $x_8 = \theta$, $x_9 = \psi$, $x_{10} = \dot{x}_7 = \dot{\phi}$, $x_{11} = \dot{x}_8 = \dot{\theta}$, and $x_{12} = \dot{x}_9 = \dot{\psi}$.

Synthesizing the motion equations of quadrotor, the state vector, and the control input variables, the state equations can be described as

$$f(X,U) = \begin{bmatrix} x_4 \\ x_5 \\ x_6 \\ -\frac{U_1}{m}\left(\cos x_7 \sin x_8 \cos x_9 + \sin x_7 \sin x_9\right) \\ -\frac{U_1}{m}\left(\cos x_7 \sin x_8 \sin x_9 - \sin x_7 \cos x_9\right) \\ g - \frac{U_1}{m}\left(\cos x_7 \cos x_8\right) \\ x_{10} \\ x_{11} \\ x_{12} \\ x_{11}x_{12}\frac{I_y - I_z}{I_x} - \frac{J_r}{I_x}x_{11}\Omega_r + \frac{L}{I_x}U_2 \\ x_{10}x_{12}\frac{I_z - I_x}{I_y} + \frac{J_r}{I_y}x_{10}\Omega_r + \frac{L}{I_y}U_3 \\ x_{10}x_{11}\frac{I_x - I_y}{I_z} + \frac{1}{I_z}U_4 \end{bmatrix}. \tag{13}$$

It can be seen from (13) that the rotation motions are independent of translational movements and full actuated, while translational motions are underactuated and depend on the rotation motions. Therefore, a control structure with inner and outer loops is designed in which the inner control loop is designed to ensure asymptotic tracking for the desired attitude and altitude and the outer loop is designed to navigate. The structure diagram is shown in Figure 3. As stabilizing attitude is the basis of controlling the quadrotor, quadrotor attitude controller is designed in this paper. In this paper, attitude control strategy of the quadrotor is firstly applying PD controller tuned by Ziegler-Nichols rules to the linear model of quadrotor after feedback linearization and then nonlinear controller consisting of the PD control and feedback linearization item acts on the quadrotor controlled object.

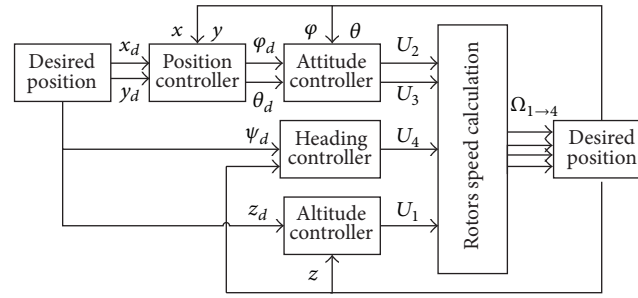

Figure 3: Quadrotor control structure.

To design attitude controller, the rotation motion equations are separately extracted and simplified, and they are given by

$$\begin{aligned} \dot{x}_{10} &= a_1 x_{11} x_{12} - a_2 x_{11}\Omega_r + b_1 U_2, \\ \dot{x}_{11} &= a_3 x_{10} x_{12} + a_4 x_{10}\Omega_r + b_2 U_3, \\ \dot{x}_{12} &= a_5 x_{10} x_{11} + b_3 U_4, \end{aligned} \tag{14}$$

where $a_1 = (I_y - I_z)/I_x, a_2 = J_r/I_x, a_3 = (I_z - I_x)/I_y, a_4 = J_r/I_y$, $a_5 = (I_x - I_y)/I_z, b_1 = L/I_x, b_2 = L/I_y$, and $b_3 = 1/I_z$.

4. Controller Design Principle

4.1. Feedback Linearization Theory. The smaller the rotor inertia of quadrotor is, the smaller the impact of gyroscopic effect is. Therefore, during the design of attitude controller, the simplified rotation motion equations are derived by ignoring the influence of the gyroscopic effect item as

$$\begin{aligned} \dot{x}_{10} &= a_1 x_{11} x_{12} + b_1 U_2, \\ \dot{x}_{11} &= a_3 x_{10} x_{12} + b_2 U_3, \\ \dot{x}_{12} &= a_5 x_{10} x_{11} + b_3 U_4. \end{aligned} \tag{15}$$

In order to obtain a linear model to make further control easily realize, in this paper, a feedback linearization technique is adopted to linearize a nonlinear system. The control inputs U_2, U_3, and U_4 are chosen as

$$\begin{aligned} U_2 &= f_2(x_{10}, x_{11}, x_{12}) + U_2^{\#}, \\ U_3 &= f_3(x_{10}, x_{11}, x_{12}) + U_3^{\#}, \\ U_4 &= f_4(x_{10}, x_{11}, x_{12}) + U_4^{\#}, \end{aligned} \tag{16}$$

where $U_2^{\#}$, $U_3^{\#}$, and $U_4^{\#}$ are new inputs. On this basis, in order to obtain a linear model, the following equations still demand to be met:

$$\begin{aligned} a_1 x_{11} x_{12} + b_1 f_2(x_{10}, x_{11}, x_{12}) &= K_2 x_{10}, \\ a_3 x_{10} x_{12} + b_2 f_3(x_{10}, x_{11}, x_{12}) &= K_3 x_{11}, \\ a_5 x_{10} x_{11} + b_3 f_4(x_{10}, x_{11}, x_{12}) &= K_4 x_{10}, \end{aligned} \tag{17}$$

where K_2, K_3, and K_4 are undetermined parameters. According to (17), the feedback linearization items f_2, f_3, and f_4 are given as

$$f_2(x_{10}, x_{11}, x_{12}) = \frac{1}{b_1}(K_2 x_{10} - a_1 x_{11} x_{12}),$$
$$f_3(x_{10}, x_{11}, x_{12}) = \frac{1}{b_2}(K_3 x_{11} - a_3 x_{10} x_{12}), \quad (18)$$
$$f_4(x_{10}, x_{11}, x_{12}) = \frac{1}{b_3}(K_4 x_{10} - a_5 x_{10} x_{11}).$$

Similarly, if considering gyroscopic effect, feedback linearization items f_2, f_3, and f_4 are derived as

$$f_2(x_{10}, x_{11}, x_{12}) = \frac{1}{b_1}(K_2 x_{10} + a_2 x_{11}\Omega_r - a_1 x_{11} x_{12}),$$
$$f_3(x_{10}, x_{11}, x_{12}) = \frac{1}{b_2}(K_3 x_{11} - a_4 x_{10}\Omega_r - a_3 x_{10} x_{12}), \quad (19)$$
$$f_4(x_{10}, x_{11}, x_{12}) = \frac{1}{b_3}(K_4 x_{10} - a_5 x_{10} x_{11}).$$

Substituting (16) into (15), meanwhile considering (17), the linear system can be obtained as

$$\dot{x}_{10} = K_2 x_{10} + b_1 U_2^{\#},$$
$$\dot{x}_{11} = K_3 x_{11} + b_2 U_3^{\#}, \quad (20)$$
$$\dot{x}_{12} = K_4 x_{12} + b_3 U_4^{\#}.$$

It can be seen from (20) that the corresponding linear closed-loop system is still stable even considering the gyroscopic effect. In order to prove the stability of the closed-loop system, in this paper, under the condition of $U_2^{\#} = U_3^{\#} = U_4^{\#} = 0$ and operating points $x_{10} = x_{11} = x_{12} = 0$, we consider the Lyapunov function

$$V(x_{10}, x_{11}, x_{12}) = 0.5\left(x_{10}^2 + x_{11}^2 + x_{12}^2\right). \quad (21)$$

Equation (21) is an attitude controller, and it is positive definite near the operating point. The first derivative of the Lyapunov function can be derived using (14) which is a model expression including gyroscopic effect item, (16) and (19); meanwhile, it can be derived using (15) which is a simplified model expression, (16) and (18). It can be seen that the above two first derivatives of the two Lyapunov functions are the same, which denotes the affair that the model including gyroscopic effect item will not affect the stability of the system. The first derivative of Lyapunov function is given by

$$\dot{V} = x_{10}\dot{x}_{10} + x_{11}\dot{x}_{11} + x_{12}\dot{x}_{12} = K_2 x_{10}^2 + K_3 x_{11}^2 + K_4 x_{12}^2. \quad (22)$$

The derivative expressed by (22) is negative definite if $K_2 < 0$, $K_3 < 0$, and $K_4 < 0$, which guarantees that the operating point of the feedback linearization system is asymptotically stable.

Considering $\dot{x}_7 = x_{10}$, $\dot{x}_8 = x_{11}$, and $\dot{x}_9 = x_{12}$, it is obvious that the feedback linearization system, that is, (20), can be described by linear decoupled differential equations of second order; namely,

$$\ddot{x}_7 = K_2 \dot{x}_7 + b_1 U_2^{\#},$$
$$\ddot{x}_8 = K_3 \dot{x}_8 + b_2 U_3^{\#}, \quad (23)$$
$$\ddot{x}_9 = K_4 \dot{x}_9 + b_3 U_4^{\#}.$$

The Laplace transformation is applied to (23), which can transform the system from time domain to frequency domain. Further, the open-loop transfer functions of controlled object quadrotor can be obtained as

$$G_1(s) = \frac{X_7(s)}{U_2^{\#}(s)} = \frac{b_1}{s^2 - K_2 s},$$
$$G_2(s) = \frac{X_8(s)}{U_3^{\#}(s)} = \frac{b_2}{s^2 - K_3 s}, \quad (24)$$
$$G_3(s) = \frac{X_9(s)}{U_4^{\#}(s)} = \frac{b_3}{s^2 - K_4 s},$$

where the system is minimum phase system only when $K_2 < 0$, $K_3 < 0$, and $K_4 < 0$.

4.2. Ziegler-Nichols PD Parameter Setting Principles. Aiming at the decoupled linear controlled object shown in (23), a simple and practical PD controller is designed. The controller parameters proportion and derivative coefficients are the corresponding proportion and derivative coefficients among the PID parameters adjusted by Ziegler-Nichols PID parameters setting rules. Ziegler-Nichols method is a PID parameter setting method based on stability analysis. The setting of the method for proportion coefficient K_P is, firstly, fixing $K_D = K_I = 0$; secondly, increasing K_P until the system begins to shock when the closed-loop system poles are on the jw axis; finally, multiplying K_P by 0.6. The final K_P is proportion coefficient after setting. Setting formula is given by

$$K_P = 0.6K_m,$$
$$K_D = \frac{K_P \pi}{4\omega_m}, \quad (25)$$
$$K_I = \frac{K_P \omega_m}{\pi},$$

where K_m is K_P value derived when the system began to shock and ω_m is the frequency of oscillation. K_m and ω_m can be determined using the root locus method. For a given transfer function of the controlled object, one can get its root locus. K_m is the gain traversing the jw axis, and the oscillation frequency of the point corresponds to ω_m.

4.3. Controller Final Form and Parameter Choice. The expressions of linear controllers $U_2^{\#}$, $U_3^{\#}$, and $U_4^{\#}$ can be written after obtaining the PID parameter value. Further, the expressions

of nonlinear controllers U_2, U_3, and U_4 also can be written. The actual control loop is discrete time system with sampling period T_s. Therefore, in MATLAB simulation, the discrete PID control applies in continuous system [27]. In this paper, a series of sampling points KT_s is selected to replace continuous time t, the integral is approximately replaced by rectangle method numerical integral, and the differential is approximately replaced by first-order backward difference; namely,

$$\begin{aligned} t &\approx kT \quad (k = 0, 1, 2, \ldots), \\ \int_0^t \text{error}(t)\, dt &\approx T \sum_{j=0}^{k} \text{error}(jT) = T \sum_{j=0}^{k} \text{error}(j), \\ \frac{d\text{error}(t)}{dt} &\approx \frac{\text{error}(kT) - \text{error}((k-1)T)}{T} \\ &= \frac{\text{error}(k) - \text{error}(k-1)}{T}. \end{aligned} \tag{26}$$

The resulting PD controllers $U_2^{\#}$, $U_3^{\#}$, and $U_4^{\#}$ are given by

$$\begin{aligned} U_2^{\#}(k) &= K_{P2}\, \text{err}\,2(k) + K_{D2} \frac{\text{err}\,2(k) - \text{err}\,2(k-1)}{T_s}, \\ U_3^{\#}(k) &= K_{P3}\, \text{err}\,3(k) + K_{D3} \frac{\text{err}\,3(k) - \text{err}\,3(k-1)}{T_s}, \\ U_4^{\#}(k) &= K_{P4}\, \text{err}\,4(k) + K_{D4} \frac{\text{err}\,4(k) - \text{err}\,4(k-1)}{T_s}, \end{aligned} \tag{27}$$

where the subscript 2 represents the roll angle loop, the subscript 3 represents the pitch angel loop, the subscript 4 represents yaw angle loop, and err $2(k)$, err $3(k)$, and err $4(k)$ represent the differences between the expected values and the actual values of the roll, pitch, and yaw angles, respectively.

Substituting (18) and (27) into (16) and sorting, nonlinear controllers U_2, U_3, and U_4 are derived as

$$\begin{aligned} U_2(k) &= \frac{1}{b_1}\left(K_2 x_{10} - a_1 x_{11} x_{12}\right) + K_{P2}\, \text{err}\,2(k) \\ &\quad + K_{D2} \frac{\text{err}\,2(k) - \text{err}\,2(k-1)}{T_s}, \\ U_3(k) &= \frac{1}{b_2}\left(K_3 x_{11} - a_3 x_{10} x_{12}\right) + K_{P3}\, \text{err}\,3(k) \\ &\quad + K_{D3} \frac{\text{err}\,3(k) - \text{err}\,3(k-1)}{T_s}, \\ U_4(k) &= \frac{1}{b_3}\left(K_4 x_{12} - a_5 x_{10} x_{11}\right) + K_{P4}\, \text{err}\,4(k) \\ &\quad + K_{D4} \frac{\text{err}\,4(k) - \text{err}\,4(k-1)}{T_s}, \end{aligned} \tag{28}$$

where K_2, K_3, and K_4 are the optimal values obtained by using a single optimization method. The goal of optimization process is to stabilize system performance and to make system have faster response and smaller overshoot amount as much as possible. The PID controller parameters are adjusted by Ziegler-Nichols principles.

5. Simulation Results

In order to test the control effect of the nonlinear controller proposed in this paper, the simulation experiment was carried out. Single control and joint control for a quadrotor were carried out, respectively. Meanwhile, the control effect comparison was done among the three nonlinear controllers which have the same feedback linearization item and the different linear control parts. The linear part of the controller adopted in this paper is a PD controller with PD parameters tuned by Ziegler-Nichols rules, while the linear parts of the other two nonlinear controllers are, respectively, PID controller with the PID controller parameters tuned by Ziegler-Nichols rules and PD controller with the PD controller parameters tuned by GA. The other two nonlinear controllers are also proposed in this paper and are used to approve the advantages of ZN-PD controller adopted in this paper. Besides, the system robust performance test was done under the condition of noise interference. In this paper, the single control is defined as controlling one of the quadrotor's attitude angles from zero initial state to the desired angle, for example, controlling pitch angle to the desired angle, while the other two attitude angles roll and yaw angles are still located in the initial state; joint control is defined as controlling all of the quadrotor's attitude angles to the expectation, namely, simultaneously controlling roll, pitch, and yaw angles to the desired angles. In this paper, we test robust performance of this system only with the interference of zero-mean white noise. The quadrotor parameters used in this paper are as follows: $m = 0.4794\,\text{kg}$, $g = 9.81\,\text{m/s}^2$, $l = 0.225\,\text{m}$, $I_x = I_y = 0.0086\,\text{kg·m}^2$, $I_z = 0.0172\,\text{kg·m}^2$, $J_{\text{rotor}} = 3.7404 \times 10^{-5}$, $b = 3.13 \times 10^{-5}$, $d = 9 \times 10^{-7}$, $K_2 = -14.6211$, $K_3 = -14.6211$, $K_4 = -32$, and $U_1 = m * g$.

The transfer function for the roll angle loop after feedback linearization is $G_1(s) = X_7(s)/U_2^{\#}(s) = b_1/(s^2 - K_2 s) = 26.1628/(s^2 + 14.6211s)$. The target value optimization diagram using GA to tune PID parameter values of this attitude loop is shown in Figure 4. The ultimate values and initial values scope of PID parameters in GA parameter optimization are shown in Table 1.

The PID parameter modulation processes for pitch angle and yaw angle loops are similar to the modulation process for roll angle loop. Just different initial values of PID parameters are applied to pitch angle and yaw angle loops. The PID parameter values tuned by Ziegler-Nichols rules and GA are shown in Table 2. The positive and negative 20 percent of PID parameters for each attitude loop tuned by Ziegler-Nichols rules are chosen as the initial values of PID parameters for GA optimization.

The control effects compare diagrams between ZN-PID (PID control with PID parameters tuned by Ziegler-Nichols rules) and GA-PID (PID control with PID parameters tuned by GA) for three attitude angle loops which are shown in Figure 5. It can be seen from Figure 5, for three attitude angle

Table 1: The ultimate values and initial values scope of PID parameters in GA parameter optimization.

	P	I	D
The ultimate PID parameter values	2.2310	2.9996	0.1969
The initial value scopes of PID parameters	[1.49344, 2.24016]	[2.97896, 4.46844]	[0.1872, 0.2808]

Table 2: PID parameter values tuned by Ziegler-Nichols rules and GA.

Attitude	PID value					
	PID parameter values tuned by Ziegler-Nichols rules			PID parameter values tuned by GA		
	P	I	D	P	I	D
Roll angle	1.8668	3.7237	0.2340	2.2310	2.9996	0.1969
Pitch angle	1.8572	3.6941	0.2334	2.1756	3.0239	0.2022
Yaw angle	1.5064	3.0067	0.1887	1.8013	2.479	0.1528

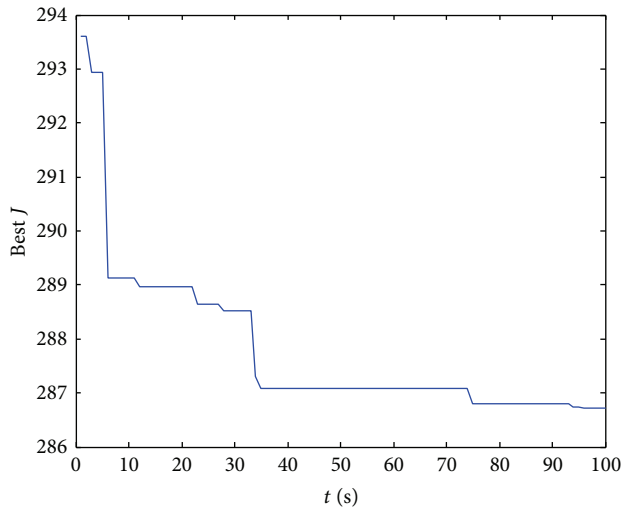

Figure 4: The target value optimization diagram using GA to tune PID parameter values of roll angle loop.

loops, the control effects of GA-PID are all better than those of ZN-PID.

The following ZN-PD control (PD control with PD parameters tuned by Ziegler-Nichols rules), GA-PD control (PD control with PD parameters tuned by GA), and ZN-PID control (PID control with PID parameters tuned by Ziegler-Nichols rules), respectively, stand for the linear control parts of three attitude controllers appearing in this paper. GA-PD control and ZN-PID control are used to compare control effect with ZN-PD control adopted in this paper. The nonlinear parts of three attitude controllers are the same. For convenience, the names of the linear control parts of three different kinds of nonlinear controllers, respectively, represent the corresponding nonlinear controllers.

The control response comparison diagrams of the single ZN-PD control and the single GA-PD are shown in Figure 6. It can be seen from Figure 6 that ZN-PD control and GA-PD control can control three attitude angles to any value in their domain of definition; for the roll and pitch angle loops, the control effects of GA-PD are better than the one of ZN-PD; for the yaw angle loop, GA-PD control has a large overshoot while ZN-PD quickly and without overshoot reaches the desired value.

For the quadrotor controlled object, the larger overshoot is fatal since it often leads to instability. The domains of definition of three attitude angles ϕ, θ, and ψ are $-\pi/2 < \phi < \pi/2$, $-\pi/2 < \theta < \pi/2$, and $-\pi < \psi < \pi$, respectively. Simulation experiments demonstrate that ZN-PID control can only control every attitude angle to 0.24 rad. The ZN-PD control and the ZN-PID control effect comparison is done when separately controlling an attitude angle to the desired angle, while the rest attitude angles remain 0. The control effect comparison diagrams are shown in Figure 7. It can be seen from the Figure 7 that ZN-PD control is apparently superior to the ZN-PID control. ZN-PD control can quickly and without overshoot control an attitude angle to its expectation and interactive responses among three attitude angles under the ZN-PD control are smaller than those under the ZN-PID control.

The further control effects compare between ZN-PD control and GA-PD control and can be seen from Figures 8 and 9. The control response curves jointly control three attitude angles to their expectations and are shown in Figure 8. It can be seen from Figure 8 that the ZN-PD controller can jointly control three attitude angles to arbitrary angle within the scope of (0.5,1,0.4) (rad), while simulation experiments demonstrate that GA-PD control can only jointly control three attitude angles to arbitrary angle within the scope of (0.5,1,0.33) (rad). The control effect comparison diagrams between ZN-PD and GA-PD of jointly controlling roll angle, pitch angle, and yaw angle to the expectations 0.5 rad, 1 rad, and 0.33 rad are shown in Figure 9. It can be seen from Figure 9 that ZN-PD control can make attitude angles quickly reach to the desired values and has smaller negative overshoot than GA-PD control in roll angle loop. It is obvious that the control effect of ZN-PD is better than one of GA-PD in jointly controlling three angles to the expectations.

It can be seen by synthesizing Figures 6, 8, and 9 that the control effect of ZN-PD is superior to the one of GA-PD. It can be seen by synthesizing Figures 6, 7, 8, and 9 that the control effect of ZN-PD is superior to the one of ZN-PID and GA-PD. In a word, the attitude controller adopted

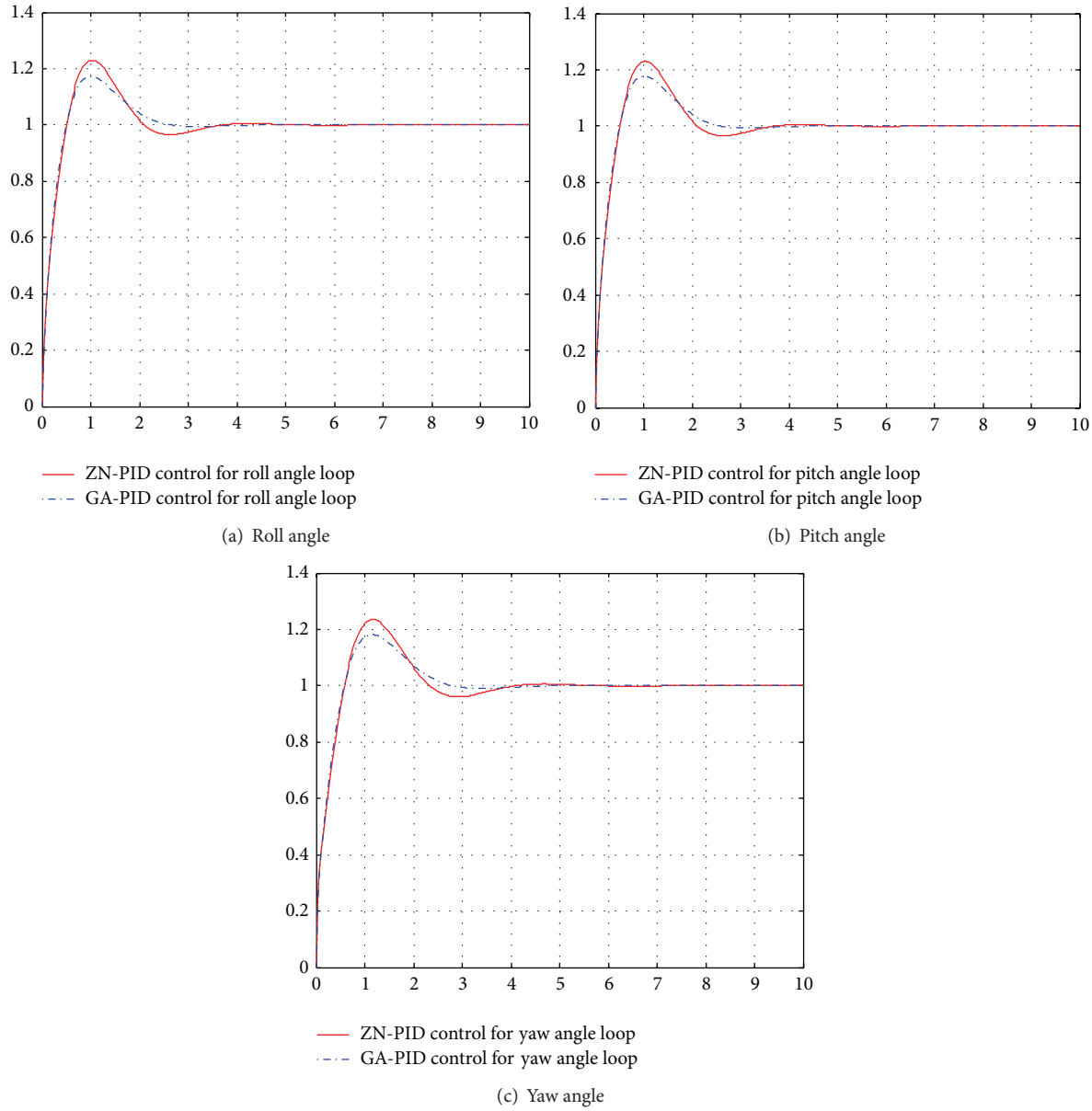

(a) Roll angle

(b) Pitch angle

(c) Yaw angle

Figure 5: The control effects compare diagrams between ZN-PID and GA-PID for three attitude angles. (a) The control effects compare diagram of the roll angle loop. (b) The control effects compare diagram of the pitch angle loop. (c) The control effects compare diagram of the yaw angle loop.

by this paper is simple and has very good control effect. The robustness tests for the ZN-PD control are shown in Figures 8 and 10. Figure 8 corresponds to the joint ZN-PD control response curve without noise interference. Figure 10 corresponds to the joint ZN-PD control response curve with noise interference. It can be seem from Figures 8 and 10 that the controller design method proposed in this paper is highly robust.

The robustness of ZN-PD controller results from the controller constituent. From the perspective of the frequency domain, in PID control, integral acts on low frequency band of the system to improve the stability of the system, and differential acts on middle frequency band of the system to improve the dynamic performance of system. But, in quadrotor control, the ZN-PD control effect is better than the ZN-PID control effect; the reason is that the integrator characteristics contradict the characteristics of quadrotor controlled object. The essence of increasing the integrator is adding a pole, which can eliminate the steady-state error of the system. But strong integral action will increase the amount of overshoot so as to make the system unstable. Nevertheless, quadrotor is a controlled object with narrow domain of definition, and the domains of definition of three attitude angles ϕ, θ, and ψ are $-\pi/2 < \phi < \pi/2$, $-\pi/2 < \theta < \pi/2$, and $-\pi < \psi < \pi$, respectively. Therefore, when integrator acts on the quadrotor controlled object,

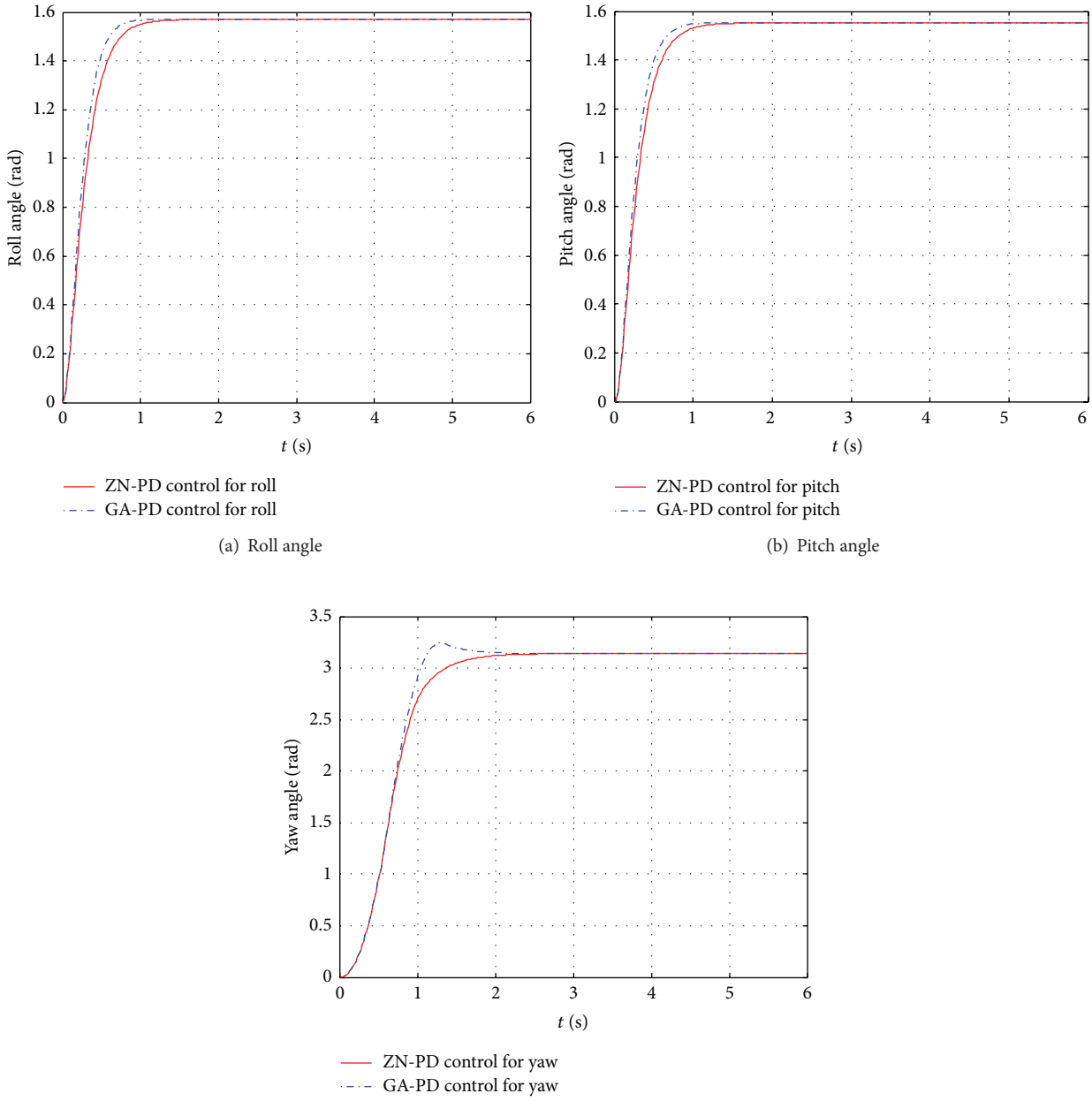

(a) Roll angle

(b) Pitch angle

(c) Yaw angle

FIGURE 6: The control effects compare diagrams between ZN-PD and GA-PD of separately controlling an attitude angle to the desired angle, while the rest attitude angles remain 0. (a) The control effects compare diagram of the roll angle. (b) The control effects compare diagram of the pitch angle. (c) The control effects compare diagram of the yaw angle.

quadrotor will become unstable as long as producing certain amount of overshoot, while this amount of overshoot will not affect the stability of the controlled object with wide domain of definition. When the noise interference is added to the quadrotor, the larger overshoot will appear in ZN-PID control, but the large overshoot will not appear because the integral action is not included and differential control can reduce overshoot and speed up the response in ZN-PD control.

The GA-PD control is an intelligent control method; it should have better control effect than ZN-PD control. But it can be seen from the simulation experiment proceeded in this paper that, in single control, for the roll and pitch angle loops, the control effects of GA-PD are better than those of ZN-PD, but, for the yaw angle loop, GA-PD control has a large overshoot while ZN-PD can quickly and without overshoot reach the desired value. For the quadrotor controlled object, the larger overshoot is fatal, which can be seen from the joint

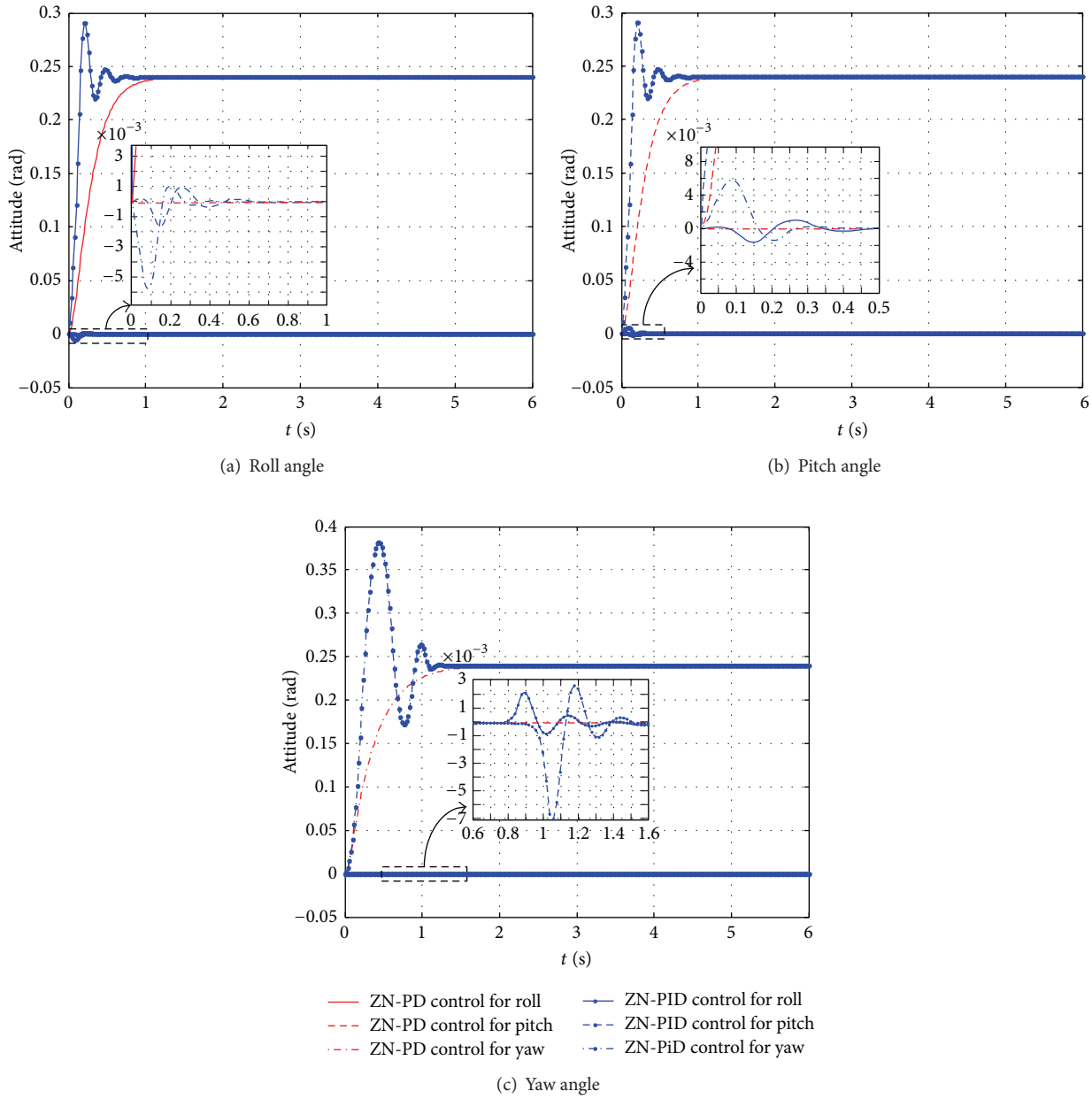

(a) Roll angle

(b) Pitch angle

(c) Yaw angle

Figure 7: The control effects compare diagrams between ZN-PD and ZN-PID of separately controlling an attitude angle to the desired angle, while the rest attitude angles remain 0. (a) The control effects compare diagram of the roll angle. (b) The control effects compare diagram of the pitch angle. (c) The control effects compare diagram of the yaw angle.

control. GA-PD control can only jointly control three attitude angles to arbitrary angle within the scope of (0.5, 1, 0.33) (rad) which is smaller than (0.5, 1, 0.4) (rad) of ZN-PD. the smaller the maximum angle is, the more the chance of unstable in afterward position control is. Meanwhile, the control effect of GA-PD is worse than the one of ZN-PD in jointly controlling three attitudes to the small values between GA-PD and ZN-PD. Moreover, the GA-PD control costs more system resources and more adjusting time, and further has the worst real-time which is more than the ZN-PD control. Therefore, the ZN-PD controller is selected in this paper.

In one word, the control effect of ZN-PD control proposed in this paper is superior to the control effects of ZN-PID and GA-PD. ZN-PD control is a simple and practical method.

6. Conclusion

The attitude controller adopted by this paper is a nonlinear controller. It consists of a linear control part and a nonlinear control part, where the linear control part is a PD controller which parameters were tuned by Ziegler-Nichols rules, and

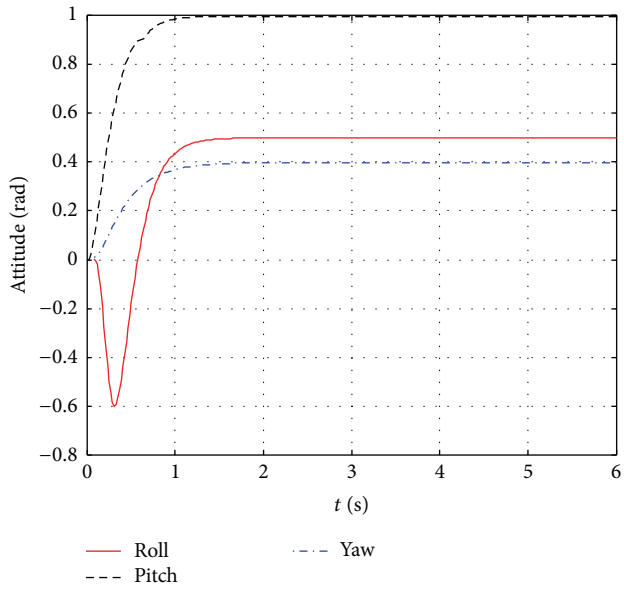

Figure 8: ZN-PD control responses of jointly controlling three attitude angles to the expectations.

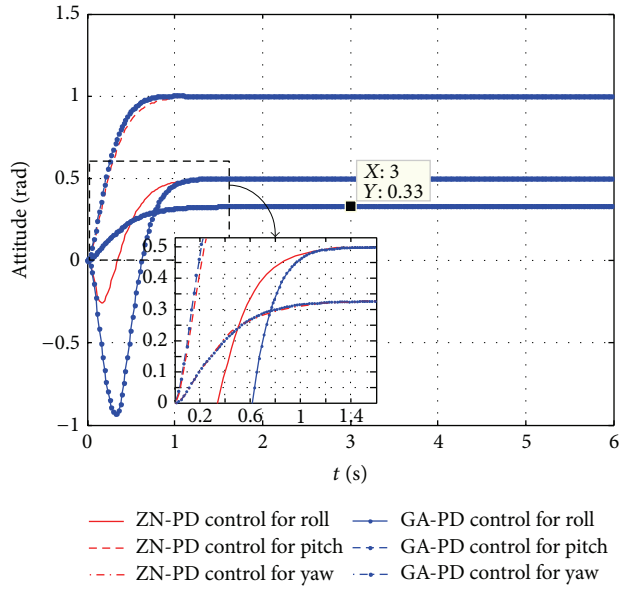

Figure 9: The control effects compare diagram between ZN-PD and GA-PD of jointly controlling three attitude angles to the expectations.

the nonlinear control part is a feedback linearization item which converts a nonlinear system into a linear system. The control effect of the attitude controller adopted by this paper is better than the control effects of the other two nonlinear controllers. The nonlinear parts of the other two nonlinear controllers are the same as the nonlinear part of the attitude controller proposed in this paper. The linear parts are, respectively, PID controller with the PID controller parameters tuned by Ziegler-Nichols rules and PD controller with the PD controller parameters tuned by GA. Besides,

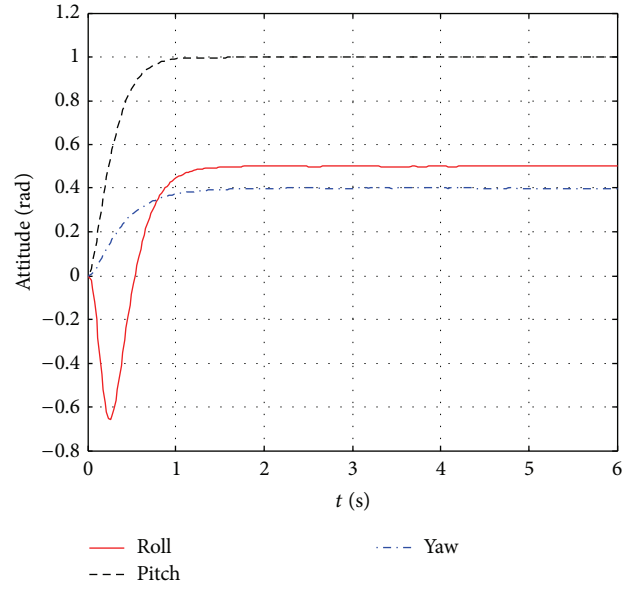

Figure 10: ZN-PD control responses with noise interference of jointly controlling three attitude angles to the expectations.

the attitude controller adopted by this paper is highly robust and the controller design method is a simple and practical one in engineering. The controller design ideas can also be used to other nonlinear controlled objects.

Conflict of Interests

The authors declare that there is no conflict of interests regarding the publication of this paper.

Acknowledgments

This work is supported by the key program of the National Natural Science Foundation of China (Grant no. 61039003), the National Natural Science Foundation of China (Grant no. 41274038), the Aeronautical Science Foundation of China (Grant no. 2013ZC51027), the Aerospace Innovation Foundation of China (CASC201102), and the Fundamental Research Funds for the Central Universities.

References

[1] K. Peng, G. Cai, B. M. Chen, M. Dong, L. Y. Lum, and T. H. Lee, "Design and implementation of an autonomous flight control law for a UAV helicopter," *Automatica*, vol. 45, no. 10, pp. 2333–2338, 2009.

[2] A. Isidori, L. Marconi, and A. Serrani, "Robust nonlinear motion control of a helicopter," *IEEE Transactions on Automatic Control*, vol. 48, no. 3, pp. 413–426, 2003.

[3] G. V. Raffo, M. G. Ortega, and F. Rubio, "An integral predictive/nonlinear H_∞ control structure for a quadrotor helicopter," *Automatica*, vol. 46, no. 1, pp. 29–39, 2010.

[4] A. Nagaty, S. Saeedi, C. Thibault, M. Seto, and H. Li, "Control and navigation framework for quadrotor helicopters," *Journal of Intelligent & Robotic Systems*, vol. 70, no. 1–4, pp. 1–12, 2013.

[5] H. Liu, Y. Bai, G. Lu, and Y. Zhong, "Robust attitude control of uncertain quadrotors," *IET Control Theory and Applications*, vol. 7, no. 11, pp. 1583–1589, 2013.

[6] C. T. Tony and W. MacKunisy, "Robust attitude tracking control of a quadrotor helicopter in the presence of uncertainty," in *Proceedings of the 51st IEEE Conference on Decision and Control (CDC '12)*, pp. 937–942, Maui, Hawaii, USA, December 2012.

[7] A. A. Mian and D. Wang, "Modeling and backstepping-based nonlinear control strategy for a 6 DOF quadrotor helicopter," *Chinese Journal of Aeronautics*, vol. 21, no. 3, pp. 261–268, 2008.

[8] V. Mistler, A. Benallegue, and N. K. M'Sirdi, "Exact linearization and noninteracting control of a 4 rotors helicopter via dynamic feedback," in *Proceedings of the 10th IEEE International Workshop on Robot and Human Communication*, pp. 586–593, September 2001.

[9] S. Bouabdallah, P. Murrieri, and R. Siegwart, "Design and control of an Indoor micro quadrotor," in *Proceedings of the IEEE International Conference on Robotics and Automation*, pp. 4393–4398, New Orleans, La, USA, May 2004.

[10] S. Bouabdallah, A. Noth, and R. Siegwart, "PID vs LQ control techniques applied to an indoor micro quadrotor," in *Proceedings of the IEEE/RSJ International Conference on Intelligent Robots and Systems (IROS '04)*, pp. 2451–2456, Sendal, Japan, October 2004.

[11] B. Erginer and E. Altuğ, "Modeling and PD control of a quadrotor VTOL vehicle," in *Proceedings of the IEEE Intelligent Vehicles Symposium*, pp. 894–899, Istanbul, Turkey, June 2007.

[12] R. A. García, F. R. Rubio, and M. G. Ortega, "Robust PID control of the quadrotor helicopter," in *Proceedings of the 2nd IFAC Conference on Advances in PID Control (PID '12)*, pp. 229–234, Brescia, Italy, March 2012.

[13] K. U. Lee, Y. H. Yun, W. Chang, J. B. Park, and Y. H. Choi, "Modeling and altitude control of quad-rotor UAV," in *Proceedings of the 11th International Conference on Control, Automation and Systems*, pp. 1897–1902, KINTEX, Gyeonggi-do, Korea, October 2011.

[14] Z. T. Dydek, A. M. Annaswamy, and E. Lavretsky, "Adaptive control of quadrotor UAVS in the presence of actuator uncertainties," in *Proceedings of the AIAA Infotech at Aerospace*, pp. 3416–3424, Atlanta, Georgia, April 2010.

[15] I. Palunko and R. Fierro, "Adaptive control of a quadrotor with dynamic changes in the center of gravity," in *Proceedings of the 18th IFAC World Congress*, pp. 2626–2631, Milano, Italy, August 2011.

[16] T. Dierks and S. Jagannathan, "Output feedback control of a quadrotor UAV using neural networks," *IEEE Transactions on Neural Networks*, vol. 21, no. 1, pp. 50–66, 2010.

[17] A. Rabhi, M. Chadli, and C. Pegard, "Robust fuzzy control for stabilization of a quadrotor," in *Proceedings of the IEEE 15th International Conference on Advanced Robotics: New Boundaries for Robotics*, pp. 471–475, Tallinn, Estonia, June 2011.

[18] B. Erginer and E. Altuğ, "Design and implementation of a hybrid fuzzy logic controller for a quadrotor VTOL vehicle," *International Journal of Control, Automation and Systems*, vol. 10, no. 1, pp. 61–70, 2012.

[19] S. Bouabdallah and R. Siegwart, "Full control of a quadrotor," in *Proceedings of the IEEE/RSJ International Conference on Intelligent Robots and Systems (IROS '07)*, pp. 153–158, IEEE, San Diego, Calif, USA, October-November 2007.

[20] K. Z. Meguenni, M. Tahar, M. R. Benhadria, and Y. Bestaoui, "Fuzzy integral sliding mode based on backstepping control synthesis for an autonomous helicopter," *Journal of Aerospace Engineering*, vol. 227, no. 5, pp. 751–765, May 2012.

[21] C. Nicol, C. J. B. MacNab, and A. Ramirez-Serrano, "Robust adaptive control of a quadrotor helicopter," *Mechatronics*, vol. 21, no. 6, pp. 927–938, 2011.

[22] Z. Song and K. Sun, "Adaptive backstepping sliding mode control with fuzzy monitoring strategy for a kind of mechanical system," *ISA Transactions*, vol. 53, no. 1, pp. 125–133, 2014.

[23] M. A. M. Basri, A. R. Husain, and K. A. Danapalasingam, "Robust chattering free backstepping sliding mode control strategy for autonomous quadrotor helicopter," *International Journal of Mechanical & Mechatronics Engineering*, vol. 14, no. 3, pp. 36–44, 2014.

[24] K. J. Åström and T. Hägglund, "The future of PID control," *Control Engineering Practice*, vol. 9, no. 11, pp. 1163–1175, 2001.

[25] J. G. Ziegler and N. B. Nichols, "Optimum settings for automatic controllers," *Transactions of the American Society of Mechanical Engineers*, vol. 64, pp. 759–768, 1942.

[26] A. M. Azzam, *A study on autonomous flight control of quadrotors [Ph.D. thesis]*, Beihang University, 2010.

[27] J. K. Liu, "The common PID control systems," in *Advanced PID Control Matlab Simulation*, X. Deng, Ed., pp. 71–93, Publishing House of Electronics Industry Press, 2nd edition, 2004.

Hindawi Publishing Corporation
The Scientific World Journal
Volume 2014, Article ID 139028, 12 pages
http://dx.doi.org/10.1155/2014/139028

Review Article

Distributed Cooperative Regulation for Multiagent Systems and Its Applications to Power Systems: A Survey

Jianqiang Hu,[1] Yaping Li,[2] Taiyou Yong,[2] Jinde Cao,[3,4] Jie Yu,[5] and Wenbo Mao[2]

[1] *School of Automation, Southeast University, Nanjing 210096, China*
[2] *China Electric Power Research Institute, Nanjing 210003, China*
[3] *Research Center for Complex Systems and Network Sciences, Department of Mathematics, Southeast University, Nanjing 210096, China*
[4] *Department of Mathematics, Faculty of Science, King Abdulaziz University, Jeddah 21589, Saudi Arabia*
[5] *School of Electrical Engineering, Southeast University, Nanjing 210096, China*

Correspondence should be addressed to Jinde Cao; jdcao@seu.edu.cn

Received 21 July 2014; Accepted 11 August 2014; Published 27 August 2014

Academic Editor: Wenwu Yu

Copyright © 2014 Jianqiang Hu et al. This is an open access article distributed under the Creative Commons Attribution License, which permits unrestricted use, distribution, and reproduction in any medium, provided the original work is properly cited.

Cooperative regulation of multiagent systems has become an active research area in the past decade. This paper reviews some recent progress in distributed coordination control for leader-following multiagent systems and its applications in power system and mainly focuses on the cooperative tracking control in terms of consensus tracking control and containment tracking control. Next, methods on how to rank the network nodes are summarized for undirected/directed network, based on which one can determine which follower should be connected to leaders such that partial followers can perceive leaders' information. Furthermore, we present a survey of the most relevant scientific studies investigating the regulation and optimization problems in power systems based on distributed strategies. Finally, some potential applications in the frequency tracking regulation of smart grids are discussed at the end of the paper.

1. Introduction

The regulating of collective behaviors for multiple interacting units is of great importance for networked interconnected systems in practical engineering [1]. Because of the development of communication technologies, the past decade has witnessed a remarkable increase in the investigation of cooperative control of events in a multiagent system, where local interactions among the events can emerge some captivating phenomena, such as synchronization [2], consensus [3, 4], swarming [5], flocking [6], and rendezvous [7]. This does not come as a surprise since such cooperative phenomenon lies in the heart of many real scenarios, ranging from some natural phenomena (school of fish, bird flock, and herding) to physics/biology and social networks, as well as engineering applications designed by networked control systems or coordination control problems among multiple subsystems.

Generally, for a large-scale multiagent system, there are always three kinds of control strategies: centralized control, decentralized control, and distributed control. The main ideas about these control strategies can be seen from Figure 1. Centralized and decentralized controls are always employed in the practical engineering applications, such as in the automatic generation control (AGC) of the power system; the participation rate for each AGC unit is received at the terminal station from the dispatching center (in a centralized way) and grid friendly household appliances which can reduce the consumption of active power by local frequency detection of the power system (in a decentralized way). While for some application fields distributed control is better than the centralized control and decentralized control in terms of easy implementation, low complexity, high robustness, and good scalability, such as in the formation flying of satellites, it is costly and inefficient to control every satellite by a way of

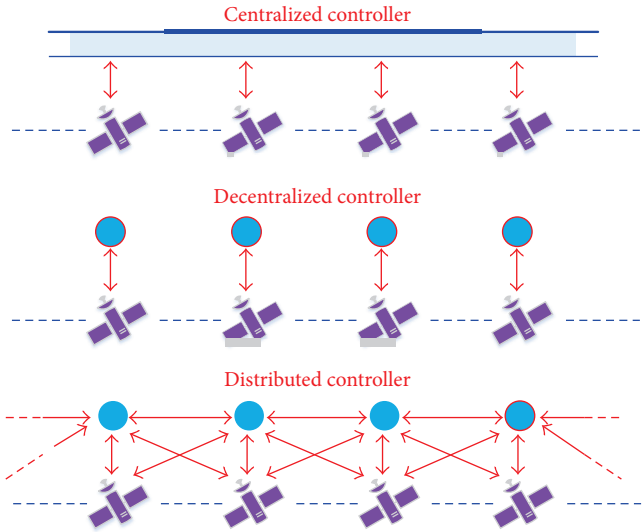

Figure 1: Three kinds of control strategies [8].

centralized control. The same is valid for underwater repair done by multiple underwater robots.

Cooperative control studies can be traced back to the synchronization control of the master-slave system [9], where there is a communication link between the node of the master system and the node of the slave system, which is also known as the drive-response system. Along with the development of communication technologies and the increasing number of the controlled plants, distributed cooperative control has become popular in recent years. As one kind of basic coordination problem, cooperative tracking is an interesting research topic subjected to one leader or multiple leaders. In fact, most of the practical problems are affiliated to tracking control problems subjected to one or multiple leaders, such as in power systems, the tracking of the expected regulation of the active and reactive power outputs of multiple photovoltaic (PV) generators [10], and the tracking of the reference voltage/frequency for the interconnected distributed generation (DGs) [11].

When there is only one leader and multiple followers in the multiagent network, the corresponding tracking problem is affiliated to consensus tracking or pinning consensus; when there are multiple leaders and multiple followers in the multiagent network, such a tracking problem is the containment control. For a multiagent system, consensus tracking control has been introduced in Hong et al. [12], where the state of the leader is time varying and not measured; in order to track such a leader, a neighbor-based local controller together with a neighbor-based state estimation rule was proposed for each autonomous agent such that all agents could follow the leader. Dimarogonas et al. [13] introduced a leader-based containment control strategy for multiple unicycle agents, where the leaders could converge to a desired formation and the followers could converge to the convex hull of the leaders' final positions.

This paper reviews some recent progress in leader-following tracking control, mainly the pinning consensus problem with a single leader and containment control problem with multiple leaders and its applications in power systems. The rest of this paper is organized as follows. We start by introducing the pinning consensus (leader-following consensus) problem in Section 2. Section 3 provides the basic description about the multiple objective tracking problem for leader-following systems (containment control). Furthermore, the methods on how to choose the pinned nodes are summarized in Section 4. Section 5 discusses some related studies on the regulation and optimization dispatch problems in the area of power systems by distributed strategies. Some potential applications for tracking control in power systems are discussed in Section 6.

The basic preparation for cooperative control is the communication network, so it is reasonable to introduce some fundamental concepts about networks as follows.

A directed graph (or digraph) $\mathcal{G} = (\mathcal{V}, \mathcal{E})$ is used to represent the communication topology in a networked multiagent system, where $\mathcal{V} = \{1, 2, \ldots, N\}$ is the finite set of the agents and $\mathcal{E}$ is the set of edges. The edge $e_{ij} = (i, j) \in \mathcal{E}$ indicates that the agent j can receive the information from the agent i. A graph with the property that $e_{ij} \in \mathcal{E}$ implies $e_{ji} \in \mathcal{E}$ is said to be undirected. $\mathcal{G}$ is called strongly connected if between any pair of distinct nodes $i, j \in \mathcal{V}$ there is a directed path from node i to node j, and $\mathcal{G}$ is said to be weakly connected if replacing all of its directed edges with undirected edges appears to be a connected undirected graph. A directed tree is a digraph, where every node, except the root, has exactly one parent node. A spanning tree of $\mathcal{G}$ is a directed tree whose node set is $\mathcal{V}$ and whose edge set is a subset of $\mathcal{E}$. For a digraph $\mathcal{G}$, the adjacency matrix $\mathcal{A} \in \mathbb{R}^{N\times N}$ is defined as $a_{ij} \geq 0$, in which $a_{ij} = 1 \Leftrightarrow e_{ji} = (j, i) \in \mathcal{E}$, while $a_{ij} = 0$ if $e_{ji} \notin \mathcal{E}$, and it is further required that self-links are not allowed; that is, $a_{ii} = 0$. The Laplacian matrix L is defined as $L = \mathcal{D} - \mathcal{A}$, where $\mathcal{D}$ is a diagonal matrix with $d_{ii} = \sum_{j\neq i} a_{ij}$.

2. Pinning Consensus of Multiagent Systems

For a multiagent tracking network, the communication structure denotes the direction of information flow, by which agents are connected to each other. Pinning consensus means there are one leader agent and multiple followers in the system and to design a control strategy such that the followers can track the leader. The objective information can be viewed as the root node for the communication network; if there exists a directed path from the root to each agent, then all the agents can track the objective successfully, that is, the simplest star-network topology (see Figure 2); all units are pinned by the control center for the objective information.

Recently, distributed pinning control becomes very popular due to their flexibility and computational efficiency based on the sparse communication network. In fact, such an idea comes from the pinning synchronization of complex dynamical networks. Pinning control can be found in the literature [14, 15], where the authors turned to seek the minimum density of controllers for controlling the spatially extended chaotic systems. With the discoveries of the small-world network [16] and the scale-free network [17], complex networks have witnessed unprecedented developments in

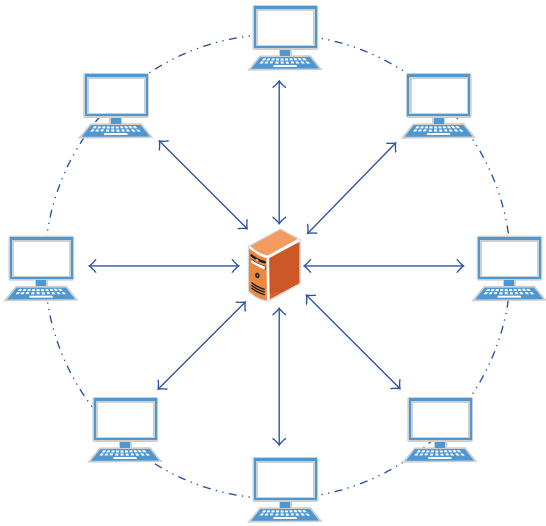

Figure 2: The communication structure for centralized control.

various fields, and the discussions of synchronization problems for complex networks have been extensively launched. However, in practice, the state variables of some network nodes are not observable or measured. Therefore, it is necessary to investigate the possibility of pinning a coupled network by adding controllers to those nodes, which can be measured or controlled.

2.1. Consensus of Multiagent Systems. One of the basic tasks in a multiagent system is the consensus of each agent's state. Consensus control has been subject to fundamental research as well as being an important theoretical preparation for other cooperation control problems, such as robotic coordination, distributed computation, and satellite formation flying. Generally, distributed consensus protocols are designed for the multiagent system. In such a distributed mode, each agent perceives the information of its neighboring agents and then responds according to the consensus protocol in real time, under which consensus can be achieved.

In a system of N agents, each characterized by a state variable $x_i(t) \in \mathbb{R}^n$ subject to a control input $u_i(t) \in \mathbb{R}^n$, is given as follows:

$$\dot{x}_i(t) = Ax_i(t) + Df\left(t, x_i(t)\right) + Bu_i(t), \tag{1}$$

where $i = 1, 2, \ldots, N$.

Consensus control means to design a distributed communication protocol such that the state of each agent can reach agreement as $t \to \infty$; that is,

$$\lim_{t\to\infty} \left\| x_i(t) - x_j(t) \right\| = 0, \quad \forall i, j = 1, 2, \ldots, N. \tag{2}$$

Given a communication topology $\mathcal{G}$ for the N multiagent system with the adjacency matrix $A = (a_{ij})_{N\times N}$ describing the interaction among agents, the consensus objective can be achieved by the following distributed consensus protocol:

$$u_i(t) = -c\sum_{j=1}^{N} a_{ij} K\left(x_i(t) - x_j(t)\right), \tag{3}$$

where $i = 1, 2, \ldots, N$; and c, K are the coupling strength and the feedback gain matrix to be determined.

Under the consensus protocol, the networked multiagent system turns out to be the following vector form:

$$\begin{aligned}\dot{x}(t) = {} & \left(I_N \otimes A\right) x(t) + \left(I_N \otimes D\right) f(t, x) \\ & - c\left(L \otimes BK\right) x(t),\end{aligned} \tag{4}$$

where $x(t) = (x_1^T(t), \ldots, x_N^T(t))^T$, $f(t, x) = (f(t, x_1)^T, \ldots, f(t, x_N)^T)^T$, and L is the Laplacian matrix of the communication topology $\mathcal{G}$.

The rest is to analyze the consensus convergence and the convergence rate of the close-loop system (4) under fixed/switching undirected or directed communication topology and so on.

Remark 1. In fact, system (1) is quite general, since it covers the multiagent systems with integrator-type dynamics, linear dynamics, and nonlinear dynamics; meanwhile, first-order, second-order, and higher-order multiagent system are all possible [18, 19].

2.2. Pinning Originated from Complex Dynamical Networks. A closely related research topic to consensus is the synchronization of complex dynamical networks. The complex dynamical network is coupled with lots of dynamic nodes, and all the nodes will achieve synchronization spontaneously if the coupling strength is sufficiently large. However, in most practical cases, the coupling strength is small and the network needs to be controlled to a desired homogeneous trajectory. The *pinning control strategy* was proposed in [20] for the scale-free dynamical network, where specifically and randomly pinning schemes were employed to synchronize the dynamical network. Furthermore, Li et al. [21] proposed the concept of virtual control and studied the pining control problem for a complex dynamical network. The concept of *pinning controllability* had been introduced in [1] for general complex dynamical networks, where networks are defined in which two different layers of dynamical nodes coexist: the uncontrolled sites and the reference (controlled) ones. It has been shown that the latter plays the role of leading the whole network towards a given (desired) reference evolution. Chen et al. [22] proved that a single controller can pin a coupled complex network to a homogenous trajectory if the network coupling strength is sufficiently large. In [23], the authors established some sufficient conditions for global pinning controllability of a generic network of coupled oscillators to some desired solutions. The authors in [24] considered the stochastic pinning synchronization of coupled dynamical system with Markovian switching couplings, where the coupling matrix and pinning feedback gain follow a common Markovian switching sequence. So far, pinning synchronization for complex dynamical networks has been extensively addressed; for more details see [25–30] and references therein.

However, the challenging problem for pinning control is which nodes should be pinned and at least how many nodes should be pinned for undirected or directed network

structures. Recently, Liu et al. [31] developed analytical tools to study the controllability of an arbitrary complex directed network based on the theory of maximum matching, which can identify the set of driver nodes with time-dependent control. The authors [32] further investigated the observability of complex systems. Yu et al. [33] investigated how to choose an optimal node to realize the pinning controllability of the complex network based on the cut graph theory. And recently, in [34], the optimal choice for the k ($k < N$) follower nodes to be pinned can be approximately solved by minimizing the maximal distance in the communication graph from the leader to the followers. Such a k-pinning problem has been transformed to a nonconvex optimization problem. The authors in [35] introduced an analytical approach to select leader agents, in order to minimize the total mean-square error of the follower agents in the presence of noisy communication links.

2.3. Consensus Tracking of Multiagent System. In a one-dimensional integrator multiagent system, by integrating the distributed consensus protocol to the node system, then the following coupled system appears:

$$\dot{x}_i = -\sum_{j=1}^{N} a_{ij}\left(x_i - x_j\right), \quad i = 1, 2, \ldots, N. \tag{5}$$

In vector notation, the consensus protocol (5) takes the form $\dot{x} = -Lx$, where L is the corresponding Laplacian matrix of the communication topology $\mathcal{G}$. Under such protocol, the multiagent system will achieve consensus on a common state; that is, all $x_i(t)$ will converge to a common value x_∞ as $t \to \infty$. If the graph $\mathcal{G}$ has a directed spanning tree, then all the eigenvalues of Laplacian matrix L have nonnegative real parts and zero is an eigenvalue with the right eigenvector $\mathbf{1}_N$ and the left eigenvector $\omega = \{\omega_1, \ldots, \omega_N\}$, where $\sum_{i=1}^{N} \omega_i = 1$, $\omega_i \geq 0$. It follows that the consensus subspace $\mathbf{1}_N$ is exponentially stable, the consensus value is the weighted average of the initial sates $x_\infty = \sum_{i=1}^{N} \omega_i x_i(0)$, and the rate of convergence is not worse than $\mathrm{Re}\{\lambda_2(L)\}$; that is, $\|x_i(t) - x_\infty\| \leq \|x_i(0) - x_\infty\| e^{-\mathrm{Re}\{\lambda_2(L)\}t}$.

However, the consensus value x_∞ in the above formula is not always the expected final state in practice. In order to control the multiagent system converging to a given objective value, the distributed pinning consensus protocol is introduced. The so-called "distributed pinning control" means only a small fraction of nodes in the network are pinned by the control center to the objective trajectory and the rest of the nodes communicated with each other to achieve the expected networked tracking.

The following distributed pinning protocol is given in [36]:

$$\dot{x}_i = -\sum_{j=1}^{N} a_{ij}\left(x_i - x_j\right) - d_i\left(x_i - \theta\right), \tag{6}$$

where $i = 1, 2, \ldots, N$ and the pinning control gain $d_i \geq 0$ and $d_i = 0$ indicates there is no control over the agent i and θ is an expected consensus state.

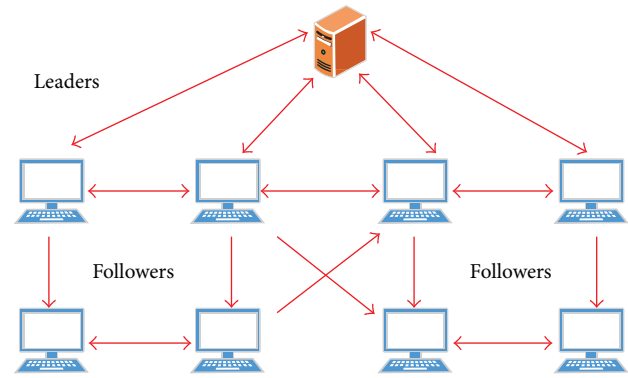

Figure 3: Pinning control structure of multiagent system.

Furthermore, Song et al. [37] investigated pinning consensus problems for second-order nonlinear multiagent systems with general network topologies and addressed what kind of agents and how many agents should be pinned. Based on the method of model predictive control (MPC) and pinning control, the authors in [38] showed that the consensus performances (i.e., the convergence speed towards consensus) could be improved, as the pinning nodes can be used to provide an accurate future state trajectory prediction due to the availability of the objective information shared with these nodes. The authors in [39] investigated finite-time distributed consensus problem for multiagent systems using a binary consensus protocol and the pinning control scheme. By using the Lie algebra theory, a linear node-and-node pinning method was proposed in [40] to achieve a consensus for the case of a directed multiagent network which does not contain a directed spanning tree.

In fact, leader-following consensus can be regarded as pinning consensus as well. Leader-follower models were introduced in the literature [12, 41, 42] where agents in the system can be categorized as leaders and followers. A leader can be viewed as an objective node which can perceive more information in order to guide the whole group, while a follower usually responds to the commands received from the leaders and other connected agents. If there exists only one leader in the network, the leader-following consensus is the general pinning consensus problem; see Figure 3.

Leader-follower models have been extensively studied in the literature in terms of controllability, formation, and target tracking [43–45]. The authors in [46] investigated the distributed tracking control for leader-follower multiagent system with measurement noises and directed interconnection topology. By using the iterative learning approach, tracking control problems were considered in [47] for multiagent systems which were described by both discrete-time and continuous-time models, where all agents in a directed graph were enabled to track a time-varying reference trajectory perfectly over a finite interval. Based on distributed discontinuous controllers with static/adaptive coupling gains, consensus tracking problem for linear multiagent systems was investigated such that all the followers could converge to the leader whose control input was nonzero and not available

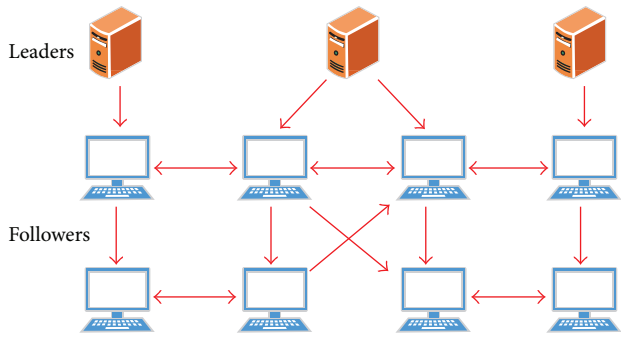

Figure 4: Containment control structure of leader-following multiagent system.

to any follower [48]. Xu et al. [49] considered the leader-following consensus of nonlinear multiagent system under switching topologies where the union of all the topologies was jointly connected. While for consensus tracking, the corresponding literature can be seen from [19, 50–52] and references therein. The pinning control strategy for multiagent systems can not only help us to better understand the mechanisms of natural collective phenomena, but also benefit applications in mobile sensor/robot networks [53–55].

3. Containment Control of Leader-Following Networks

In the previous section, we mainly reviewed the leader-following consensus problems, where there is only one leader in the multiagent network. Containment control problem arises in the presence of multiple leaders and multiple followers in a multiagent network (see Figure 4) where its control objective is to drive all the followers into the convex hull spanned by the leaders. Motivated by numerous natural phenomena and some requirements of engineering applications, such as moving of migratory birds, earth monitoring satellites, and smart autonomous robots which can steer clear of obstacles, containment control has attracted substantial attention from various research communities.

Containment control is a combination of formation and rendezvous problem and as such it is of interest for UAV formation control, robot swarms, and attitude control of rigid bodies [13]. The authors in [56, 57] investigated the problem of driving a collection of mobile robots to a given target location in the context of partial difference equations by a decentralized control strategy for the followers, and the following agents would stay in the convex polytope spanned by dedicated leader agents, whose dynamics were given by a hybrid Stop-Go policy according to a decentralized formation control strategy. At this point, the leaders stop and let the followers settle back into the leader polytope before they start moving again. Inspired by [57], the authors in [58] furthermore considered a hierarchical model predictive control (MPC) structure for containment and distributed sensing in a leader-following multiagent architecture.

Containment control problems are further carried out in the single-/double-integrator agents with multiple stationary or dynamic leaders under fixed undirected/directed communication topologies [59–62] by distributed protocol. The authors [63] studied the containment control for continuous-time/discrete-time multiagent systems by proposing a new protocol which exploited the control input information of neighbors. While the containment control for linear multiagent system [64–66] has been considered recently, such as necessary and sufficient conditions were given in [67, 68] for discrete-time linear multiagent systems under both the state feedback and output feedback protocol cases. Robust H_∞ containment controls for uncertain linear/nonlinear multiagent systems were further investigated recently in [69, 70]. On the other hand, the containment control for nonlinear multiagent systems has been investigated as well, such as containment for second-order nonlinear multiagent systems [71], finite-time containment for multiple Lagrangian systems [72], and multiple rigid body systems [73]. Distributed containment control problems were discussed in [74, 75] for nonlinear Euler-Lagrange systems with parametric uncertainties by introducing estimator or adaptive control law under a directed communication topology. Some other nonlinear multiagent system cases were studied in [76, 77].

On the other hand, switching communication topology is an attractive research area, which has been considered in the designing of the distributed protocol. As a kind of time-varying communication topology, switching always follows two different cases: random switching and Markov switching. Under the assumption that the union of undirected graphs is jointly connected, [78] considered the containment control problem in leader-following networks. By considering the dynamically/randomly switching topologies, [79] investigated the mean-square containment control for multiagent systems with transmission noises. The almost surely asymptotic containment was considered in [80] for a second-order multiagent system under the switching of a continuous-time irreducible Markov chain.

Generally, the containment control problem of a group of N nonlinear agents with the dynamic of ith agent can be described as follows:

$$\begin{aligned} \dot{x}_i &= Ax_i + Df\left(t, x_i\right) + Bu_i, \quad i \in \mathcal{V}_F, \\ \dot{x}_i &= Ax_i + Df\left(t, x_i\right), \quad i \in \mathcal{V}_L, \end{aligned} \tag{7}$$

where $x_i \in \mathbb{R}^n$ and $u_i \in \mathbb{R}^m$ are the state and the control input of ith agent and $\mathcal{V}_F \triangleq \{1, \ldots, M\}$ and $\mathcal{V}_L \triangleq \{M+1, \ldots, N\}$ denote the followers' set and the leaders' set, respectively.

The distributed containment control protocol based on the real-time state information feedback for the followers in system (7) is given as

$$u_i = \alpha K \sum_{j=1}^{N} a_{ij}\left(x_j - x_i\right), \quad i \in \mathcal{V}_F, \tag{8}$$

where α and K are the positive coupling strength and the feedback gain matrix for the protocol and a_{ij} is the element of the adjacency matrix of the directed communication topology $\mathcal{G}$.

Protocol (8) is said to solve the containment control problem, if for any initial sates, all followers asymptotically converge to the convex hull spanned by the leaders. That is,

$$\lim_{t\to\infty} d(x_i, \Omega) = 0, \quad \forall i \in \mathcal{V}_F, \tag{9}$$

where $\Omega = \{\sum_{i=1}^{N-M} \alpha_i x_{M+i} \mid \alpha_i \geq 0, \sum_{i=1}^{N-M} \alpha_i = 1\}$ is the convex combination of the leaders' states.

In the above discussion (since 2010), there is a basic assumption that there is no communication among leaders. That is, the leaders are controlled in a centralized way. In fact leaders may communicate with each other so as to maintain a fixed formation or expected running space (as stated in [56]). Such a leader-following model presents a hierarchical structure with two layers, where the upper layer denotes the set of leaders and the lower layer represents the set of followers. The leaders communicate with each other such that a formation control objective can be achieved, and the followers communicate with each other such that they can converge to the formation based on the designed protocol. In [81], finite-time formation control has been considered for a group of agents where the global formation information was only available for navigational leaders; meanwhile, the other following agents regulated their positions by the local information in a distributed manner. Cooperative control has been investigated in [82] such that the leaders converged to a formation and the followers moved into the convex hull spanned by the leaders final positions under switching topologies. It deserves further investigations of distributed-distributed cooperative control in leader-following structures.

4. How to Choose the Pinning Nodes

As for a multiagent system, if the communication networks are prescribed, then the pinning consensus problem reduced to find the pinning nodes according to the network structure. On the other hand, pinning is related to the designing of an efficient communication network for the multiagent system according to the controllability and observability of each plant. When pinning a multiagent system, the most challenging problems are what kinds of nodes should be pinned and what is the minimum number of the pinned nodes. Up to now, some effective pinning schemes have been proposed for the directed/undirected complex networks, as reported in the literature.

When the communication network is undirected, one can choose randomly a set of nodes or specifically the most highly connected nodes to be pinned [20]. On the other hand, one can also utilize the following centrality methods to choose the pinning nodes, such as: local centrality [83], betweenness centrality [84, 85], closeness centrality [86], eigenvector centrality [87], subgraph centrality [88], PageRank centrality [89], LeaderRank centrality [90], and some applications [91, 92]. These centrality methods can be utilized to rank the nodes in the network according to the communication structure. High centrality nodes are always viewed as more important nodes in networks and they should be pinned first. However, the performance is evaluated and determined by the convergence rate under the minimal number of pinned nodes under the same pinning gains.

When the communication network is directed, how to select the appropriate pinned nodes is quite a challenging problem. In the literature, there have been several pinning strategies proposed. In [93], it is suggested to pin the roots of trees in a spanning forest of the interaction graph. Some high ControlRank (CR) nodes [94] have been chosen to be pinned. One can also make use of the closeness centrality of the weighted directed networks method [95] to decide whether the nodes should be pinned or not. In [96], the authors have proposed a selective method based on the pinned candidates set composed of the nodes whose out-degree is bigger than their in-degree. Illuminated by the idea in [96], it is considered that if there is a directed edge from the ith node to the jth node, the dynamical behavior of the node j will then be impacted by the dynamics of the node i to a great extent. The manipulating procedure is summarized as follows.

(i) For a given digraph with $G^{(0)}$ as its Laplacian matrix, the in-degrees and out-degrees of the nodes are defined as $\deg_{\text{in}}(i) = \sum_{j=1, j\neq i}^{N} G_{ij}^{(0)}$ and $\deg_{\text{out}}(i) = \sum_{i=1, i\neq j}^{N} G_{ij}^{(0)}$.

(ii) Let $\deg_{\text{diff}}(i) = \deg_{\text{out}}(i) - \deg_{\text{in}}(i)$ $(i = 1, 2, \ldots, N)$ be the degree differences of the digraph $G^{(0)}$.

(iii) For the nodes with zero in-degrees, they should be pinned first since those nodes can be viewed as leaders of the network.

(iv) Rearrange the remaining nodes in descending order according to their degree differences, and choose the pinning nodes according to the degree differences.

In summary, there exist many kinds of node ranking methods with respect to undirected networks and directed networks. However, the basic problem comes for a given large-scale communication network, which nodes should be pinned and at least how many nodes should be pinned, instead of checking each method one by one. This problem is a network optimization problem that remains to be further explored. Some recent progress with respect to optimization methods on how to choose the optimal pinning nodes can be seen in [33–35].

5. Cooperative Control in Power Systems

With the development of smart grids and the interconnection of multiple large-scale regional power grids, power system has increasingly developed into a supersized artificial network. Such a network consists of cross-coupled primary/secondary power equipments and is supported by advanced control technologies and efficient communications networks, which has formed a smart self-healing system. Traditionally, power system stability and control were accompanied by control strategies of centralized or decentralized control and rarely involved the distributed coordination control. Owing to the expansion of network scale and the increasing number of the controlled objects, distributed

control gradually brings out its advantages in terms of better robust performance and lower cost of control. Recently, distributed control and distributed optimization are utilized to solve the emerged control and optimization problems in power systems.

5.1. Distributed Regulation. As for distributed cooperative control, consensus protocol and pinning tracking have been introduced in some application fields of power systems, especially in microgrids. Kim et al. [97] employed a cooperative control strategy to the islanded operation microsources and the energy storage system (ESS) and showed that such a control strategy could improve the control capability in the regulations of frequency and voltage. By selecting the incremental cost of each generation unit as the consensus variable, the authors in [98] introduced an incremental cost consensus (ICC) algorithm which was able to solve the conventional (centralized) economic dispatch problem of power systems in a distributed manner. Based on the cooperative control strategies, the regulation output was considered for multiple photovoltaic (PV) generators [99, 100] such that all the PVs had the same reserve ratio with respect to their maximum available power, and the regulation output for multiple distributed generators (DGs) was investigated in [101] in a distributed fashion such that these generators could be developed into a virtual power plant (VPP) in a distribution network. By input-output feedback linearization, the secondary voltage control problem was converted to a linear second-order tracking consensus problem [102] and it was shown that the distributed structure could improve the system reliability. Similarly, distributed control was introduced in distribution networks for coordinating multiple energy storage (ESUs) such that the ESUs's reactive power could be used for voltage support and the active power could be utilized in managing network loading [103]. Distributed frequency synchronization of multiple isolated microgrids was investigated in [104] under the smart grid communication infrastructure.

While most of previous publications focus on the distributed regulation problems for generating/storage units, the coordination problem among multiple controllable flexible loads in distribution networks has received much attention recently. By proposing a multiagent reinforcement learning algorithm and considering the nonlinear characteristics of power systems, Daneshfar and Bevrani [105] showed that load-frequency control (LFC) performance was improved compared with traditional proportional-integral (PI) controllers. A distributed multi-agent-based load shedding algorithm was proposed in [106], which could make efficient load shedding decision based on discovered global information, where the information discovery algorithm was given in a distributed way. Zhao et al. [107] proposed a decentralized optimal load control scheme via frequency measurement, where each load estimated the total mismatch between load and generation. Meanwhile, the inconsistencies of the estimations were mitigated by an average consensus algorithm. Furthermore, frequency regulation problem was considered in [108] by formulating an optimal load control problem. By proposing a market-based control and a multiagent distributed communication model, the optimal operation problem was considered in [109] for price-response controllable loads in electrical distribution network. For an islanded microgrids, Shafiee et al. [110] investigated distributed secondary control problem by a distributed networked control system which not only could be able to restore the frequency and voltage of the microgrid but also ensures reactive power sharing. It has also been shown that averaging-based distributed controllers using communication among the generation units offer the best combination of flexibility and performance in a microgrid [111].

5.2. Distributed Optimal Dispatch. With respect to power transmission systems, three kinds of control architectures, that is, a layering of primary, secondary, and tertiary control, have formed the standard operation paradigm for power systems. Generally, primary droop control is realized in a decentralized way, and secondary frequency regulation can be performed in a centralized, decentralized, or distributed architecture. Tertiary control is affiliated to unit commitment (UC) problem and economic dispatch (ED) problem, which are always solved in a centralized way. Owning to the explosion in size and complexity of modern electric power datasets, it is increasingly important to solve such an optimization problem high efficiently. Distributed convex optimization, in particular for large-scale problems arising in power systems, statistics, and other related areas, has received considerable attention recently.

Kar and Hug [112] proposed a distributed consensus-based approach for economic dispatch problem in power systems, in which each network agent participates in a collaborative process of neighborhood message exchange and local computation. By utilizing the distributed algorithm for frequency control and optimal economic dispatch of power generators, it was shown in [113] that distributed algorithm could eventually achieve optimality and present better robustness compared with traditional (centralized) dispatch algorithms. Economic dispatch problem was solved in distributed fashion by a novel consensus-based algorithm [114], where the estimated mismatch was used as a feedback mechanism to adjust current power generation by each generator such that all generators can automatically minimize the total cost in a collective sense. Yang et al. [115] considered the problem of distributed optimal dispatch based on the distributed primal-dual subgradient algorithm for virtual power plant (VPP). Based on two parallel consensus algorithms, a distributed algorithm was presented in [116] to solve the economic power dispatch problems with transmission line losses and generator constraints.

In fact, power systems can be modeled as a hybrid system, in which control and optimization coexist. Such as in the process of the frequency regulation, generating units and controllable flexible loads will participate in the secondary frequency regulation together. How the generators and loads respond to the frequency deviation is a cooperative control problem. While, for the tertiary frequency regulation problem, UC and ED problems are solved at the dispatching center traditionally; and distributed regulation and distributed optimization can be combined together to deal with such

a multitime scale frequency regulation problem emerged in small or large power system.

6. Conclusion and Discussion

In this paper, we reviewed some recent progress in cooperative tracking control for leader-following multiagent systems and some relevant application problems in power systems by distributed regulation and optimization. Pinning control is an interesting research topic which has lots of potential applications. Although the existing theoretical results in distributed multiagent system are rich and varied, there are still many practical engineering problems to be solved which may involve the application of pinning control for large-scale interconnected systems. In the following, we mainly discussed some potential applications of pinning control in multiarea interconnected power system.

(1) The interconnected power system can be modeled as a multiagent system, where network nodes are generators and buses, flexible loads, and network links are transmission/communication lines. While, in the power system, a basic tracking problem is the LFC problem [117, 118], in which the generators have to track the changing of active power of the time-varying loads, conventional control efforts focus on the generation side, mainly determined by AGC units, the objective of which is to control the reserved generation capacity and minimize the area control error (ACE) [119, 120]. In fact, such a control scheme is the centralized control; each generator receives the frequency regulation and generation scheduling signals from the dispatching center. Distributed pinning AGC may play an even greater advantage, which will be discussed in the near future.

(2) Smart grids integrate different kinds of renewable power generations and multiple controllable flexible loads, which are connecting to the main power grid. These power generations together with AGC units and flexible loads will be involved in the primary frequency regulation of the power system together. So the basic problem comes of how do these participants coordinate with each other such that the frequency of power systems can be maintained at the normal operating range while subjected to the power balance constraints. The renewable power plants and AGC units can be categorized as the upper layer of generator cluster; flexible controllable loads are categorized as lower layer of consumer cluster. All units in each cluster can coordinate in a distributed way such that the frequency regulation is able to cope with the disturbance of the system.

(3) The frequency regulation of power systems is accomplished through a three-stage process with the fast response primary control as the first stage. Secondary control can be contributed by all the generating units and controllable loads through distributed cooperative control, while controllable flexible loads in power systems are at a large scale of both size and distribution. For any given bus node, the loads under this bus can be aggregated to several clusters with each managed by a load agent. Is it necessary for loads to interact with each other inside a load agent and for agents to interact with each other under a bus node? It is urgent to introduce distributed or decentralized management instead of centralized management owing to the increasing number of managed objects. In the third-stage process, optimal dispatch can be performed at each generating/bus agent in a distributed manner. Thus, one can conclude that the frequency regulation of power systems is carried out by decentralized control in the first layer, distributed cooperative control in the second layer, and distributed optimization in the third layer, which makes the entire regulation system become more robust and efficient.

Conflict of Interests

The authors declare that there is no conflict of interests regarding the publication of this paper.

Acknowledgments

This work was jointly supported by the State Grid Corporation of China Project (DZ71-13-045): Study on Key Technologies for Power and Frequency Control of System with "Source-Grid-Load" Interactions, the National Natural Science Foundation of China under Grants 61272530 and 11072059, the Natural Science Foundation of Jiangsu Province of China under Grant BK2012741, the Specialized Research Fund for the Doctoral Program of Higher Education under Grants 20110092110017 and 20130092110017, and the China Postdoctoral Science Foundation (2013M541582).

References

[1] F. Sorrentino, M. di Bernardo, F. Garofalo, and G. Chen, "Controllability of complex networks via pinning," *Physical Review E: Statistical, Nonlinear, and Soft Matter Physics*, vol. 75, no. 4, Article ID 046103, 2007.

[2] A. Arenas, A. Diaz-Guilera, J. Kurths, Y. Moreno, and C. Zhou, "Synchronization in complex networks," *Physics Reports*, vol. 469, no. 3, pp. 93–153, 2008.

[3] R. Olfati-Saber and R. M. Murray, "Consensus problems in networks of agents with switching topology and time-delays," *IEEE Transactions on Automatic Control*, vol. 49, no. 9, pp. 1520–1533, 2004.

[4] W. Ren and R. W. Beard, "Consensus seeking in multiagent systems under dynamically changing interaction topologies," *IEEE Transactions on Automatic Control*, vol. 50, no. 5, pp. 655–661, 2005.

[5] H. Shi, L. Wang, and T. Chu, "Swarming behavior of multi-agent systems," *Journal of Control Theory and Applications*, vol. 2, no. 4, pp. 313–318, 2004.

[6] R. Olfati-Saber, "Flocking for multi-agent dynamic systems: algorithms and theory," *IEEE Transactions on Automatic Control*, vol. 51, no. 3, pp. 401–420, 2006.

[7] H. Su, X. Wang, and G. Chen, "Rendezvous of multiple mobile agents with preserved network connectivity," *Systems and Control Letters*, vol. 59, no. 5, pp. 313–322, 2010.

[8] P. Massioni and M. Verhaegen, "Distributed control for identical dynamically coupled systems: a decomposition approach," *IEEE Transactions on Automatic Control*, vol. 54, no. 1, pp. 124–135, 2009.

[9] M. E. Yalçin, J. A. K. Suykens, and J. Vandewalle, "Master-slave synchronization of Lur'e systems with time-delay," *International Journal of Bifurcation and Chaos in Applied Sciences and Engineering*, vol. 11, no. 6, pp. 1707–1722, 2001.

[10] H. Xin, Z. Lu, Z. Qu, D. Gan, and D. Qi, "Cooperative control strategy for multiple photovoltaic generators in distribution networks," *IET Control Theory and Applications*, vol. 5, no. 14, pp. 1617–1629, 2011.

[11] A. Bidram, A. Davoudi, F. L. Lewis, and Z. Qu, "Secondary control of microgrids based on distributed cooperative control of multi-agent systems," *IET Generation, Transmission and Distribution*, vol. 7, no. 8, pp. 822–831, 2013.

[12] Y. Hong, J. Hu, and L. Gao, "Tracking control for multi-agent consensus with an active leader and variable topology," *Automatica*, vol. 42, no. 7, pp. 1177–1182, 2006.

[13] D. V. Dimarogonas, M. Egerstedt, and K. J. Kyriakopoulos, "A leader-based containment control strategy for multiple unicycles," in *Proceedings of the 45th IEEE Conference on Decision and Control (CDC '06)*, pp. 5968–5973, San Diego, Calif, USA, December 2006.

[14] H. Gang and Q. Zhilin, "Controlling spatiotemporal chaos in coupled map lattice systems," *Physical Review Letters*, vol. 72, no. 1, pp. 68–71, 1994.

[15] R. O. Grigoriev, M. C. Cross, and H. G. Schuster, "Pinning control of spatiotemporal chaos," *Physical Review Letters*, vol. 79, no. 15, pp. 2795–2798, 1997.

[16] D. J. Watts and S. H. Strogatz, "Collective dynamics of 'small-world' networks," *Nature*, vol. 393, no. 6684, pp. 440–442, 1998.

[17] A. Barabási and R. Albert, "Emergence of scaling in random networks," *Science*, vol. 286, no. 5439, pp. 509–512, 1999.

[18] Z. Li, X. Liu, M. Fu, and L. Xie, "Global H_∞ consensus of multi-agent systems with Lipschitz non-linear dynamics," *IET Control Theory and Applications*, vol. 6, no. 13, pp. 2041–2048, 2012.

[19] G. Wen, Z. Duan, G. Chen, and W. Yu, "Consensus tracking of multi-agent systems with Lipschitz-type node dynamics and switching topologies," *IEEE Transactions on Circuits and Systems. I. Regular Papers*, vol. 61, no. 2, pp. 499–511, 2014.

[20] X. F. Wang and G. Chen, "Pinning control of scale-free dynamical networks," *Physica A*, vol. 310, no. 3, pp. 521–531, 2002.

[21] X. Li, X. Wang, and G. Chen, "Pinning a complex dynamical network to its equilibrium," *IEEE Transactions on Circuits and Systems. I: Regular Papers*, vol. 51, no. 10, pp. 2074–2087, 2004.

[22] T. Chen, X. Liu, and W. Lu, "Pinning complex networks by a single controller," *IEEE Transactions on Circuits and Systems. I. Regular Papers*, vol. 54, no. 6, pp. 1317–1326, 2007.

[23] M. Porfiri and M. di Bernardo, "Criteria for global pinning-controllability of complex networks," *Automatica*, vol. 44, no. 12, pp. 3100–3106, 2008.

[24] Y. Han, W. Lu, Z. Li, and T. Chen, "Pinning dynamic systems of networks with markovian switching couplings and controller-node set," *Systems & Control Letters*, vol. 65, pp. 56–63, 2014.

[25] L. Y. Xiang, Z. X. Liu, Z. Q. Chen, F. Chen, and Z. Z. Yuan, "Pinning control of complex dynamical networks with general topology," *Physica A*, vol. 379, no. 1, pp. 298–306, 2007.

[26] J. Zhou, J. Lu, and J. Lü, "Pinning adaptive synchronization of a general complex dynamical network," *Automatica*, vol. 44, no. 4, pp. 996–1003, 2008.

[27] W. Yu, G. Chen, and J. Lü, "On pinning synchronization of complex dynamical networks," *Automatica*, vol. 45, no. 2, pp. 429–435, 2009.

[28] Q. Song and J. Cao, "On pinning synchronization of directed and undirected complex dynamical networks," *IEEE Transactions on Circuits and Systems. I: Regular Papers*, vol. 57, no. 3, pp. 672–680, 2010.

[29] W. Yu, G. Chen, J. Lü, and J. Kurths, "Synchronization via pinning control on general complex networks," *SIAM Journal on Control and Optimization*, vol. 51, no. 2, pp. 1395–1416, 2013.

[30] J. Hu, J. Liang, and J. Cao, "Synchronization of hybrid-coupled heterogeneous networks: pinning control and impulsive control schemes," *Journal of the Franklin Institute*, vol. 351, no. 5, pp. 2600–2622, 2014.

[31] Y.-Y. Liu, J.-J. Slotine, and A.-L. Barabási, "Controllability of complex networks," *Nature*, vol. 473, no. 7346, pp. 167–173, 2011.

[32] Y. Y. Liu, J. J. Slotine, and A. Barabási, "Observability of complex systems," *Proceedings of the National Academy of Sciences of the United States of America*, vol. 110, no. 7, pp. 2460–2465, 2013.

[33] W. Yu, J. Lü, X. Yu, and G. Chen, "A step forward to pinning control of complex networks: finding an optimal vertex to control," in *Proceedings of the 9th Asian Control Conference (ASCC '13)*, pp. 1–6, IEEE, Istanbul, Turkey, June 2013.

[34] G. Shi, K. C. Sou, H. Sandberg, and K. H. Johansson, "A graph-theoretic approach on optimizing informed-node selection in multi-agent tracking control," *Physica D: Nonlinear Phenomena*, vol. 267, pp. 104–111, 2014.

[35] A. Clark, L. Bushnell, and R. Poovendran, "A supermodular optimization framework for leader selection under link noise in linear multi-agent systems," *IEEE Transactions on Automatic Control*, vol. 59, no. 2, pp. 283–296, 2014.

[36] F. Chen, Z. Chen, L. Xiang, Z. Liu, and Z. Yuan, "Reaching a consensus via pinning control," *Automatica*, vol. 45, no. 5, pp. 1215–1220, 2009.

[37] Q. Song, J. Cao, and W. Yu, "Second-order leader-following consensus of nonlinear multi-agent systems via pinning control," *Systems and Control Letters*, vol. 59, no. 9, pp. 553–562, 2010.

[38] H. Zhang, M. Z. Q. Chen, and G. Stan, "Fast consensus via predictive pinning control," *IEEE Transactions on Circuits and Systems. I. Regular Papers*, vol. 58, no. 9, pp. 2247–2258, 2011.

[39] G. Chen, F. L. Lewis, and L. Xie, "Finite-time distributed consensus via binary control protocols," *Automatica*, vol. 47, no. 9, pp. 1962–1968, 2011.

[40] W. Xiong, D. W. C. Ho, and Z. Wang, "Consensus analysis of multiagent networks via aggregated and pinning approaches," *IEEE Transactions on Neural Networks*, vol. 22, no. 8, pp. 1231–1240, 2011.

[41] J. Hu and Y. Hong, "Leader-following coordination of multi-agent systems with coupling time delays," *Physica A*, vol. 374, no. 2, pp. 853–863, 2007.

[42] Y. Hong, G. Chen, and L. Bushnell, "Distributed observers design for leader-following control of multi-agent networks," *Automatica*, vol. 44, no. 3, pp. 846–850, 2008.

[43] W. Ni and D. Cheng, "Leader-following consensus of multi-agent systems under fixed and switching topologies," *Systems and Control Letters*, vol. 59, no. 3-4, pp. 209–217, 2010.

[44] K. Peng and Y. Yang, "Leader-following consensus problem with a varying-velocity leader and time-varying delays," *Physica A*, vol. 388, no. 2-3, pp. 193–208, 2009.

[45] W. Zhu and D. Cheng, "Leader-following consensus of second-order agents with multiple time-varying delays," *Automatica*, vol. 46, no. 12, pp. 1994–1999, 2010.

[46] J. Hu and G. Feng, "Distributed tracking control of leader-follower multi-agent systems under noisy measurement," *Automatica*, vol. 46, no. 8, pp. 1382–1387, 2010.

[47] D. Meng, Y. Jia, J. Du, and F. Yu, "Tracking control over a finite interval for multi-agent systems with a time-varying reference trajectory," *Systems and Control Letters*, vol. 61, no. 7, pp. 807–818, 2012.

[48] Z. Li, X. Liu, W. Ren, and L. Xie, "Distributed tracking control for linear multiagent systems with a leader of bounded unknown input," *IEEE Transactions on Automatic Control*, vol. 58, no. 2, pp. 518–523, 2013.

[49] W. Xu, J. Cao, W. Yu, and J. Lu, "Leader-following consensus of non-linear multi-agent systems with jointly connected topology," *IET Control Theory & Applications*, vol. 8, no. 6, pp. 432–440, 2014.

[50] Y. Zhao, Z. Duan, G. Wen, and Y. Zhang, "Distributed finite-time tracking control for multi-agent systems: an observer-based approach," *Systems and Control Letters*, vol. 62, no. 1, pp. 22–28, 2013.

[51] G. Wen, G. Hu, W. Yu, J. Cao, and G. Chen, "Consensus tracking for higher-order multi-agent systems with switching directed topologies and occasionally missing control inputs," *Systems & Control Letters*, vol. 62, no. 12, pp. 1151–1158, 2013.

[52] M. Diao, Z. Duan, and G. Wen, "Consensus tracking of linear multi-agent systems under networked observability conditions," *International Journal of Control*, vol. 87, no. 8, pp. 1478–1486, 2014.

[53] H. Su and X. Wang, *Pinning Control of Complex Networked Systems: Synchronization, Consensus and Flocking of Networked Systems Via Pinning*, Springer, 2013.

[54] X. Wang and H. Su, "Pinning control of complex networked systems: a decade after and beyond," *Annual Reviews in Control*, vol. 38, no. 1, pp. 103–111, 2014.

[55] G. Chen, "Pinning control and synchronization on complex dynamical networks," *International Journal of Control, Automation and Systems*, vol. 12, no. 2, pp. 221–230, 2014.

[56] G. Ferrari-Trecate, M. Egerstedt, A. Buffa, and M. Ji, "Laplacian sheep: a hybrid, stop-go policy for leader-based containment control," in *Hybrid Systems: Computation and Control*, vol. 3927 of *Lecture Notes in Computer Science*, pp. 212–226, Springer, Berlin, Germany, 2006.

[57] M. Ji, G. Ferrari-Trecate, M. Egerstedt, and A. Buffa, "Containment control in mobile networks," *IEEE Transactions on Automatic Control*, vol. 53, no. 8, pp. 1972–1975, 2008.

[58] L. Galbusera, G. Ferrari-Trecate, and R. Scattolini, "A hybrid model predictive control scheme for containment and distributed sensing in multi-agent systems," *Systems and Control Letters*, vol. 62, no. 5, pp. 413–419, 2013.

[59] Y. Cao, D. Stuart, W. Ren, and Z. Meng, "Distributed containment control for double-integrator dynamics: algorithms and experiments," in *Proceedings of the American Control Conference (ACC '10)*, pp. 3830–3835, IEEE, July 2010.

[60] J. Li, W. Ren, and S. Xu, "Distributed containment control with multiple dynamic leaders for double-integrator dynamics using only position measurements," *IEEE Transactions on Automatic Control*, vol. 57, no. 6, pp. 1553–1559, 2012.

[61] Y. Zheng and L. Wang, "Containment control of heterogeneous multi-agent systems," *International Journal of Control*, vol. 87, no. 1, pp. 1–8, 2014.

[62] K. Liu, G. Xie, and L. Wang, "Containment control for second-order multi-agent systems with time-varying delays," *Systems & Control Letters*, vol. 67, pp. 24–31, 2014.

[63] S. Liu, L. Xie, and H. Zhang, "Containment control of multi-agent systems by exploiting the control inputs of neighbors," *International Journal of Robust and Nonlinear Control*, 2013.

[64] Z. Li, W. Ren, X. Liu, and M. Fu, "Distributed containment control of multi-agent systems with general linear dynamics in the presence of multiple leaders," *International Journal of Robust and Nonlinear Control*, vol. 23, no. 5, pp. 534–547, 2013.

[65] H. Liu, G. Xie, and L. Wang, "Necessary and sufficient conditions for containment control of networked multi-agent systems," *Automatica*, vol. 48, no. 7, pp. 1415–1422, 2012.

[66] H. Liu, G. Xie, and L. Wang, "Containment of linear multi-agent systems under general interaction topologies," *Systems and Control Letters*, vol. 61, no. 4, pp. 528–534, 2012.

[67] Q. Ma, F. L. Lewis, and S. Xu, "Cooperative containment of discrete-time linear multi-agent systems," *International Journal of Robust and Nonlinear Control*, 2013.

[68] Q. Ma and G. Miao, "Distributed containment control of linear multi-agent systems," *Neurocomputing*, vol. 133, no. 10, pp. 399–403, 2014.

[69] G. Wen, Z. Duan, Y. Zhao, W. Yu, and J. Cao, "Robust containment tracking of uncertain linear multi-agent systems: a nonsmooth control approach," *International Journal of Control*, 2014.

[70] P. Wang and Y. Jia, "Robust H_∞ containment control for uncertain multi-agent systems with inherent nonlinear dynamics," *International Journal of Systems Science*, 2014.

[71] P. Wang and Y. Jia, "Distributed containment control of second-order multi-agent systems with inherent non-linear dynamics," *IET Control Theory & Applications*, vol. 8, no. 4, pp. 277–287, 2014.

[72] Z. Meng, W. Ren, and Z. You, "Distributed finite-time containment control for multiple Lagrangian systems," in *Proceedings of the American Control Conference (ACC '10)*, pp. 2885–2890, July 2010.

[73] Z. Meng, W. Ren, and Z. You, "Distributed finite-time attitude containment control for multiple rigid bodies," *Automatica*, vol. 46, no. 12, pp. 2092–2099, 2010.

[74] J. Mei, W. Ren, and G. Ma, "Distributed coordinated tracking with a dynamic leader for multiple Euler-Lagrange systems," *IEEE Transactions on Automatic Control*, vol. 56, no. 6, pp. 1415–1421, 2011.

[75] J. Mei, W. Ren, and G. Ma, "Distributed containment control for lagrangian networks with parametric uncertainties under a directed graph," *Automatica*, vol. 48, no. 4, pp. 653–659, 2012.

[76] Y. Zhang, Y. Yang, Y. Zhao, and G. Wen, "Distributed finite-time tracking control for nonlinear multi-agent systems subject to external disturbances," *International Journal of Control*, vol. 86, no. 1, pp. 29–40, 2013.

[77] S. J. Yoo, "Distributed adaptive containment control of uncertain nonlinear multi-agent systems in strict-feedback form," *Automatica*, vol. 49, no. 7, pp. 2145–2153, 2013.

[78] G. Notarstefano, M. Egerstedt, and M. Haque, "Containment in leader-follower networks with switching communication topologies," *Automatica*, vol. 47, no. 5, pp. 1035–1040, 2011.

[79] S. Liu, L. Xie, and H. Zhang, "Mean square containment control of multi-agent systems with transmission noises," *Acta Automatica Sinica*, vol. 39, no. 11, pp. 1787–1795, 2013.

[80] Y. Lou and Y. Hong, "Target containment control of multi-agent systems with random switching interconnection topologies," *Automatica*, vol. 48, no. 5, pp. 879–885, 2012.

[81] F. Xiao, L. Wang, J. Chen, and Y. Gao, "Finite-time formation control for multi-agent systems," *Automatica*, vol. 45, no. 11, pp. 2605–2611, 2009.

[82] H. Liu, L. Cheng, M. Tan, Z. Hou, Z. Cao, and M. Wang, "Containment control with multiple interacting leaders under switching topologies," in *Proceedings of the 32nd Chinese Control Conference (CCC '13)*, pp. 7093–7098, IEEE, 2013.

[83] D. Chen, L. Lü, M. Shang, Y. Zhang, and T. Zhou, "Identifying influential nodes in complex networks," *Physica A: Statistical Mechanics and its Applications*, vol. 391, no. 4, pp. 1777–1787, 2012.

[84] L. C. Freeman, "A set of measures of centrality based on betweenness," *Sociometry*, vol. 40, no. 1, pp. 35–41, 1977.

[85] M. Barthélemy, "Betweenness centrality in large complex networks," *European Physical Journal B*, vol. 38, no. 2, pp. 163–168, 2004.

[86] G. Sabidussi, "The centrality index of a graph," *Psychometrika*, vol. 31, pp. 581–603, 1966.

[87] P. Bonacich, "Some unique properties of eigenvector centrality," *Social Networks*, vol. 29, no. 4, pp. 555–564, 2007.

[88] E. Estrada and J. A. Rodríguez-Velázquez, "Subgraph centrality in complex networks," *Physical Review E: Statistical, Nonlinear, and Soft Matter Physics*, vol. 71, no. 5, Article ID 056103, 9 pages, 2005.

[89] S. Brin, "The anatomy of a large-scale hypertextual Web search engine 1," *Computer Networks*, vol. 30, no. 1–7, pp. 107–117, 1998.

[90] L. Lü, Y.-C. Zhang, C. H. Yeung, and T. Zhou, "Leaders in social networks, the delicious case," *PLoS ONE*, vol. 6, no. 6, Article ID e21202, 2011.

[91] M. Porfiri and F. Fiorilli, "Node-to-node pinning control of complex networks," *Chaos*, vol. 19, no. 1, Article ID 013122, 2009.

[92] Y. Tang, H. Gao, J. Kurths, and J. Fang, "Evolutionary pinning control and its application in UAV coordination," *IEEE Transactions on Industrial Informatics*, vol. 8, no. 4, pp. 828–838, 2012.

[93] C. W. Wu, "Localization of effective pinning control in complex networks of dynamical systems," in *Proceedings of the IEEE International Symposium on Circuits and Systems (ISCAS '08)*, pp. 2530–2533, Seattle, Wash, USA, May 2008.

[94] Y. Y. Lu and X. F. Wang, "Pinning control of directed dynamical networks based on ControlRank," *International Journal of Computer Mathematics*, vol. 85, no. 8, pp. 1279–1286, 2008.

[95] T. Opsahl, F. Agneessens, and J. Skvoretz, "Node centrality in weighted networks: Generalizing degree and shortest paths," *Social Networks*, vol. 32, no. 3, pp. 245–251, 2010.

[96] Q. Song, J. Cao, and F. Liu, "Pinning-controlled synchronization of hybrid-coupled complex dynamical networks with mixed time-delays," *International Journal of Robust and Nonlinear Control*, vol. 22, no. 6, pp. 690–706, 2012.

[97] J. Kim, J. Jeon, S. Kim et al., "Cooperative control strategy of energy storage system and microsources for stabilizing the microgrid during islanded operation," *IEEE Transactions on Power Electronics*, vol. 25, no. 12, pp. 3037–3048, 2010.

[98] Z. Zhang and M. Chow, "Convergence analysis of the incremental cost consensus algorithm under different communication network topologies in a smart grid," *IEEE Transactions on Power Systems*, vol. 27, no. 4, pp. 1761–1768, 2012.

[99] H. Xin, Z. Lu, Y. Liu, and D. Gan, "A center-free control strategy for the coordination of multiple photovoltaic generators," *IEEE Transactions on Smart Grid*, vol. 5, no. 3, pp. 1262–1269, 2014.

[100] H. Xin, Y. Liu, Z. Wang, D. Gan, and T. Yang, "A new frequency regulation strategy for photovoltaic systems without energy storage," *IEEE Transactions on Sustainable Energy*, vol. 4, no. 4, pp. 985–993, 2013.

[101] H. Xin, D. Gan, N. Li, H. Li, and C. Dai, "Virtual power plant-based distributed control strategy for multiple distributed generators," *IET Control Theory and Applications*, vol. 7, no. 1, pp. 90–98, 2013.

[102] A. Bidram, A. Davoudi, F. L. Lewis, and J. M. Guerrero, "Distributed cooperative secondary control of microgrids using feedback linearization," *IEEE Transactions on Power Systems*, vol. 28, no. 3, pp. 3462–3470, 2013.

[103] G. Mokhtari, G. Nourbakhsh, and A. Ghosh, "Smart coordination of energy storage units (ESUs) for voltage and loading management in distribution network," *IEEE Transactions on Power Systems*, vol. 28, no. 4, pp. 4812–4820, 2013.

[104] J. Giraldo, E. Mojica-Nava, and N. Quijano, "Synchronization of isolated microgrids with a communication infrastructure using energy storage systems," *International Journal of Electrical Power & Energy Systems*, vol. 63, pp. 71–82, 2014.

[105] F. Daneshfar and H. Bevrani, "Load-frequency control: a GA-based multi-agent reinforcement learning," *IET Generation, Transmission and Distribution*, vol. 4, no. 1, pp. 13–26, 2010.

[106] Y. Xu, W. Liu, and J. Gong, "Stable multi-agent-based load shedding algorithm for power systems," *IEEE Transactions on Power Systems*, vol. 26, no. 4, pp. 2006–2014, 2011.

[107] C. Zhao, U. Topcu, and S. H. Low, "Optimal load control via frequency measurement and neighborhood area communication," *IEEE Transactions on Power Systems*, vol. 28, no. 4, pp. 3576–3587, 2013.

[108] C. Zhao, U. Topcu, N. Li, and S. Low, "Design and stability of load-side primary frequency control in power systems," *IEEE Transactions on Automatic Control*, vol. 59, no. 5, pp. 1177–1189, 2014.

[109] E. F. Bompard and B. Han, "Market-based control in emerging distribution system operation," *IEEE Transactions on Power Delivery*, vol. 28, no. 4, pp. 2373–2382, 2013.

[110] Q. Shafiee, J. M. Guerrero, and J. C. Vasquez, "Distributed secondary control for islanded microgrids-a novel approach," *IEEE Transactions on Power Electronics*, vol. 29, no. 2, pp. 1018–1031, 2014.

[111] F. Dörfler and F. Bullo, "Breaking the hierarchy: distributed control & economic optimality in microgrids," *IEEE Transactions on Control of Network Systems*, 2014.

[112] S. Kar and G. Hug, "Distributed robust economic dispatch in power systems: a consensus innovations approach," in *Proceedings of the IEEE Power and Energy Society General Meeting (PES '12)*, pp. 1–8, IEEE, July 2012.

[113] R. Mudumbai, S. Dasgupta, and B. B. Cho, "Distributed control for optimal economic dispatch of a network of heterogeneous power generators," *IEEE Transactions on Power Systems*, vol. 27, no. 4, pp. 1750–1760, 2012.

[114] S. Yang, S. Tan, and J.-X. Xu, "Consensus based approach for economic dispatch problem in a smart grid," *IEEE Transactions on Power Systems*, vol. 28, no. 4, pp. 4416–4426, 2013.

[115] H. Yang, D. Yi, J. Zhao, and Z. Dong, "Distributed optimal dispatch of virtual power plant via limited communication," *IEEE Transactions on Power Systems*, vol. 28, no. 3, pp. 3511–3512, 2013.

[116] G. Binetti, A. Davoudi, F. L. Lewis, D. Naso, and B. Turchiano, "Distributed consensus-based economic dispatch with transmission losses," *IEEE Transactions on Power Systems*, vol. 29, no. 4, pp. 1711–1720, 2014.

[117] P. Bhatt, R. Roy, and S. P. Ghoshal, "Optimized multi area AGC simulation in restructured power systems," *International Journal of Electrical Power and Energy Systems*, vol. 32, no. 4, pp. 311–322, 2010.

[118] K. Naidua, H. Mokhlisa, A. H. A. Bakarb, V. Terzijac, and H. A. Illiasa, "Application of firefly algorithm with online wavelet filter in automatic generation control of an interconnected reheat thermal power system," *International Journal of Electrical Power & Energy Systems*, vol. 63, no. 4, pp. 401–413, 2014.

[119] H. Bevrani, *Robust Power System Frequency Control*, Springer, 2008.

[120] M. D. Ilic' and Q. Liu, "Toward sensing, communications and control architectures for frequency regulation in systems with highly variable resources," in *Control and Optimization Methods for Electric Smart Grids*, pp. 3–33, Springer, 2012.

Hindawi Publishing Corporation
The Scientific World Journal
Volume 2014, Article ID 130643, 10 pages
http://dx.doi.org/10.1155/2014/130643

Research Article

Consensus Tracking for Multiagent Systems with Nonlinear Dynamics

Runsha Dong

The State Key Laboratory for Turbulence and Complex System, Department of Mechanics and Engineering Science, College of Engineering, Peking University, Beijing 100871, China

Correspondence should be addressed to Runsha Dong; dongrunsha@pku.edu.cn

Received 4 June 2014; Accepted 5 July 2014; Published 14 August 2014

Academic Editor: Wenwu Yu

Copyright © 2014 Runsha Dong. This is an open access article distributed under the Creative Commons Attribution License, which permits unrestricted use, distribution, and reproduction in any medium, provided the original work is properly cited.

This paper concerns the problem of consensus tracking for multiagent systems with a dynamical leader. In particular, it proposes the corresponding explicit control laws for multiple first-order nonlinear systems, second-order nonlinear systems, and quite general nonlinear systems based on the leader-follower and the tree shaped network topologies. Several numerical simulations are given to verify the theoretical results.

1. Introduction

There have been a lot of recent researches paying attention to the problem of multiagent cooperative control which means a group of agents working cooperatively to achieve coverage, formation, and consensus [1–5]. The consensus problem, known as agreement on certain quantities of interest for groups of agents, is one of the major research directions. Consensus tracking means consensus with a dynamical leader [6, 7]. It is considered as a manner of cooperative behaviors and has also drawn far more attention.

In the pioneering work on consensus tracking of Ren [8], consensus with a constant reference state and with a time-varying reference state is analyzed for the first-order integrator systems. However, even in the second case, the dynamics of the time-varying reference state is assumed to have no explicit external input. Later, many variants of the consensus tracking algorithms are developed for various system models. In [9], a control algorithm is proposed for the problems of consensus tracking while those homogenous follower agents are with dynamics of first-order linear integrator and the leader is governed by the different dynamics. In [10], a consensus tracking algorithm is proposed and analyzed for the second-order integrator dynamics which is also a linear system model. And in [6], the author designs several consensus tracking algorithms for the agents with first-order (and second-order) integrator dynamics. We note that both the follower agents and the leader are with linear dynamics, and the leader has an upper bounded external input.

Li et al. [11] propose an observer-based algorithm for the problem of consensus tracking for multiagent systems with general linear dynamics. In the recent literature [12], the problem of multiple first-order nonlinear systems tracking several leaders is studied under the assumption that these leaders have no explicit external input. In [13], the consensus tracking problem is studied for the case that the dynamics of both the leader and the followers are of the second-order nonlinearity, under the assumption that the leader has no external input.

Nonlinear dynamics are now studied in the consensus problem from various perspectives such as [14–17]. In [16, 17], the effective consensus tracking laws are developed for multiagent systems modeled as higher-order dynamics with nonlinear terms under switching directed topologies. By contrast, this paper discusses the consensus tracking problem for multiagent systems with general nonlinear systems and the very special cases (the first-order and the second-order nonlinear systems) under tree topologies. The network of groups of nonlinear systems is a kind of coupled nonlinear systems with linear coupling (linearly coupled ordinary differential equations) [18] which is widely used in nature and engineering to describe the models of spike-burst neural activity, the transitions of n-patch metapopulation, the dynamics of linearly coupled Chua circuits [13, 18],

the coupled oscillator systems [19], epidemiology, ecology [20], and so on.

In those papers mentioned above, some focus on the problem that the linear follower agents track a leader who is governed by an external input, yet others focus on the problem that the nonlinear follower agents track a leader who has no explicit external input. In the practical network with a linear or a nonlinear leader, the external input is unavoidable or even is important for guiding the group to behave correctly. Thus, the study of consensus tracking for a group of nonlinear agents with the leader having an external input will be significative. In this paper, we consider the problem of consensus tracking for the network of a group of $N + 1$ identical nonlinear agents, in which one agent indexed by r and governed by its external input is assigned to be the leader, and the other agents indexed by $1, \ldots, N$ are regarded as the followers. The nonlinear dynamics of agents in this paper are described by the first-order (resp., the second-order and the general) nonlinear equations like (1) in [12] (resp., (3) in [21] and (1) in [22]) which will be introduced later.

We have noted that the intrinsic dynamics of the leader in [12] which is specified by $\dot{x}_r = f(t, x_r)$ have no explicit external input, where x_r is the state of the leader, f is the nonlinear vector field, and t is the time. However, it can be interpreted as the fact that each follower has known the detailed measurements of the leader's external input $u(t)$ all the time and the consensus algorithm for the follower could cancel out the impact of the leader's external input. Though the equation $f(t, x_r)$ is theoretically capable of including the situation of $f(t, x_r) + u(t)$, the given Lipschitz condition for the f in [12] will limit the choice of the control input $u(t)$ or sometimes there will even be no choice. However, in this paper, we relax this condition and assume that each follower only knows the upper bound of the leader's input in advance and there are no other limitations. There is a similar situation in [21].

Due to the existence of nonlinearity in the agents' dynamics and the external input of the leader, the existing consensus algorithms are not applicable to our problem. By synthetically using the Lipschitz conditions, the variable structure technique [6], the feedback linearization technique [22], and the Lyapunov theory, all three control algorithms for consensus tracking under the undirect or the tree shaped communication topology are effectively designed.

The remainder of the paper is organized as follows. In Section 2, some notations and basic concepts in graph theory that will be used in this paper are introduced. Section 3 is the main text that establishes the consensus tracking algorithms for nonlinear systems. Section 4 shows several simulation results. Finaly, Section 5 draws conclusions to this paper.

2. Background and Preliminaries

We use $\|\cdot\|$ to denote the Euclidean norm and $\|\cdot\|_1$ 1-norm. Let $\mathbf{1}^n$, $\mathbf{0}^n$ denote $n \times 1$ column vectors with all components being ones and zeros, respectively. I_n is used to denote the $n \times n$ identity matrix. And $\otimes$ stands for the kronecker product. A function f is said to be of class C^k if the derivatives $f', f'', \ldots, f^{(k)}$ exist and are continuous. The superscript T means the transpose of a matrix. For a matrix M, $M > 0$ denotes that M is positive definite.

Since graph theory plays an important role in modeling the communication topology of the network of the multiagent systems, some basic concepts in graph theory that will be used in this paper are introduced in the following.

In the problem of nonlinear consensus tracking, a kind of communication topology of N follower agents is modeled as an undirected graph $\mathcal{G} = \{\mathcal{V}, \mathcal{E}, A\}$, where $\mathcal{V} = \{1, 2, \ldots, i, \ldots, N\}$ is a set of N integers, with the number i which means the ith vertex representing the ith agent, and $\mathcal{E} \subset \mathcal{V} \times \mathcal{V}$ is an edge set in which each edge is denoted by a pair of vertices (i, j). In an undirected graph, $(i, j) \in \mathcal{E}$ is equivalent to $(j, i) \in \mathcal{E}$. The set of neighbors of agent i is denoted by $\mathcal{N}_i = \{j \in \mathcal{V} : (i, j) \in \mathcal{E}\}$. $A = [a_{ij}] \in \mathbb{R}^{N \times N}$ is a weighted adjacency matrix of $\mathcal{G}$, where $a_{ii} = 0$ and $a_{ij} = 1$ if $(i, j) \in \mathcal{V}$ or 0 otherwise. The Laplacian of $\mathcal{G}$ is defined as $L = D - A$, where $D = \mathrm{diag}(\deg_1, \ldots, \deg_N)$ and $\deg_i = \sum_{j=1}^{N} a_{ij}$ [23]. A path in an undirected graph $\mathcal{G}$ is a sequence of edges in the form of $(i_1, i_2), (i_2, i_3), \ldots$, where $i_k \in \mathcal{V}$. An undirected graph is connected if there exists a path between every two vertices.

For a directed graph, $(i, j) \in \mathcal{E}$ does not necessarily mean $(j, i) \in \mathcal{E}$. A directed path is a sequence of directed edges in the form of $(i_1, i_2), (i_2, i_3), \ldots$, where $i_k \in \mathcal{V}$. The tree shaped communication topology is modeled as the tree shaped graph (a directed graph) in which each vertex has only one parent vertex except for one vertex called the root. To study the problem of nonlinear consensus tracking, a leader adjacency matrix H is defined as $H = \mathrm{diag}(h_1, h_2, \ldots, h_i, \ldots, h_N)$, where $h_i = 1$ if the leader's information is available to the ith follower agent and $h_i = 0$ otherwise. The undirect graph $\mathcal{G}$ with one additional vertex representing a leader is used to model the leader-follower communication topologies in this paper.

3. Nonlinear Consensus Tracking

3.1. Consensus Tracking for the First-Order Nonlinear Dynamics. We start by considering the first-order nonlinearity case: N followers labeled as $1, 2, \ldots, N$ are described by the following first-order nonlinear ordinary differential equation:

$$\dot{x}_i = f(t, x_i) + u_i, \quad i = 1, \ldots, N, \tag{1}$$

where $x_i \in \mathbb{R}^n$ is the state vector representing the position of agent i, $f : \mathbb{R}^n \times \mathbb{R} \to \mathbb{R}^n$ is a uniformly continuously differentiable vector-valued function, and $u_i \in \mathbb{R}^n$ is the control input. The communication topology of these N followers is modeled as an undirected graph $\mathcal{G} = \{\mathcal{V}, \mathcal{E}, A\}$. The corresponding Laplacian matrix and adjacency matrix are denoted by L and A. We aim to design a control algorithm $u_i, i = 1, \ldots, N$, such that

$$\lim_{t \to \infty} \|x_i(t) - x_r(t)\| = 0, \tag{2}$$

where $x_r \in \mathbb{R}^n$ is the state vector representing the position of the leader which is specified by

$$\dot{x}_r = f(t, x_r) + u_r. \tag{3}$$

Note that u_r is the external input of the leader and $u_r \neq \mathbf{0}^n$. If the limit (2) is finally achieved, then we say that the first-order nonlinear followers (1) with the control algorithm asymptotically track the leader (3).

As in most existing works on networks of nonlinear agents [12, 13, 21, 24], we give an assumption of Lipschitz-like condition as follows.

Assumption 1. There exists $\rho > 0$ such that the vector field $f : \mathbb{R}^n \times \mathbb{R} \to \mathbb{R}^n$ satisfies $\|f(t,p) - f(t,q)\| \leq \rho\|p - q\|$, for all $p, q \in \mathbb{R}^n$.

In order to guarantee these N followers could track the leader, the necessary connectivity is required from the point of view of graph theory. For this, we further make the following assumption.

Assumption 2. The undirected graph $\mathcal{G}$ which models the network topology of N followers is connected and at least one follower is informed about the state of the leader.

To deal with the problem of consensus tracking for the network with the first-order nonlinear agents, we propose a control algorithm for (1) as

$$u_i = -\alpha_i(t)\left[\sum_{j\in\mathcal{N}_i}\left(x_i - x_j\right) + h_i\left(x_i - x_r\right)\right] - \omega\,\mathrm{sgn}\left[\sum_{j\in\mathcal{N}_i}\left(x_i - x_j\right) + h_i\left(x_i - x_r\right)\right], \tag{4}$$

where $\alpha_i(t)$ is the adaptive gain [13] for agent i and it is specified by

$$\dot{\alpha}_i(t) = \beta_i\left[\sum_{j\in\mathcal{N}_i}\left(x_i - x_j\right) + h_i\left(x_i - x_r\right)\right]^T \times \left[\sum_{j\in\mathcal{N}_i}\left(x_i - x_j\right) + h_i\left(x_i - x_r\right)\right], \tag{5}$$

where $\mathrm{sgn}(\cdot)$ is the signum function, $\omega > \|u_r\|$, β_i is any positive constant, and h_i is used for describing whether agent i is informed about the state of the leader, as we introduced in Section 2, and we denote that $H = \mathrm{diag}(h_1, h_2, \ldots, h_i, \ldots, h_N)$. The column stack vectors of x_i $(i \in \mathcal{V})$ and $f(t, x_i)$ $(i \in \mathcal{V})$ are denoted by x and $F(t,x)$, respectively. By applying the control algorithms (4) and (5) into the input of the system (1), the closed-loop system is then rewritten as follows:

$$\dot{x} = -\left(\alpha(t)\otimes I_n\right)\left[\left(L\otimes I_n\right)x + \left(H\otimes I_n\right)\left(x - \left(\mathbf{1}^N\otimes I_n\right)x_r\right)\right] - \omega\,\mathrm{sgn}\left[\left(L\otimes I_n\right)x + \left(H\otimes I_n\right)\left(x - \left(\mathbf{1}^N\otimes I_n\right)x_r\right)\right] + F(t,x), \tag{6}$$

where $\alpha(t) \triangleq \mathrm{diag}(\alpha_1(t), \alpha_2(t), \ldots, \alpha_N(t))$.

Then, the main result on the problem of consensus tracking for the network with first-order nonlinear agents is proposed by the following theorem.

Theorem 3. *If Assumptions 1 and 2 are satisfied, then the first-order nonlinear followers* (1) *with the control algorithms* (4) *and* (5) *asymptotically track the leader* (3).

Proof. Let $\tilde{x}_i = x_i - x_r$ and $\tilde{x} \triangleq [\tilde{x}_1, \tilde{x}_2, \ldots, \tilde{x}_N]^T$. Then, we have

$$\dot{\tilde{x}} = F(t,x) - 1_N\otimes f\left(t, x_r\right) - \left(\alpha(t)\otimes I_n\right)\left[\left(L+H\right)\otimes I_n\right]\tilde{x} - \omega\,\mathrm{sgn}\left(\left[\left(L+H\right)\otimes I_n\right]\tilde{x}\right) - \left(\mathbf{1}^N\otimes I_n\right)u_r. \tag{7}$$

From Assumption 2 and Lemma 1 in [13], the matrix $M \triangleq L + H$ is positive definite. Consider a Lyapunov function candidate

$$V = \frac{1}{2}\tilde{x}^T\left(M\otimes I_n\right)\tilde{x} + \sum_{i=1}^{N}\frac{1}{2\beta_i}\left(\alpha_i(t) - \alpha_0\right)^2, \tag{8}$$

where α_0 is chosen such that

$$\alpha_0 \geq \frac{\rho\lambda_{\max}(M)}{\lambda_{\min}(M)^2}. \tag{9}$$

The derivative of V along the system (7) satisfies

$$\begin{aligned}\dot{V}(t) &= \tilde{x}^T\left(M\otimes I_n\right)\dot{\tilde{x}} + \frac{1}{\beta_i}\sum_{i=1}^{n}\left(\alpha_i(t) - \alpha_0\right)\dot{\alpha}_i(t)\\ &= \tilde{x}^T\left(M\otimes I_n\right)\left[F(t,x) - 1_N\otimes f\left(t,x_r\right)\right]\\ &\quad - \left[\left(M\otimes I_n\right)\tilde{x}\right]^T\left(\alpha(t)\otimes I_n\right)\left(M\otimes I_n\right)\tilde{x}\\ &\quad - \omega\left[\left(M\otimes I_n\right)\tilde{x}\right]^T\left[\mathrm{sgn}\left(\left(M\otimes I_n\right)\tilde{x}\right) + \left(1^N\otimes I_n\right)u_r\right]\\ &\quad + \left[\left(M\otimes I_n\right)\tilde{x}\right]^T\left(\alpha(t)\otimes I_n\right)\left[\left(M\otimes I_n\right)\tilde{x}\right]\\ &\quad - \alpha_0\left[\left(M\otimes I_n\right)\tilde{x}\right]^T\left[\left(M\otimes I_n\right)\tilde{x}\right]\\ &\leq \rho\lambda_{\max}(M)\|\tilde{x}\|^2 - \left(\omega - \|u_r\|\right)\left\|\left(M\otimes I_n\right)\tilde{x}\right\|_1\\ &\quad - \alpha_0\lambda_{\min}(M)^2\|\tilde{x}\|^2.\end{aligned} \tag{10}$$

From (9) and $\omega > \|u_r\|$, it is easy to obtain that $\dot{V} < 0$. Therefore, $\tilde{x} \to \mathbf{0}$ as $t \to \infty$. It follows that $\lim_{t\to\infty}\|x_i(t) - x_r(t)\| = 0$. That is, the first-order nonlinear followers (1) track the leader (3) asymptotically. □

3.2. Consensus Tracking for the Second-Order Nonlinear Dynamics. Next, we discuss the second-order nonlinearity case. Suppose that each of the N followers is described by

$$\begin{aligned}\dot{x}_i &= v_i,\\ \dot{v}_i &= f\left(t, x_i, v_i\right) + u_i,\end{aligned} \tag{11}$$

where, $i = 1, \ldots, N$, $x_i \in \mathbb{R}$ and $v_i \in \mathbb{R}$ are the state representing the position and the velocity of agent i, respectively. $f : \mathbb{R} \times \mathbb{R} \times \mathbb{R} \to \mathbb{R}$ is the intrinsic dynamics. $u_i \in \mathbb{R}$ is the control input. The problem is to design u_i for each of the N followers to track the leader which is specified by

$$\begin{aligned} \dot{x}_r &= v_r, \\ \dot{v}_r &= f\left(t, x_r, v_r\right) + u_r, \end{aligned} \tag{12}$$

such that, for each agent i,

$$\begin{aligned} \lim_{t \to \infty} \left\| x_i\left(t\right) - x_r\left(t\right) \right\| &= 0, \\ \lim_{t \to \infty} \left\| v_i\left(t\right) - v_r\left(t\right) \right\| &= 0, \end{aligned} \tag{13}$$

where $x_r \in \mathbb{R}$ and $v_r \in \mathbb{R}$ are, respectively, the position and velocity of the leader. If limits (13) are finally achieved, then we say that the second-order nonlinear followers (11) with the designed control algorithm asymptotically track the leader (12). Before studying this problem, we give some assumptions.

Assumption 4. There exist $\rho_1 > 0$ and $\rho_2 > 0$ such that the vector field $f : \mathbb{R} \times \mathbb{R} \times \mathbb{R} \to \mathbb{R}$ satisfies $\|f(t, x, y) - f(t, z, w)\| \le \rho_1 \|x - z\| + \rho_2 \|y - w\|$, for all $x, y, z, w \in \mathbb{R}$.

Remark 5. Compared with Assumption 1, it is easy to see that both of the assumptions are Lipschitz-like conditions.

Similar to the first-order case in Section 3.1, we give the same assumption on communication topology of the network as Assumption 2 to guarantee these N followers with dynamics of (11) could track the leader with dynamics of (12). And $M = L + H$ here also represents the communication topology of the network, where L and H are the same as in Section 3.1.

Then, we propose the following control algorithm applied for the system (11):

$$\begin{aligned} u_i = &-\sum_{j=1}^{N} a_{ij} \left[\left(x_i - x_j\right) + \alpha \left(v_i - v_j\right) \right] \\ &- h_i \left[\left(x_i - x_r\right) + \alpha \left(v_i - v_r\right) \right] \\ &- w \operatorname{sgn} \left\{ \sum_{j=1}^{N} a_{ij} \left[\gamma \left(x_i - x_j\right) + \left(v_i - v_j\right) \right] \right. \\ &\left. + h_i \left[\gamma \left(x_i - x_r\right) + \left(v_i - v_r\right) \right] \right\}, \end{aligned} \tag{14}$$

where $\alpha > 0$ is a constant gain, γ is a positive constant which is to be designed, and ω is a constant that satisfies $\omega > \|u_r\|$. Before going any further, we define two matrices P_γ and Q_γ associated with γ. For a matrix M (let λ_M be the maximal eigenvalue of the M) and the constants $\alpha > 0$, $\rho_1 > 0$ and $\rho_2 > 0$, P_γ, and Q_γ are defined by

$$\begin{aligned} P_\gamma &\triangleq \begin{bmatrix} \frac{1}{2}\left(M^2 - \gamma\lambda_M I - \lambda_M \rho_1 \rho_2 I - \alpha\gamma M^2\right) & \frac{\gamma}{2}M \\ \frac{\gamma}{2}M & \frac{1}{2}M \end{bmatrix}, \\ Q_\gamma &\triangleq \begin{bmatrix} \gamma M^2 - \frac{\lambda_M}{2}\gamma^2 I - \frac{\lambda_M}{2}{\rho_1}^2 I & 0_{N\times N} \\ 0_{N\times N} & \alpha M^2 - \gamma M - \frac{\lambda_M}{2} I - \frac{\lambda_M}{2}{\rho_2}^2 I \end{bmatrix}. \end{aligned} \tag{15}$$

Then, we have the following lemma.

Lemma 6. *Given the matrix M and the constants $\rho_1 > 0$, $\rho_2 > 0$, for any constant $\alpha > 0$, if γ satisfies*

$$\gamma \in \left\{ \gamma \mid \max\left(0, c_4\right) < \gamma < \min\left\{c_1, c_2, c_3, c_5, c_6\right\} \right\} \tag{16}$$

or

$$\gamma \in \left\{ \gamma \mid \max\left(0, c_4, c_5, c_6\right) < \gamma < \min\left\{c_1, c_2, c_3\right\} \right\}, \tag{17}$$

then $P_\gamma = P_\gamma^T > 0$ and $Q_\gamma = Q_\gamma^T > 0$, where

$$\begin{aligned} c_1 &\triangleq \frac{1 + \lambda_M - \rho_1\rho_2}{1 + \alpha\lambda_M}, \\ c_2 &\triangleq \sqrt{\frac{\left(1 + \alpha\lambda_M\right)^2}{4} + \lambda_M - \rho_1\rho_2} - \frac{\left(1 + \alpha\lambda_M\right)}{2}, \\ c_3 &\triangleq \sqrt{\lambda_M^2 + 2\left(\alpha - 1\right)\lambda_M - \left(\rho_1^2 + \rho_2^2\right)} + \left(\lambda_M - 1\right), \\ c_4 &\triangleq \lambda_M - \sqrt{\lambda_M^2 - \rho_1^2}, \\ c_5 &\triangleq \lambda_M + \sqrt{\lambda_M^2 - \rho_1^2}, \\ c_6 &\triangleq \alpha\lambda_M - \frac{1}{2}\left(1 + \rho_1^2\right). \end{aligned} \tag{18}$$

Proof. Since M is a positive definite matrix, it can be diagonalized as $M = \Gamma^{-1}\Lambda\Gamma$, where $\Lambda = \operatorname{diag}(\lambda_1, \lambda_2, \ldots, \lambda_N)$ and $\lambda_1 \ge \lambda_2 \ge \cdots \ge \lambda_N$. We define that

$$\widetilde{\Gamma} = \begin{bmatrix} \Gamma & 0_{N\times N} \\ 0_{N\times N} & \Gamma \end{bmatrix}. \tag{19}$$

It then follows that

$$P_\gamma = \widetilde{\Gamma}^{-1} \underbrace{\begin{bmatrix} \frac{1}{2}\left(\Lambda^2 - \gamma\lambda_M I - \lambda_M\rho_1\rho_2 I - \alpha\gamma\Lambda^2\right) & \frac{\gamma}{2}\Lambda \\ \frac{\gamma}{2}\Lambda & \frac{1}{2}\Lambda \end{bmatrix}}_{\widetilde{P}_\gamma} \widetilde{\Gamma}. \tag{20}$$

Let η be any eigenvalue of the matrix $\widetilde{P}_\gamma$. Since Λ is a diagonal matrix and $\widetilde{P}_\gamma$ is symmetric, it follows that η is real and satisfies

$$\left[\eta - \frac{1}{2}\left(\lambda_i^2 - \gamma\lambda_M - \lambda_M\rho_1\rho_2 - \alpha\gamma\lambda_i^2\right)\right]\left[\eta - \frac{1}{2}\lambda_i\right] - \frac{\gamma^2}{4}\lambda_i^2 = 0. \tag{21}$$

That is,

$$\eta^2 - \left[\frac{1}{2}\left(\lambda_i^2 - \gamma\lambda_M - \lambda_M\rho_1\rho_2 - \alpha\gamma\lambda_i^2\right) + \frac{1}{2}\lambda_i\right]\eta + \frac{1}{4}\lambda_i\left(\lambda_i^2 - \gamma\lambda_M - \lambda_M\rho_1\rho_2 - \alpha\gamma\lambda_i^2\right) - \frac{\gamma^2}{4}\lambda_i^2 = 0. \tag{22}$$

Note that $\eta > 0$ if and only if

$$\frac{1}{2}\left(\lambda_i^2 - \gamma\lambda_M - \lambda_M\rho_1\rho_2 - \alpha\gamma\lambda_i^2\right) + \frac{1}{2}\lambda_i > 0,$$
$$\frac{1}{4}\lambda_i\left(\lambda_i^2 - \gamma\lambda_M - \lambda_M\rho_1\rho_2 - \alpha\gamma\lambda_i^2\right) - \frac{\gamma^2}{4}\lambda_i^2 > 0, \tag{23}$$

which means

$$\gamma < \frac{1 + \lambda_M - \rho_1\rho_2}{1 + \alpha\lambda_M} \triangleq c_1,$$
$$\gamma < \sqrt{\frac{\left(1 + \alpha\lambda_M\right)^2}{4} + \lambda_M - \rho_1\rho_2} - \frac{\left(1 + \alpha\lambda_M\right)}{2} \triangleq c_2. \tag{24}$$

By a similar analysis, we have

$$Q_\gamma = \widetilde{\Gamma}^{-1}\underbrace{\begin{bmatrix}\gamma\Lambda^2 - \frac{\lambda_M}{2}\gamma^2 - \frac{\lambda_M}{2}\rho_1^2 & 0_{N\times N}\\ 0_{N\times N} & \alpha\Lambda^2 - \gamma\Lambda - \frac{\lambda_M}{2} - \frac{\lambda_M}{2}\rho_2^2\end{bmatrix}}_{\widetilde{Q}_\gamma}\widetilde{\Gamma}. \tag{25}$$

Let μ be any eigenvalue of the matrix $\widetilde{Q}_\gamma$. Then, one has

$$\left[\mu - \left(\gamma\lambda_i^2 - \frac{\lambda_M}{2}\gamma^2 - \frac{\lambda_M}{2}\rho_1^2\right)\right] \times \left[\mu - \left(\alpha\lambda_i^2 - \gamma\lambda_i - \frac{\lambda_M}{2} - \frac{\lambda_M}{2}\rho_2^2\right)\right] = 0. \tag{26}$$

And $\mu > 0$ if and only if

$$\gamma\lambda_i^2 - \frac{\lambda_M}{2}\gamma^2 - \frac{\lambda_M}{2}\rho_1^2 + \alpha\lambda_i^2 - \gamma\lambda_i - \frac{\lambda_M}{2} - \frac{\lambda_M}{2}\rho_2^2 > 0,$$
$$\left(\gamma\lambda_i^2 - \frac{\lambda_M}{2}\gamma^2 - \frac{\lambda_M}{2}\rho_1^2\right)\left(\alpha\lambda_i^2 - \gamma\lambda_i - \frac{\lambda_M}{2} - \frac{\lambda_M}{2}\rho_2^2\right) > 0, \tag{27}$$

which means

$$\gamma < \sqrt{\lambda_M^2 + 2(\alpha - 1)\lambda_M - \left(\rho_1^2 + \rho_2^2\right)} + \left(\lambda_M - 1\right) \triangleq c_3,$$
$$c_4 \triangleq \lambda_M - \sqrt{\lambda_M^2 - \rho_1^2} < \gamma < \lambda_M + \sqrt{\lambda_M^2 - \rho_1^2} \triangleq c_5, \tag{28}$$
$$\gamma < \alpha\lambda_M - \frac{1}{2}\left(1 + \rho_1^2\right) \triangleq c_6,$$

or

$$\gamma < \sqrt{\lambda_M^2 + 2(\alpha - 1)\lambda_M - \left(\rho_1^2 + \rho_2^2\right)} + \left(\lambda_M - 1\right) \triangleq c_3,$$
$$\gamma > \lambda_M + \sqrt{\lambda_M^2 - \rho_1^2} \triangleq c_5, \tag{29}$$
$$\gamma > \alpha\lambda_M - \frac{1}{2}\left(1 + \rho_1^2\right) \triangleq c_6.$$

In summary, if γ satisfies $\gamma \in \{\gamma \mid \max(0, c_4) < \gamma < \min\{c_1, c_2, c_3, c_5, c_6\}\}$ or $\gamma \in \{\gamma \mid \max(0, c_5, c_6) < \gamma < \min\{c_1, c_2, c_3\}\}$, then both the matrix $\widetilde{P}_\gamma$ and the matrix $\widetilde{Q}_\gamma$ are positive definite. Since $\widetilde{P}_\gamma$ and $\widetilde{Q}_\gamma$ have the same eigenvalues as that of P_γ and Q_γ, we have $P_\gamma = P_\gamma^T > 0$ and $Q_\gamma = Q_\gamma^T > 0$ when γ satisfies $\gamma \in \{\gamma \mid \max(0, c_4) < \gamma < \min\{c_1, c_2, c_3, c_5, c_6\}\}$ or $\gamma \in \{\gamma \mid \max(0, c_5, c_6) < \gamma < \min\{c_1, c_2, c_3\}\}$. □

Then, the main result follows.

Theorem 7. *Suppose that Assumptions 2 and 4 are satisfied; if* $\alpha > 0$ *and* $\gamma \in \{\max\{0, c_4\} < \gamma < \min\{c_1, c_2, c_3, c_5, c_6\}\} \cup \{\max(0, c_5, c_6) < \gamma < \min\{c_1, c_2, c_3\}\}$, *where* c_i, $i = 1, 2, \ldots, 6$, *are defined as in Lemma 6, then the second-order nonlinear followers* (11) *with the control algorithms* (14) *asymptotically track the leader* (12).

Proof. Let $\tilde{x}_i = x_i - x_r$ and $\tilde{v}_i = v_i - v_r$. And let $\tilde{x} = [\tilde{x}_1, \tilde{x}_2, \ldots, \tilde{x}_N]^T$, $\tilde{v} = [\tilde{v}_1, \tilde{v}_2, \ldots, \tilde{v}_N]^T$. We rewrite the closed-loop system of (11) using the control algorithm (14) as

$$\dot{\tilde{x}} = \tilde{v},$$
$$\dot{\tilde{v}} = F(t, x, v) - 1_N \otimes f(t, x_r, v_r) - M\tilde{x} - \alpha M\tilde{v} - \beta\,\mathrm{sgn}\{M(\gamma\tilde{x} + \tilde{v})\} - 1_N \otimes u_r, \tag{30}$$

where

$$F(t, x, v) = \left[f(t, x_1, v_1), f(t, x_2, v_2), \ldots, f(t, x_N, v_N)\right]^T. \tag{31}$$

Consider a Lyapunov function candidate

$$V = \begin{bmatrix}\tilde{x}^T & \tilde{v}^T\end{bmatrix} P_\gamma \begin{bmatrix}\tilde{x}\\ \tilde{v}\end{bmatrix} = \frac{1}{2}\tilde{x}^T\left(M^2 - \gamma\lambda_M I - \lambda_M\rho_1\rho_2 I - \alpha\gamma M^2\right)\tilde{x} + \tilde{x}^T\gamma M\tilde{v} + \frac{1}{2}\tilde{v}^T M\tilde{v}. \tag{32}$$

From Lemma 6, one has $V > 0$. The derivative of V along the system (30) is

$$\dot{V} = \tilde{x}^T\left(M^2 - \gamma\lambda_M I - \lambda_M\rho_1\rho_2 I - \alpha\gamma M^2\right)\tilde{v} + \tilde{v}^T\gamma M\tilde{v}^T + \tilde{x}^T\gamma M\dot{\tilde{v}} + \tilde{v}^T M\dot{\tilde{v}}$$

$$
\begin{aligned}
&= \tilde{x}^T \left(M^2 - \gamma\lambda_M I - \lambda_M\rho_1\rho_2 I - \alpha\gamma M^2\right)\tilde{v} \\
&\quad + \tilde{v}^T \gamma M \tilde{v}^T + \left(\gamma\tilde{x}^T + \tilde{v}^T\right) M \\
&\quad \times \left\{F(t,x,v) - 1_N \otimes f(t,x_r,v_r)\right\} \\
&\quad - \left(\gamma\tilde{x}^T + \tilde{v}^T\right) M \left(M\tilde{x} + \alpha M\tilde{v}\right) \\
&\quad - \left(\gamma\tilde{x}^T + \tilde{v}^T\right) M \left\{\beta \operatorname{sgn}\left[M\left(\gamma\tilde{x} + \tilde{v}\right)\right] + 1_N \otimes u_r\right\}.
\end{aligned} \tag{33}
$$

For the vectors $x, y \in \mathbb{R}^N$ and the matrix $0 < M = M^T \in \mathbb{R}^{N\times N}$, we define

$$
\langle x, y\rangle = x^T M y, \qquad \|x\|_M = \langle x, x\rangle^{1/2} = \left(x^T M x\right)^{1/2}. \tag{34}
$$

From Cauchy-Schwarz inequality, one has

$$
\begin{aligned}
&\|xy\|_M^2 \le \|x\|_M \|y\|_M, \\
&x^T M y \le \left(x^T M x\right)^{1/2} \times \left(y^T M y\right)^{1/2}, \qquad (ab)^{1/2} \le \frac{1}{2}(a+b).
\end{aligned} \tag{35}
$$

It follows that

$$
\begin{aligned}
&\left(\gamma\tilde{x}^T + \tilde{v}^T\right) M \left\{F(t,x,v) - 1_N \otimes f(t,x_r,v_r)\right\} \\
&\le \sqrt{\left(\gamma\tilde{x}^T + \tilde{v}^T\right) M \left(\gamma\tilde{x} + \tilde{v}\right) \left(\rho_1\tilde{x}^T + \rho_2\tilde{v}^T\right) M \left(\rho_1\tilde{x} + \rho_2\tilde{v}\right)} \\
&\le \frac{\lambda_M}{2} \\
&\quad \times \left(\gamma^2\tilde{x}^T\tilde{x} + 2\gamma\tilde{x}^T\tilde{v} + \tilde{v}^T\tilde{v} + \rho_1^2\tilde{x}^T\tilde{x} + 2\rho_1\rho_2\tilde{x}^T\tilde{v} + \rho_2^2\tilde{v}^T\tilde{v}\right) \\
&= \frac{\lambda_M\gamma^2}{2}\tilde{x}^T\tilde{x} + \lambda_M\gamma\tilde{x}^T\tilde{v} + \frac{\lambda_M}{2}\tilde{v}^T\tilde{v} \\
&\quad + \frac{\lambda_M}{2}\rho_1^2\tilde{x}^T\tilde{x} + \lambda_M\rho_1\rho_2\tilde{x}^T\tilde{v} + \frac{\lambda_M}{2}\rho_2^2\tilde{v}^T\tilde{v}, \\
\dot{V} &\le \tilde{x}^T \left(M^2 - \gamma\lambda_M I - \lambda_M\rho_1\rho_2 I - \alpha\gamma M^2\right)\tilde{v} \\
&\quad + \tilde{v}^T\gamma M\tilde{v}^T - \left(\gamma\tilde{x}^T + \tilde{v}^T\right) M^2 \left(\tilde{x} + \alpha\tilde{v}\right) \\
&\quad + \frac{\lambda_M\gamma^2}{2}\tilde{x}^T\tilde{x} + \lambda_M\gamma\tilde{x}^T\tilde{v} + \frac{\lambda_M}{2}\tilde{v}^T\tilde{v} + \frac{\lambda_M}{2}\rho_1^2\tilde{x}^T\tilde{x} \\
&\quad + \lambda_M\rho_1\rho_2\tilde{x}^T\tilde{v} + \frac{\lambda_M}{2}\rho_2^2\tilde{v}^T\tilde{v} \\
&\quad - \left(\gamma\tilde{x}^T + \tilde{v}^T\right) M \left\{\beta \operatorname{sgn}\left\{M\left(\gamma\tilde{x} + \tilde{v}\right)\right\} + 1_N \otimes u_r\right\} \\
&= \tilde{x}^T M^2\tilde{v} - \gamma\lambda_M\tilde{x}^T\tilde{v} - \lambda_M\rho_1\rho_2\tilde{x}^T\tilde{v} - \alpha\gamma\tilde{x}^T M^2\tilde{v} \\
&\quad + \tilde{v}^T\gamma M\tilde{v}^T - \gamma\tilde{x}^T M^2\tilde{x} - \tilde{x}^T M^2\tilde{v} - \gamma\alpha\tilde{x}^T M^2\tilde{v} \\
&\quad - \alpha\tilde{v}^T M^2\tilde{v} + \frac{\lambda_M\gamma^2}{2}\tilde{x}^T\tilde{x} + \lambda_M\gamma\tilde{x}^T\tilde{v} + \frac{\lambda_M}{2}\tilde{v}^T\tilde{v} \\
&\quad + \frac{\lambda_M}{2}\rho_1^2\tilde{x}^T\tilde{x} + \lambda_M\rho_1\rho_2\tilde{x}^T\tilde{v} + \frac{\lambda_M}{2}\rho_2^2\tilde{v}^T\tilde{v} \\
&\quad - \left(\beta - \|u_r\|\right)\left\|M\left(\gamma\tilde{x} + \tilde{v}\right)\right\|_1 \\
&= -\begin{bmatrix}\tilde{x}^T & \tilde{v}^T\end{bmatrix} Q_\gamma \begin{bmatrix}\tilde{x} \\ \tilde{v}\end{bmatrix} - \left(\beta - \|u_r\|\right)\left\|M\left(\gamma\tilde{x} + \tilde{v}\right)\right\|_1.
\end{aligned} \tag{36}
$$

From Lemma 6 that $Q_\gamma > 0$ and $\beta - \|u_r\| > 0$, we have $\dot{V} < 0$. Equivalently, it follows that as $t \to \infty$, $\tilde{x}_i \to 0$, $\tilde{v}_i \to 0$, which means $x_i \to x_r$, $v_i \to v_r$ as $t \to \infty$. And then the second-order nonlinear followers (11) with the control algorithms (14) asymptotically track the leader (12). □

Remark 8. In order to deal with the nonlinear term of the agents' dynamics in Theorem 7, one key procedure is the definition of the inner product (34) and the application of Cauchy-Schwarz inequality.

Remark 9. The result in Theorem 7 for multiagent systems with $x_i \in \mathbb{R}$ and $v_i \in \mathbb{R}$ is also suitable for agents with dynamics evolved in higher-order dimension; that is, $x_i \in \mathbb{R}^n$ and $v_i \in \mathbb{R}^n$.

3.3. Consensus Tracking for the General Nonlinear Dynamics. In the general nonlinear case, suppose that a network system with N followers represented by the following nonlinear equation:

$$
\dot{x}_i = f(x_i, u_i), \quad i = 1, 2, \ldots, N, \tag{37}
$$

where $x_i \in \mathbb{R}^n$ is the state vector of the ith follower and $u_i \in \mathbb{R}^p$ is the control input. And a leader is given by

$$
\dot{x}_r = f(x_r, u_r), \tag{38}
$$

where $x_r \in \mathbb{R}^n$ and $u_r \in \mathbb{R}^p$ are, respectively, the state and the control input of the leader. The function $f(x_i, u_i)$ will be C^2 with regard to x_i and u_i, and so is $f(x_r, u_r)$. We aim to give an explicit control law u_i for each follower such that

$$
\lim_{t\to\infty} \left\|x_i(t) - x_r(t)\right\| = 0. \tag{39}
$$

If the limit (39) is finally achieved, then we say that the general nonlinear followers (37) with the control algorithm asymptotically track the leader (38).

Remark 10. Note that the differential equation (37) can describe the models of many kinds of mechanical system such as nonholonomic system and underactuated system.

Throughout the subsequent analysis we assume that the network topology satisfies the following two assumptions.

Assumption 11. The graph of the network topology is tree shaped with the leader as the root node, where the tree shaped graph means each node has only one parent node except the root node.

Assumption 12. For the network system, each agent knows the measurement of the control input of its parent agent at the same time.

Assumption 12 illustrates that each agent is a cooperative partner with its neighbors. Due to the very general nonlinear dynamics and the goal of nonlinear consensus tracking, it is necessary for an agent to know the input of its parent agent. Motivated by the consensus analysis in [25], where the tool of incidence matrix is used to model the error system, we number the edges in the tree shaped graph according to the length of the path which is indirectly connected to the root node shown in Figure 4.

In order to propose the consensus tracking algorithm for agents (37), we make some preparation. The following analysis is based on the *proposition 1* in [22]. For the tree shaped graph, each follower node i in the form of (37) tracks the trajectory of its parent node j in the form of (37) (or (38)), where both $x_i(t)$, $x_j(t)$ and $u_i(t)$, $u_j(t)$ are bounded. And we denote

$$A_{ij}(t) := \frac{\partial f}{\partial x_i}\left(x_j(t), u_j(t)\right),$$
$$B_{ij}(t) := \frac{\partial f}{\partial u_i}\left(x_j(t), u_j(t)\right). \tag{40}$$

Let $\Phi_{ij}(t, t_0) \in \mathbb{R}^{n\times n} \times \mathbb{R}$ be the state transition matrix of $A_{ij}(t)$; that is, $\Phi_{ij}(t, t_0)$ satisfies $\dot{\Phi}_{ij}(t, t_0) = A_{ij}(t)\Phi_{ij}(t, t_0)$ with $\Phi_{ij}(t_0, t_0) = I$. Further, for a given constant $\alpha > 0$, we define

$$H_{ij}(t_0, t) = \int_{t_0}^{t} \exp\left(6\alpha\left(t_0 - \tau\right)\right)\Phi_{ij}\left(t_0, \tau\right)B_{ij}(\tau)\,B_{ij}(\tau)^T\Phi_{ij}(t_0, \tau)^T d\tau. \tag{41}$$

If there exists a constant δ such that $H_{ij}(t, t+\delta)$ is bounded away from singularity uniformly in t, then define $P_{ij}(t)$ as follows:

$$P_{ij}(t) := H_{ij}^{-1}(t, t+\delta). \tag{42}$$

If there exist two numbers p_{ij}^m and p_{ij}^M such that

$$0 < p_{ij}^m I < P_{ij}(t) < p_{ij}^M I, \quad \forall t \in \mathbb{R}_+, \tag{43}$$

then, for any function $\gamma_{ij}(t) : \mathbb{R}_+ \to [1/2, \infty)$, continuous and bounded, we propose the following linear time-varying feedback control law:

$$u_i(t) = u_j(t) - \gamma_{ij}(t)\,B_{ij}(t)^T P_{ij}(t)\left[x_i(t) - x_j(t)\right]. \tag{44}$$

Now we have the main result as follows.

Theorem 13. *If Assumptions 11 and 12 are satisfied, then the general nonlinear followers* (37) *with the control algorithms* (44) *asymptotically track the leader* (38).

Proof. Let

$$x_i(t) - x_j(t) = \widetilde{x}_{ij}(t),$$
$$u_i(t) - u_j(t) = \widetilde{u}_{ij}(t), \tag{45}$$

where x_j and u_j are the state and the input of agent j and the agent j is the parent agent of agent i. For simplicity, we denote $\widetilde{x}_{ij}(t)$ in the multiagent systems by $e_k(t)$, $k = 1, 2, \ldots, m$, like in Figure 4, where m is the number of edges in the graph of the network topology, and $e = [e_1, e_2, \ldots, e_m]^T$. Similarly, let $P(t) = \mathrm{diag}(P_1(t), P_2(t), \ldots, P_m(t))$, where $P_k(t)$, $k = 1, 2, \ldots, m$, represent the matrix $P_{ij}(t)$, $i \in \mathcal{V}$, $j \in \mathcal{V} \cup \{r\}$ (r represents the leader in the network), and each is described by (42). Consider a Lyapunov function candidate

$$V = \sum_{k=1}^{m} V_k = \sum_{k=1}^{m} e_k^T P_k e_k. \tag{46}$$

Note that

$$\widetilde{u}_k(t) = \widetilde{u}_{ij}(t) = -\gamma_{ij}(t)\,B_{ij}(t)^T P_{ij}(t)\,\widetilde{x}_{ij}(t) = -\gamma_k(t)\,B_k(t)^T P_k(t)\,e_k(t). \tag{47}$$

In addition, one has

$$\begin{aligned}
\dot{e}_k(t) &= A_k(t)\,e_k(t) + B_k(t)\,\widetilde{u}_k(t) + o\left(e_k(t), \widetilde{u}_k(t), t\right),\\
\dot{P}_k(t) &= -P_k(t)\,\dot{H}_k(t)\,P_k(t),\\
\dot{H}_k(t) &= \dot{H}_{ij}(t, t+\delta)\\
&= 6\alpha H_k(t) + A_k(t)\,H_k(t) + H_k(t)\,A_k(t)^T\\
&\quad + \exp(-6\alpha\delta)\,\Phi_k(t, t+\delta)\,B_k(t+\delta)\\
&\quad \times B_k(t+\delta)^T\Phi_k(t, t+\delta)^T - B_k(t)\,B_k(t)^T.
\end{aligned} \tag{48}$$

Since $\gamma_k(t) \geq 1/2$, $k = 1, 2, \ldots, m$, from the control algorithm (44) and the notation (45) and

$$\left\|\widetilde{u}_k\right\| = \left\|-\gamma_k B_k^T P_k e_k\right\| \leq K\left\|e_k\right\|, \quad K < \infty, \tag{49}$$

we have

$$o\left(e_k(t), \widetilde{u}_k(t), t\right) = \widehat{o}\left(e_k(t), t\right),$$
$$\lim_{\|e_k\|\to 0}\sup_{t\geq 0}\frac{\left\|\widehat{o}\left(e_k(t), t\right)\right\|}{\left\|e_k(t)\right\|} = 0. \tag{50}$$

Then,

$$\begin{aligned}
\dot{V}_k(e_k, t) &= -e_k(t)^T 6\alpha P_k(t)\,e_k(t)\\
&\quad - e_k(t)^T\left(2\gamma_k(t) - 1\right)P_k(t)\,B_k(t)\,B_k(t)^T P_k(t)\,e_k(t)\\
&\quad - e_k(t)^T\Big[\exp(-6\alpha\delta)\,P_k(t)\,\Phi_k(t, t+\delta)\,B_k(t+\delta)\\
&\qquad \times B_k(t+\delta)^T\Phi_k(t, t+\delta)^T P_k(t)\Big]\,e_k(t)\\
&\quad + 2e_k(t)^T P_k(t)\,\widehat{o}\left(e_k(t), t\right)\\
&\leq -4\alpha p_k^m\left\|e_k\right\|^2.
\end{aligned} \tag{51}$$

It follows that $\dot{V} < 0$ and $\widetilde{x}_{ij} \to 0$, $\widetilde{u}_{ij} \to 0$ as $t \to \infty$. At the same time, $\lim_{t\to\infty}\|x_i(t) - x_r(t)\| = 0$ is satisfied and the consensus tracking problem is solved. □

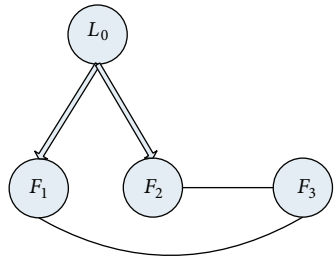

Figure 1: The undirected graph for a group of three followers with a leader. Here L_0 denotes the leader and F_i, $i = 1, 2, 3$, denote the followers. The direct arrows represent the information flow from the leader to the follower and the indirect edges represent the bidirectional information flow between followers.

Remark 14. For an undirected connected graph which contains a tree shaped subgraph, or a directed graph which contains a directed spanning tree, we can choose such a tree as Assumption 11 required. However, such a directed tree is unfavorable for implementing the distributed control since in such case each follower has to know the information of the global communication topology. So, it is worth discussing the general undirected (or directed) communication topologies and it will be a direction of the future research.

Remark 15. It has been shown that systems (1) and (11) are the special cases of system (37). However, the analysis for convergence of closed system is completely different. Though, in each case, the communication topologies are relatively simple.

4. Simulation Results

In this section, three numerical simulation examples are given to illustrate the theoretical results. Consider the first example, a network of three followers with a leader shown in Figure 1. Assume that the dynamics of the follower agents with $n = 2$ are described by the following equations:

$$f(t, x_i) = \begin{pmatrix} x_{i1} \sin t \\ x_{i2} \cos t \end{pmatrix},$$
$$f(t, x_r) = \begin{pmatrix} x_{r1} \sin t \\ x_{r2} \cos t \end{pmatrix}. \tag{52}$$

The control input of the leader is given by $u_r = [1, 1]^T$. Choose $\beta_i = 1$ for $i = 1, 2, 3$ and $\omega = 1.5$. Note that $1.5 > \|u_r\| = \sqrt{2}$. The initial values of the error between the multiple followers and the leader, which is described by $\tilde{x}_{ij} = x_{ij} - x_{rj}$, $i = 1, 2, 3$, $j = 1, 2$, are given as $[0.1, -0.2, 0.3, -0.1, 0.4, 0.2]^T$. Then the results of consensus tracking are shown in Figure 2, where $x_1 = [x_{11}, x_{21}, x_{31}]^T$ and $x_2 = [x_{12}, x_{22}, x_{32}]^T$. Since $\tilde{x}_{ij} \to 0$ as t moves on, consensus tracking is finally achieved.

The second example is also given for the graph in Figure 1, which characterizes the communication channel among the three followers and a leader. The dynamics of each follower and the leader are specified by the following equations, respectively:

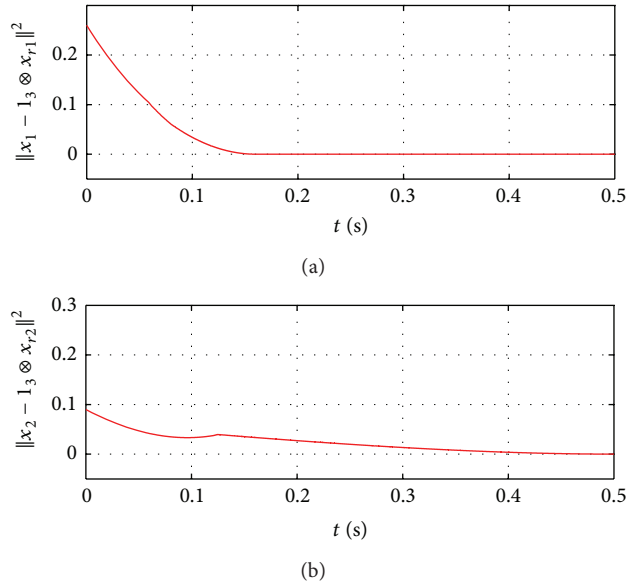

Figure 2: Consensus tracking for the first-order nonlinear systems.

$$\begin{aligned} \dot{x}_i &= v_i, \\ \dot{v}_i &= x_i \sin(t) + v_i \cos(t) + u_i, \\ \dot{x}_r &= v_r, \\ \dot{v}_r &= x_r \sin(t) + v_r \cos(t) + u_r. \end{aligned} \tag{53}$$

Note that

$$M = \begin{bmatrix} 2 & 0 & -1 \\ 0 & 2 & -1 \\ -1 & -1 & 2 \end{bmatrix}, \tag{54}$$

and $\lambda_M = 3.4142$, $\rho_1 = \rho_2 = 1$. Choose $\alpha = 1$; then it is easy to compute that

$$\begin{aligned} c_1 &= 0.7735, \quad & c_2 &= 0.4921, \quad & c_3 &= 5.5217, \\ c_4 &= 0.1497, \quad & c_5 &= 6.6787, \quad & c_6 &= 2.4142. \end{aligned} \tag{55}$$

Choose $\gamma = 0.45 \in \{\gamma \mid \max(0, c_4) < \gamma < \min\{c_1, c_2, c_3, c_5, c_6\}\}$. Given the initial values as $\tilde{x}_1(0) = 1$, $\tilde{x}_2(0) = 2$, $\tilde{x}_3(0) = 3$, $\tilde{v}_1(0) = 4$, $\tilde{v}_2(0) = 5$, and $\tilde{v}_3(0) = 6$, the results of consensus tracking are shown in Figure 3.

Now let us see the third example. In the case of the general nonlinear dynamics, the graph of the network topology is shown in Figure 4.

We consider each agent's dynamics to be a simple nonholonomic system specified by the equations as follows:

$$\begin{aligned} \dot{x}_1 &= u_1, \\ \dot{x}_2 &= u_2, \\ \dot{x}_3 &= x_2 u_1. \end{aligned} \tag{56}$$

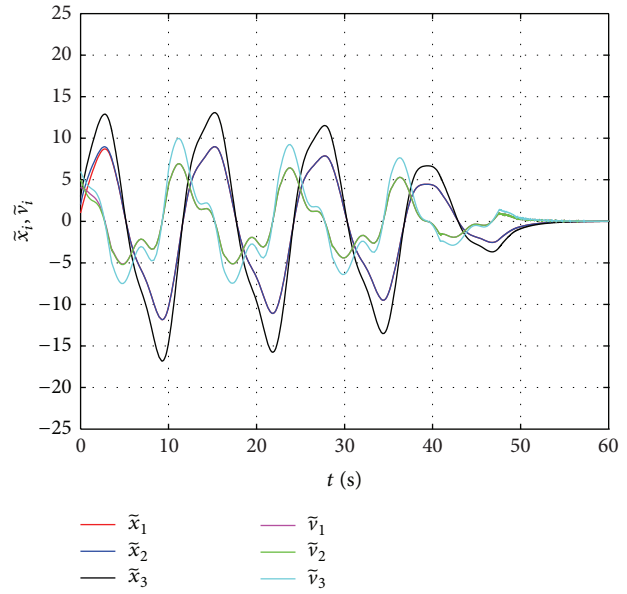

Figure 3: Consensus tracking for the second-order nonlinear systems.

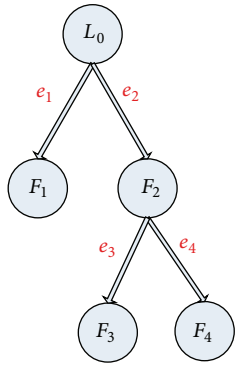

Figure 4: The tree shaped graph for a network of four followers with a leader, where L_0 denotes the leader and F_i, $i = 1, 2, 3, 4$, denote the followers. The direct arrows represent the information flow from the parent agent to the child agent.

Assume that the trajectory and the control input of the leader are, respectively, described by $x^{L_0} = (0, t, 0)$ and $u^{L_0} = (0, 1)$, where the superscript L_0 means the leader. Choose $\delta = 0.1$ and $\gamma_{ij}(t) = 1$. For the initial value of F_i, $i = 1, 2, 3, 4$, given by $x^{F_1}(0) = (0.4, -0.6, 0.4)$, $x^{F_2}(0) = (-0.8, 1.2, 1.8)$, $x^{F_3}(0) = (0, 2.4, 1.4)$, and $x^{F_4}(0) = (1, -3.8, 2.8)$, the norm results of tracking error $e_1(t) = x^{F_1} - x^{L_0}$, $e_2(t) = x^{F_2} - x^{L_0}$, $e_3(t) = x^{F_3} - x^{F_2}$, and $e_4(t) = x^{F_4} - x^{F_2}$ are shown in Figure 5.

Since e_i, $i = 1, 2, 3, 4$, converge to 0 as time moves on, consensus tracking is achieved asymptotically.

5. Conclusion

In this paper, we studied the problem of nonlinear consensus tracking via the variable structure technique, the feedback linearization technique, and the Lyapunov theory when there is a leader governed by the external input. Suppose that the leader's external input is upper bounded and a connectivity requirement for the network topology is satisfied; we proposed the consensus tracking algorithms for the followers with the first-order nonlinear dynamics, the second-order nonlinear dynamics, and the general nonlinear dynamics to asymptotically track the corresponding nonlinear leader. And several numerical simulations were given to show the effectiveness of our algorithms. The future works include the study of nonlinear consensus tracking in the general directed network topologies.

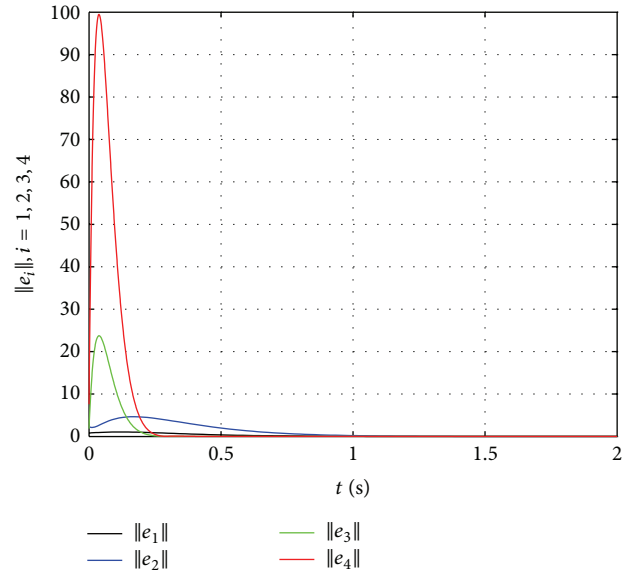

Figure 5: The norm of error e_i, $i = 1, 2, 3, 4$, versus time.

Conflict of Interests

The author declares that there is no conflict of interests regarding the publication of this paper.

References

[1] R. M. Murray, "Recent research in cooperative control of multivehicle systems," *Journal of Dynamic Systems, Measurement and Control*, vol. 129, no. 5, pp. 571–583, 2007.

[2] Q. Hui and W. M. Haddad, "Distributed nonlinear control algorithms for network consensus," *Automatica*, vol. 44, no. 9, pp. 2375–2381, 2008.

[3] Z. H. Qu, *Cooperative Control of Dynamical Systems*, Springer, London, UK, 2009.

[4] W. Ren and Y. C. Cao, *Distributed Coordination of Multi-agent Networks*, Springer, London, UK, 2011.

[5] G. Wen, G. Hu, W. Yu, J. Cao, and G. Chen, "Consensus tracking for higher-order multi-agent systems with switching directed topologies and occasionally missing control inputs," *Systems & Control Letters*, vol. 62, no. 12, pp. 1151–1158, 2013.

[6] Y. C. Cao and W. Ren, "Distributed coordinated tracking with reduced interaction via a variable structure approach," *IEEE Transactions on Automatic Control*, vol. 57, no. 1, pp. 33–48, 2012.

[7] W. Ren, "Consensus tracking under directed interaction topologies: algorithms and experiments," *IEEE Transactions on Control Systems Technology*, vol. 18, no. 1, pp. 230–237, 2010.

[8] W. Ren, "Multi-vehicle consensus with a time-varying reference state," *Systems and Control Letters*, vol. 56, no. 7-8, pp. 474–483, 2007.

[9] Y. G. Hong, J. P. Hu, and L. X. Gao, "Tracking control for multi-agent consensus with an active leader and variable topology," *Automatica*, vol. 42, no. 7, pp. 1177–1182, 2006.

[10] W. Ren, "On consensus algorithms for double-integrator dynamics," *IEEE Transactions on Automatic Control*, vol. 53, no. 6, pp. 1503–1509, 2008.

[11] Z. K. Li, Z. S. Duan, and L. Huang, "Leader-follower consensus of multi-agent systems," in *Proceedings of the American Control Conference (ACC '09)*, pp. 3256–3261, St. Louis, Mo, USA, June 2009.

[12] J. Mei, W. Ren, and G. Ma, "Distributed containment control for multiple nonlinear systems with identical dynamics," in *Proceedings of the 30th Chinese Control Conference (CCC '11)*, pp. 6544–6549, Yantai, China, July 2011.

[13] H. S. Su, G. R. Chen, X. F. Wang, and Z. L. Lin, "Adaptive second-order consensus of networked mobile agents with nonlinear dynamics," *Automatica*, vol. 47, no. 2, pp. 368–375, 2011.

[14] D. V. Dimarogonas, M. Egerstedt, and K. J. Kyriakopoulos, "A leader-based containment control strategy for multiple unicycles," in *Proceeding of the 45th IEEE Conference on Decision and Control (CDC '06)*, pp. 5968–5973, San Diego, Calif, USA, December 2006.

[15] Z. Qu, J. Chunyu, and J. Wang, "Nonlinear cooperative control for consensus of nonlinear and heterogeneous systems," in *Proceedings of the 46th IEEE Conference on Decision and Control (CDC '07)*, pp. 2301–2308, December 2007.

[16] G. Wen, Z. Duan, W. Yu, and G. Chen, "Consensus of second-order multi-agent systems with delayed nonlinear dynamics and intermittent communications," *International Journal of Control*, vol. 86, no. 2, pp. 322–331, 2013.

[17] G. Wen, Z. Duan, G. Chen, and W. Yu, "Consensus tracking of multi-agent systems with Lipschitz-type node dynamics and switching topologies," *IEEE Transactions on Circuits and Systems. I. Regular Papers*, vol. 61, no. 2, pp. 499–511, 2014.

[18] W. L. Lu and T. P. Chen, "New approach to synchronization analysis of linearly coupled ordinary differential systems," *Physica D*, vol. 213, no. 2, pp. 214–230, 2006.

[19] J. F. Heagy, T. L. Carroll, and L. M. Pecora, "Synchronous chaos in coupled oscillator systems," *Physical Review E*, vol. 50, no. 3, pp. 1874–1885, 1994.

[20] J. A. Jacquez, *Compartmental Analysis in Biology and Medicine*, University of Michigan Press, Ann Arbor, Mich, USA, 2nd edition, 1985.

[21] Q. Song, J. D. Cao, and W. W. Yu, "Second-order leader-following consensus of nonlinear multi-agent systems via pinning control," *Systems & Control Letters*, vol. 59, no. 9, pp. 553–562, 2010.

[22] G. Walsh, D. Tilbury, S. Sastry, and R. A. Murray, "Stabilization of trajectories for systems with nonholonomic constraints," *IEEE Transactions on Automatic Control*, vol. 39, no. 1, pp. 216–222, 1994.

[23] C. Godsil and G. Royle, *Algebraic Graph Theory*, Springer, New York, NY, USA, 2001.

[24] W. W. Yu, G. R. Chen, M. Cao, and J. Kurths, "Second-order consensus for multiagent systems with directed topologies and nonlinear dynamics," *IEEE Transactions on Systems, Man, and Cybernetics B: Cybernetics*, vol. 40, no. 3, pp. 881–891, 2010.

[25] D. V. Dimarogonas and K. H. Johansson, "Stability analysis for multi-agent systems using the incidence matrix: quantized communication and formation control," *Automatica*, vol. 46, no. 4, pp. 695–700, 2010.

Hindawi Publishing Corporation
The Scientific World Journal
Volume 2014, Article ID 394828, 12 pages
http://dx.doi.org/10.1155/2014/394828

Research Article

A Novel Memristive Multilayer Feedforward Small-World Neural Network with Its Applications in PID Control

Zhekang Dong,[1] Shukai Duan,[1] Xiaofang Hu,[2] Lidan Wang,[1] and Hai Li[3]

[1] *School of Electronics and Information Engineering, Southwest University, Chongqing 400715, China*
[2] *Department of MBE, City University of Hong Kong, Hong Kong*
[3] *Department of ECE, University of Pittsburgh, Pittsburgh, PA 15261, USA*

Correspondence should be addressed to Shukai Duan; duansk@swu.edu.cn

Received 16 June 2014; Accepted 17 July 2014; Published 14 August 2014

Academic Editor: Jinde Cao

Copyright © 2014 Zhekang Dong et al. This is an open access article distributed under the Creative Commons Attribution License, which permits unrestricted use, distribution, and reproduction in any medium, provided the original work is properly cited.

In this paper, we present an implementation scheme of memristor-based multilayer feedforward small-world neural network (MFSNN) inspirited by the lack of the hardware realization of the MFSNN on account of the need of a large number of electronic neurons and synapses. More specially, a mathematical closed-form charge-governed memristor model is presented with derivation procedures and the corresponding Simulink model is presented, which is an essential block for realizing the memristive synapse and the activation function in electronic neurons. Furthermore, we investigate a more intelligent memristive PID controller by incorporating the proposed MFSNN into intelligent PID control based on the advantages of the memristive MFSNN on computation speed and accuracy. Finally, numerical simulations have demonstrated the effectiveness of the proposed scheme.

1. Introduction

In 1971, Professor Chua theoretically formulated and defined the memristor and described that the memristance (short for resistor of a memristor) is characterized by the relationship between the electrical charge q and flux φ passing through a device [1]. However, it was only after the first physical realization of the memristor in nanoscale at Hewlett-Packard (HP) Lab in 2008 that it immediately garnered extensive interests among numerous researchers [2–4]. The reported experiments confirmed that the memristor possesses switching characteristic, memory capacity, and continuous input and output property. Due to these unique properties, memristors are being explored for many potential applications in the areas of nonvolatile memory [5, 6], very-large-scale integrated (VLSI) circuit [7], artificial neural networks [8–10], digital image processing [11–13], and signal processing and pattern recognition [14]. At present, a considerable number of models of different complexity have been proposed in the literatures, such as Pickett's model [15], spintronic memristor model [16], nonlinear ionic drift model [17], boundary condition-based model [18], and threshold adaptive memristor model [19]. These published models exhibit desired nonlinearity of nanoscale structures. This paper still applies the TiO_2 memristor model on account of its simplified expressions and the same ideal physical behaviors.

Brain neural network emerges from the interactions of dozens, perhaps hundreds, of brain regions, each containing millions of neurons [20]. They are highly evolved nervous systems capable of high-speed information processing, real-time integration of information across segregated sensory channels, and brain regions [20, 21]. In order to obtain the similar intelligence of human brain, artificial neural network is designed to imitate the human brain not merely on architecture but also on work patterns. The connection structure of artificial neural networks is generally divided into feedforward, feedback, single-layer, multilayer, and so forth. Most of these connection architectures are approximately regular. However, the bioneurological researches show that brain neural network has random features to a certain degree and exhibits "small-world" effectiveness, that is, high levels of clustering and short average path length [22]. Therefore,

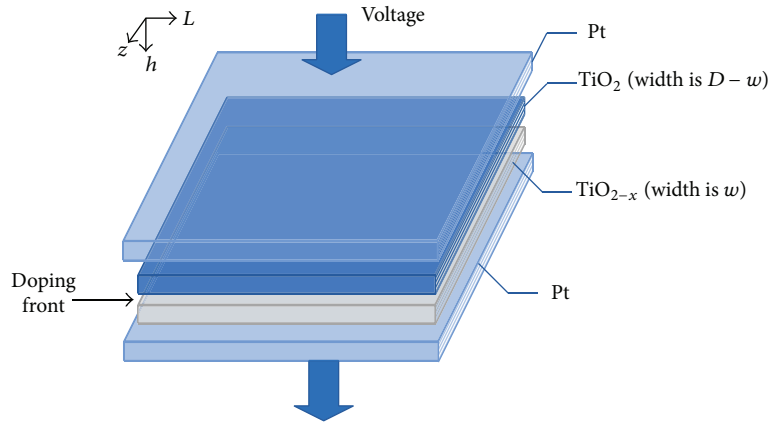

Figure 1: Schematic model of the HP memristor.

it becomes a hot issue to design bionics neural network with randomness in architecture based on the background of neurobiology.

Notably, Watts and Strogatz revealed a significant effect that is in common among complex networks. They pointed out that the real architecture of network is nearly a middle model between regular connection and random connection and defined it as small-world network (WS model) in 1998 [23]. Over the past several years, a large number of investigations on complex networks have provided new insight into biological neural networks. Bassett concluded that human brain functional networks have small-world network topology derived from a series of magneto encephalography experiments [22]. Douw et al. found that the cognition is related to the resting-state small-world network topology [24]. In literature [25], the authors applied small-world properties into prefrontal cortex that correlate with predictors of psychopathology risk, which holds promise as a potential neurodiagnostic for young children. Taylor has studied the protein structures and binding based on small-world network strategies and has made great progress [26]. Simard built up a small-world neural network through rewiring the regular connections and found that the small-world neural network has faster learning speed and smaller error than that of the regular network and random network with the same size [27]. In this paper, we incorporate the memristor into the multilayer feedforward small-world neural network to build up a new type of memristive neural network that is easy of VLSI implementation and closer to biological networks. Furthermore, based on the proposed memristive neural network, a novel memristive intelligent PID controller is put forward. The nanoscale memristor is beneficial for easily adjusting the PID control parameters and the hardware realization of modern intelligent microcontrol system.

This paper is organized as follows. In Section 2, we derive the mathematical model of a nonlinear memristor which takes into account the nonlinear dopant drift effect nearby the terminals and the boundary conditions and give its Simulink model correspondingly. Following that, the concepts and design algorithm of the memristive small-world neural network are described in detail in Section 3. Section 4 designs a memristive PID controller by combining the proposed neural network with the standard PID control theory. In order to guarantee the feasibility and effectiveness of the proposed scheme, the computer simulations are performed in Section 5. Finally, we give the conclusions in Section 6.

2. The Nonlinear Memristor Model

2.1. The Mathematical Model of the Memristor. A memristor or memristive device is essentially a two-terminal passive electronic element with memory capacity. Its memristance state depends on the amplitude, polarity, and duration of the external applied power. The physical model of the HP memristor from [28], shown in Figure 1, consists of a two-layer thin film (thickness $D \approx 10\,\text{nm}$) of TiO_2 sandwiched between two platinum electrodes. One of the layers, which is described as TiO_{2-x}, is doped with oxygen vacancies (called dopants) and thus it exhibits high conductivity. The width w of the doped region is modulated depending on the amount of electric charge passing through the memristor. The other TiO_2 layer owning an insulating property has a perfect 2 : 1 oxygen-to-titanium ratio, and this layer is referred to the undoped region. Generally, an external excitation $v(t)$ applied across the memristor may cause the charged dopants to drift and the boundary between the two regions would be moved correspondingly with the total memristance changed eventually.

The total resistance of the memristor, M, is a sum of the resistances of the doped and undoped regions:

$$M(t) = R_{\text{on}}\left(\frac{w(t)}{D}\right) + R_{\text{off}}\left(1 - \frac{w(t)}{D}\right), \tag{1}$$

where R_{on} and R_{off} are the limited values of the memristance for $w = D$ and $w = 0$, respectively. Setting the internal state variable as $x = w/D, \in [0, 1]$, (1) can be rewritten as

$$M(t) = R_{\text{off}} + (R_{\text{on}} - R_{\text{off}})\, x(t). \tag{2}$$

When $t = 0$, the initial memristance is

$$M_0 = R_{\text{off}} + (R_{\text{on}} - R_{\text{off}})\, x_0. \tag{3}$$

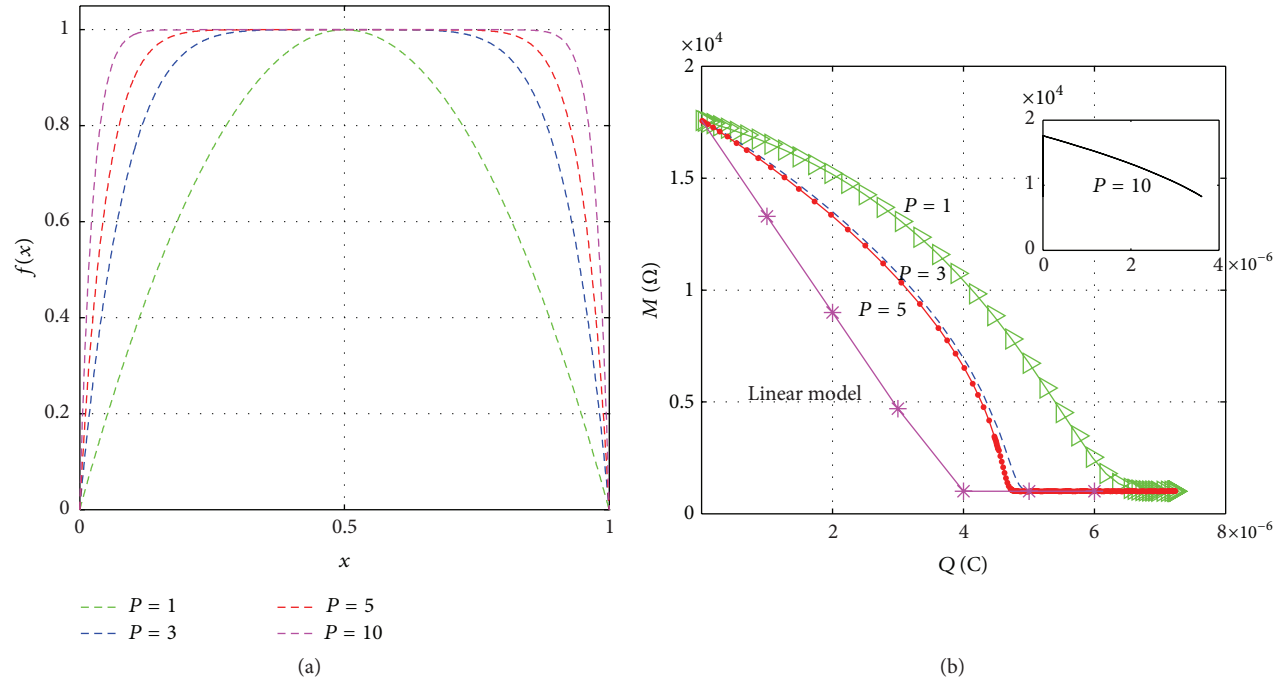

FIGURE 2: The influence of different values of the integer P on the memristor. (a) Joglekar window function for $P = 1$, $P = 3$, $P = 5$, and $P = 10$. (b) Relationship between memristance versus charge for the nonlinear memristor model. As the integer P increases, the graphs tend to linearity.

The movement speed of the boundary between the doped and undoped regions depends on the resistance of doped area, the passing current, and other factors according to the state equation:

$$\frac{dx}{dt} = ki(t) f(x), \qquad k = \frac{\mu_v R_{\mathrm{ON}}}{D^2}, \tag{4}$$

where $\mu_v \approx 10^{-14}\,\mathrm{m^2\,s^{-1}\,V^{-1}}$ is the average ionic mobility parameter. As we all known, small voltages can yield enormous electric fields in nanoscale devices, which can secondarily produce significant nonlinearities in the ionic transport. As for a memristive device, these nonlinearities are manifested particularly at the thin film edges, especially at the two boundaries. This phenomenon, called nonlinear dopant drift, can be simulated by multiplying a proper window function $f(x)$ on the right side of (4). Based on [28], there are several kinds of classical window functions, such as Joglekar window function and Biolek window function. This paper chooses the Joglekar window function which can be described by

$$f(x) = 1 - (2x - 1)^{2P}, \tag{5}$$

where P is a positive integer called the control parameter.

Figure 2(a) exhibits the behavior of the Joglekar window function for different values of P. Figure 2(b) shows the graphs of the memristance versus charge of the memristor. As the value of P becomes smaller, the nonlinearity increases. On the other hand, as the integer P increases, the model tends to the linear model. Based upon this, as well as the literature [3, 28], we set the value of the integer $P = 1$ in this window function and obtain

$$f(x) = 4x - 4x^2. \tag{6}$$

Substituting (6) into (4),

$$\int_{x_0}^{x(t)} \left(\frac{1}{x(\tau)} + \frac{1}{1 - x(\tau)}\right) dx(\tau) = \int_0^t 4ki(\tau)\, d\tau, \tag{7}$$

where the internal state variable satisfies $x(\tau) \in [x_0, x(t)]$ and the integration time is $0 \le \tau \le t$.

Assume $q_0 = 0$; we can get

$$\frac{x(t)}{1 - x(t)} = \frac{x_0}{1 - x_0} \times e^{4kq(t)}. \tag{8}$$

The initial value of the state variable can be expressed as

$$x_0 = \frac{R_{\mathrm{off}} - R_0}{\Delta R}. \tag{9}$$

Then, the expression of $x(t)$ can be calculated as

$$x(t) = 1 - \frac{1}{Ae^{4kq(t)} + 1}, \tag{10}$$

where A is a constant and its value is determined by R_{off}, R_{on}, and R_0:

$$A = \frac{R_{\mathrm{off}} - R_0}{R_0 - R_{\mathrm{on}}}. \tag{11}$$

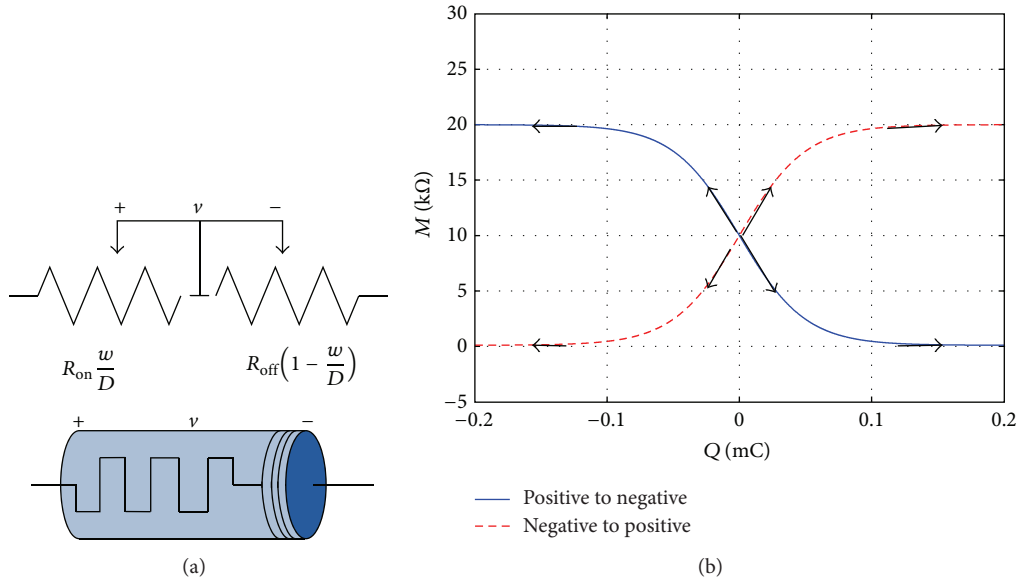

Figure 3: The nonlinear memristor model and its characteristic curves. (a) The equivalent circuit of the memristor and its 3D symbol. (b) The relationship between memristance and the charge.

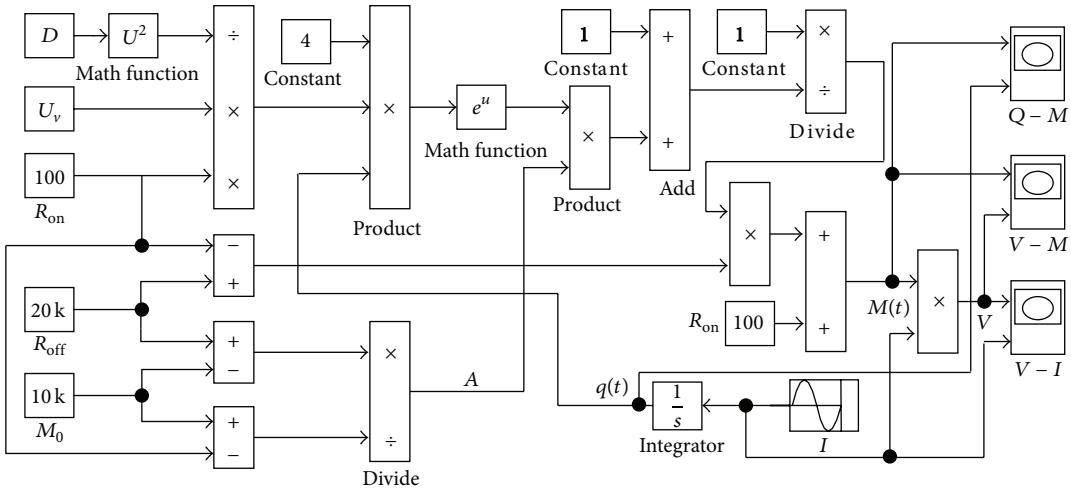

Figure 4: The Simulink model of the nonlinear memristor.

Combining (2)–(11), the resistance of memristor can be rewritten as

$$M(t) = R_{on} + \Delta R \frac{1}{Ae^{4kq(t)} + 1}, \quad (12)$$

where $\Delta R = R_{off} - R_{on}$.

Giving a sine stimulus to the memristor, we get the simulation results using MATLAB software. It is noteworthy that the memristor is a two-terminal element with polarity, which is shown in Figure 3(a). When the current flows into the memristive device from the positive pole to the negative pole, one can get the relationship curve (the blue line) between memristance and charge through it as shown in Figure 3(b). On the contrary, when the current flows into the memristor from the negative pole to the positive pole, the relationship curve is denoted by the red dashed line. When the charge is close to or exceeds the charge threshold values, the resistance of the memristor reaches and stays at R_{on} and R_{off}, respectively. Notably, the threshold value denotes the quantity of electric charge required when the memristance reaches the limit resistance. The parameters of the model are $R_{on} = 100\,\Omega$, $R_{off} = 20\,k\Omega$, $M_0 = 10\,k\Omega$, $D = 10\,nm$, and $\mu_v \approx 10^{-14}\,m^2 s^{-1} V^{-1}$. Moreover, the simulation results in Figure 3(b) are consistent with the results concluded by Adhikari et al. in [8, 29].

2.2. The Simulink Model of the Memristor. For the sake of analyzing the characteristics of the memristor model comprehensively, a Simulink model is built upon (2)–(12) and illustrated in Figure 4. The model mainly consists of input and output modules, internal operation modules (multipliers,

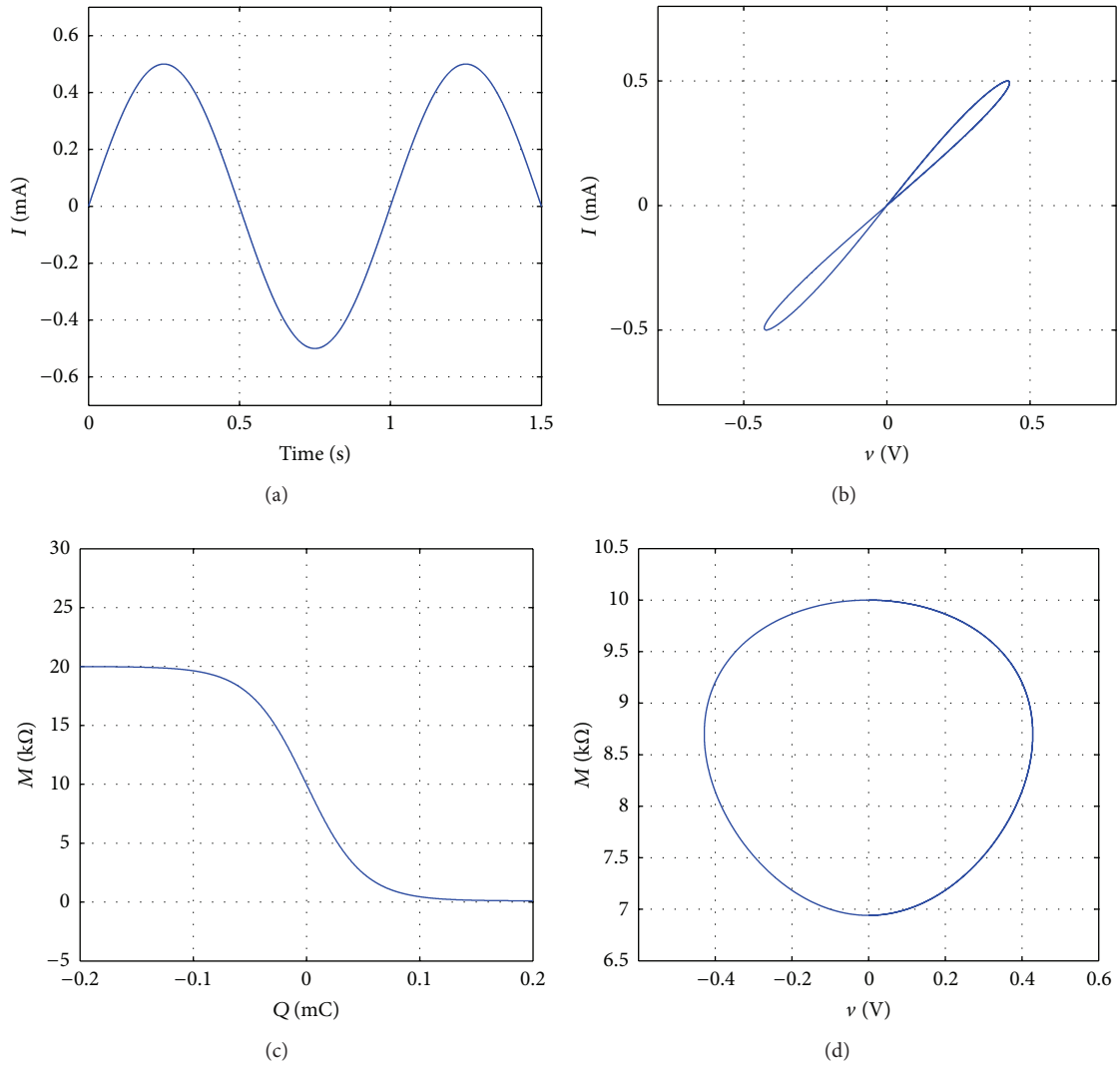

Figure 5: The results of the memristor Simulink model. (a) The input current source. (b) Relationship between the current i and the voltage v. (c) Relationship between the memristance M and the charge q. (d) Relationship between the memristance M and the voltage v.

adders, and modules), and parameter control modules. The model parameters are the same as those in Figure 3. The signal stimulus applied into the memristor is a sinusoidal current source with amplitude of 0.5 mA and frequency of 1 Hz.

The simulation results are exhibited in Figure 5. The current flowing through the memristor is shown in Figure 5(a). The typical hysteresis loop in Figure 5(b) shows its switching characteristic; that is, the memristance can switch between high resistance and low resistance. Figure 5(c) illustrates that the memristance is a nonlinear function of the flow of charge as discussed previously. Figure 5(d) shows the relationship between the memristance M and the charge q. Notably, in the part of the higher memristance state, the change ratio of the memristance is low, while, in the part of the lower memristance state, the change ratio of the memristance is high.

3. The Memristive Multilayer Feedforward Small-World Neural Network

3.1. The Multilayer Feedforward Small-World Neural Network. Generally, small-world phenomenon indicates that a network has highly concentrated local connections and also includes a few random long connections. In real world, a large number of networks have the small-world effect, such as disease transmission network, social network, and the food chain network [22]. As is known to all, in the classical multilayer feedforward neural network, such as BP network, the ith neuron in the lth layer v_i^l only connects its neighboring neuron sets V^{l-1} and V^{l+1}. In addition, all connections are feedforward and no connections exist between neurons within the same layer. This kind of network can be considered as a regular network. Based on [27] and the construction process of WS small world model, we introduce Algorithm 1

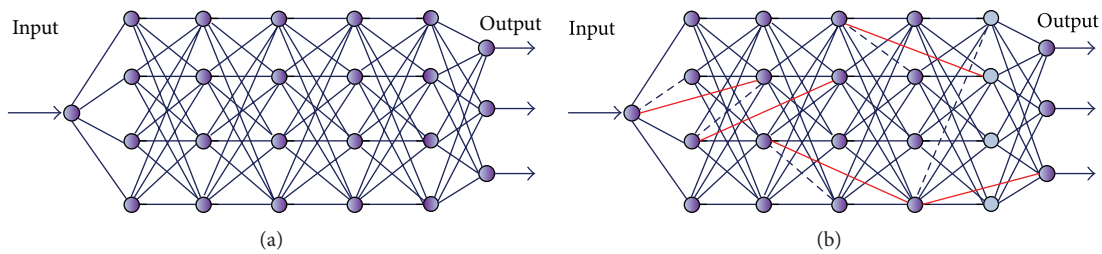

Figure 6: The construction progress of the multilayer feedforward WS small-world neural network. (a) The regular network ($P = 0$). (b) The multilayer feedforward WS small-world neural network ($0 < P < 1$).

```
Set the network has L layers
Set each layer has n_l nodes
For h = 1 To L − 2
    p_1(h) = αe^{−β(h+2)}
For l_1 = 1 To L − 2
  For n_l = 1 To n_l
    For n_2 = 1 To n_l
      If rand < p
        w^{l_1(l_1+1)}_{n_1 n_2} = 0
n_3 = randint(1, n_l)
  t = 1
While t = 1
  p_2 = rand
  For l_2 = L − 2 To l_1 + 2
      If p_2 < p_1(l_2)
        b^{l_1 l_2}_{n_1 n_3} = rand
        t = 0
        Break
      Finish!
```

Algorithm 1: Constructive procedure of the small-world neural network.

which is used to construct multilayer feedforward neural network model according to the rewiring probability. The specific construction process is given as follows.

Step 1. Initialization: assuming the number of the network layers is L, each layer has n_l neuron nodes and the rewiring probability is P.

Step 2. Generate the multilayer feedforward regular neural network, as shown in Figure 6(a).

Step 3. As shown in Algorithm 1 where $p_1(h)$ is the probability to select reconnection layer, selection probability between two neurons decreases exponentially. α and β are the distance coefficients, rand and randint both are MATLAB functions, the former is used to generate a number between $(0, 1)$ randomly, and the latter can be used to randomly generate an integer from 1 to n_l. Since the connections of the $(L - 1)$th layer cannot generate new long-connections if they are disconnected, the connections of the last two layers are not reconnected in the network.

As shown in Figure 6(a), when the rewiring probability $P = 0$, the connection of the network maintains completely regular mode. Nonetheless, when P ranges from 0 to 1, the long cross-layer connections are generated according to the rewiring probability P and the probability of reconnection layer selecting. The resulting structure is between completely regular and random connection mode, as shown in Figure 6(b).

More specially, we set the network connection matrix as W, where W^l denotes the connection submatrix between the lth layer and the $(l + 1)$th layer. $w_{ij}^l \in R$ is the connection weight between the neuron i of the lth layer and the neuron j of the $(l + 1)$th layer. If there exists connection between these two neurons, then $w_{ij}^l \neq 0$; otherwise, $w_{ij}^l = 0$. Therefore, the regular network connection matrix can be expressed as the following equation:

$$W = \begin{pmatrix} 0 & W^1 & 0 & 0 & 0 & 0 & 0 \\ 0 & 0 & W^2 & 0 & 0 & 0 & 0 \\ 0 & 0 & 0 & W^3 & 0 & 0 & 0 \\ 0 & 0 & 0 & 0 & W^4 & 0 & 0 \\ 0 & 0 & 0 & 0 & 0 & W^5 & 0 \\ 0 & 0 & 0 & 0 & 0 & 0 & W^6 \\ 0 & 0 & 0 & 0 & 0 & 0 & 0 \end{pmatrix}, \quad (13)$$

in which the number zero means no connection exists between the corresponding layers. As for multilayer feedforward small-world neural network, because of the reconnection performance, the connection matrix changes into as

$$W' = \begin{pmatrix} 0 & W^1 & B_1^3 & B_1^4 & B_1^5 & B_1^6 & B_1^7 \\ 0 & 0 & W^2 & B_2^4 & B_2^5 & B_2^6 & B_2^7 \\ 0 & 0 & 0 & W^3 & B_3^5 & B_3^6 & B_3^7 \\ 0 & 0 & 0 & 0 & W^4 & B_4^6 & B_4^7 \\ 0 & 0 & 0 & 0 & 0 & W^5 & B_5^7 \\ 0 & 0 & 0 & 0 & 0 & 0 & W^6 \\ 0 & 0 & 0 & 0 & 0 & 0 & 0 \end{pmatrix}, \quad (14)$$

where W^l represents the reconnection submatrix between the lth layer and the $(l + 1)$th layer, and the $B_l^{l'}$ is the submatrix between two nonadjacent layers, which $l \in \{1, 2, \ldots 5\}$, $l' \in \{3, 4, \ldots 7\}$.

3.2. The Combination of the MFSNN and the Memristor

3.2.1. The Memristive Synapse. The nanoscale memristor has high potential of information storage on account of the nonvolatility with respect to long periods of power-down, so it can be used as electric synapse in the artificial neural networks, and the primary reasons are manifold. Firstly, as a kind of analog component, this device can realize weight updating continuously. Moreover, the memristor possesses the capacity of information storage due to the nonvolatility. This feature is consistent with the memory ability of the neurons in human's brain. Additionally, the memristive neural network can be further integrated in crossbar array which has significant advantages in better information processing capacity and huger storage.

According to the nonlinear memristor model in Section 2, the memristive conductance can be calculated from (12) as

$$G(t) = \frac{1}{M(t)} = \frac{1}{R_{\text{on}} + \Delta R\left(1/\left(Ae^{4kq(t)} + 1\right)\right)}. \quad (15)$$

Differentiating (15) with respect to time t, we can be obtain

$$\frac{dG(t)}{dt} = \frac{4kAe^{4kq(t)}\Delta R}{\left(R_{\text{on}}Ae^{4kq(t)} + R_{\text{off}}\right)^2} \times \frac{dq(t)}{dt}, \quad (16)$$

where the current $i(t) = dq(t)/dt$. Notably, when $\Delta t \to 0$, $dG(t) \approx \Delta G$. Hence, the rate of the memristive conductance ΔG can be described as the synapse weight update rule. The relationship curve between the rate of the memristive conductance change and the current is shown in Figure 7. When the current is tiny, the memristive conductance is almost invariant. While the current tends to ±4 mA, the memristive conductance changes suddenly. So the current threshold value of the memristive synapse can be set as $|I_{\text{th}}| = 4$ mA.

3.2.2. The Memristive Activation Function. In the standard MFSNN, the activation function for each neuron is usually the nonlinear Sigmoid function. Particularly, the activation function of the hidden layer adopts bipolar Sigmoid function, but the output layer activation function is unipolar Sigmoid function.

Based on the constitutive relationship of the memristor, a lot of nonlinear curves can be simulated and substituted [5, 6, 11, 12]. Based on the Simulink model of the nonlinear memristor described in Section 2, we get its simplified Simulink model accordingly as shown in Figure 8(a). Furthermore, we design a package of the memristive device (in Figure 8(b)) which can be considered as a system with single-input and double-output. In this system, the input variable is the current I, and the output variable is the memristance $M(t)$ and charge $q(t)$, respectively.

Then, the behavior of the output curve can be adjusted efficiently by the parameter control module, gain module, and internal operation module, which is crucial to implement the activation function in the neural network. Here, we set

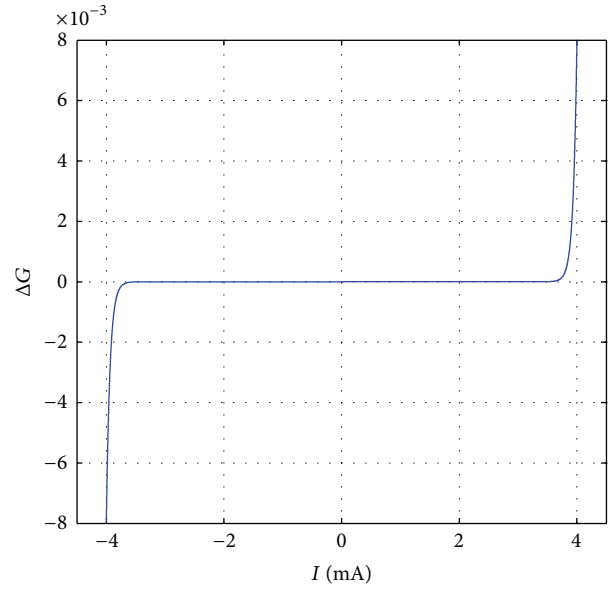

Figure 7: The relationship curve between the rate of the memristive conductance change and the current.

the activation functions for the hidden layer and output layer neurons of the memristive MFSNN as $h(x)$ and $y(x)$, respectively.

Figure 9(a) exhibits the constructing principle diagram of the memristive activation function in the hidden layer, in which the red dotted line frame represents the parameter adjustment area. K_1 is the adjustable gain which is used for controlling the shape of the activation function, and K_2 is the fixed gain whose value is $K_2 = 10^{-4}$. The suitable parameters of the memristor are chosen as $R_{\text{on}} = 100\,\Omega$, $R_{\text{off}} = 20\,\text{k}\Omega$, $M_0 = 10\,\text{k}\Omega$, $D = 10\,\text{nm}$, and $\mu_v \approx 10^{-14}\text{m}^2\text{s}^{-1}\text{V}^{-1}$. The input signal is a sinusoidal current with an amplitude of 0.5 mA and a frequency of 1 Hz. Notably, the polarity of the voltage applied into the memristor is opposite to the polarity of the memristor itself; that is, the current flows through the memristor from the negative polar to the positive polar. Figure 9(b) shows the memristive activation function of the hidden layer, and its shape varies with different values of K_1.

Similarly, Figure 10(a) is the constructing principle diagram of the activation function of the output layer. In the parameter adjustment part (the red dotted line frame), K_3 is an adjustable gain and K_4 is the fixed gain whose value is $K_4 = 2 \times 10^{-4}$. The parameters are the same with the simulation in Figure 9. Figure 10(b) shows the memristive activation function of the output layer. Obviously, as the value of K_3 increases, the graphs tend to flatten.

4. The Memristive Intelligent PID Controller

So far, the PID control has found widespread applications in the modern control field. By adjusting the control action of the proportion, integration, and differentiation, we get an interactive nonlinear relationship among these control variables. The neural network has the ability of expressing

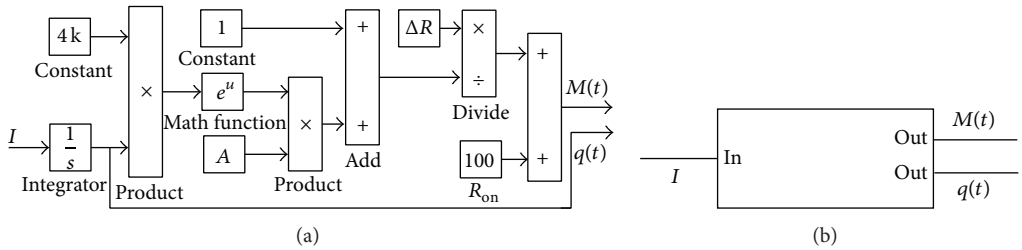

Figure 8: The simplified memristor model. (a) The simplified Simulink model of the memristor. (b) The package of the memristor.

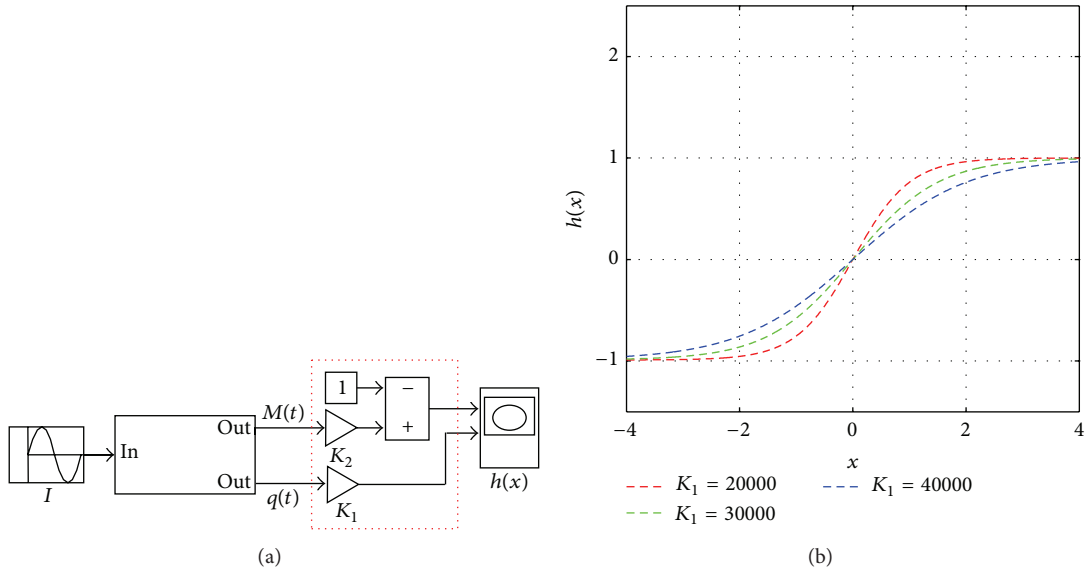

Figure 9: The principle diagram of the memristive activation function in the hidden layer. (a) The Simulink model of the memristive activation function in the hidden layer. (b) The curve of the memristive activation function $h(x)$.

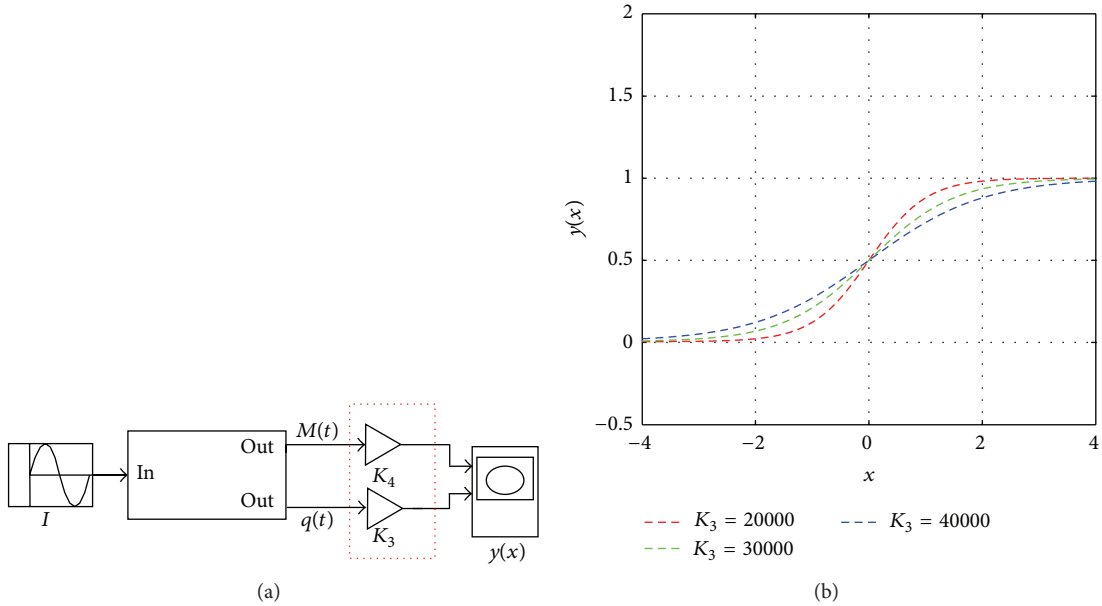

Figure 10: The principle diagram of the memristive activation function of the output layer. (a) The Simulink model of the memristive activation function of the output layer. (b) The curve of the memristive activation function $y(x)$.

the nonlinearity, which can be used in the PID control for implementing the optimal nonlinear relationship among control variables. In this work, we build up a more intelligent PID controller with the parameters (k_p, k_i, and k_d) self-tune based on the presented memristive multilayer feedforward small-world neural network.

According to the literature [30], the classical incremental digital PID control algorithm can be described as

$$\begin{aligned} u(k) &= u(k-1) + k_p\left(e(k) - e(k-1)\right) \\ &\quad + k_i e(k) + k_d\left(e(k) - 2e(k-1) + e(k-2)\right), \end{aligned} \tag{17}$$

where the k_p, k_i, and k_d are the coefficient of the proportion, integration, and differentiation, respectively.

In Figure 11, the ANN is the memristive multilayer feedforward small-world neural network. Its learning algorithm consisted of the backward error propagation and the forward input signal propagation. Different from the traditional multilayer feedforward neural network, the state of the neurons in each layer not only affects the state of the neurons in the next layer but also affects the state of the neurons in the cross-layer.

Based on the novel neural network presented in Section 3, we set the j, i, and l that represent the input layer, hidden layer, and output layer, respectively. The number of the input layer is 1 which is same with that of the output layer, and the number of the hidden layer is S. x_i represents the input vector of the network, then the set of the input samples is $O_j^1 = [x_1, x_2, x_3, \ldots, x_N]$. The number of the input vectors is dependent on the complexity of the system. Notably, the superscript 1 represents the first layer in the whole neural network.

The input and output vectors of the first hidden layer can be expressed as

$$\begin{aligned} \mathrm{net}_i^{i_1}(k) &= \sum_{j=0}^{N} w_{ij}^{i_1} O_j^1 \\ O_i^{i_1}(k) &= h\left(\mathrm{net}_i^{i_1}(k)\right) \\ i &= 1, 2, 3, \ldots, Q, \end{aligned} \tag{18}$$

where the superscript i_1 denotes the first hidden layer of the network and $h(x)$ is the memristive bipolar sigmoid function proposed in Section 3.

By that analogy, the input and output vectors of the Sth hidden layer can be written as

$$\begin{aligned} \mathrm{net}_i^{i_s}(k) &= \sum_{j=0}^{N} w_{ij}^{i_s} O_j^1 + \sum_{a=1}^{s-1}\sum_{b=1}^{s} w_{i_a i_s}^{i_s} \mathrm{net}_b^{i_s}(k) \\ O_i^{i_s}(k) &= h\left(\mathrm{net}_i^{i_s}(k)\right) \\ i &= 1, 2, 3, \ldots, Q. \end{aligned} \tag{19}$$

Finally, the input and output vectors of the output layer can be obtained as

$$\begin{aligned} \mathrm{net}_l^{s+2}(k) &= \sum_{j=0}^{N} w_{il}^{s+2} O_j^1 + \sum_{a=1}^{s}\sum_{b=1}^{s} w_{i_a l}^{s+2} \mathrm{net}_b^{s+2}(k) \\ O_l^{s+2}(k) &= y\left(\mathrm{net}_l^{s+2}(k)\right) \\ l &= 1, 2, 3, \end{aligned} \tag{20}$$

where $y(x)$ denotes the memristive unipolar sigmoid function. The three nodes of the output layer are corresponding with the nonnegative adjustable parameters k_p, k_i, and k_d of the PID controller, respectively.

From [27], we conclude the weight update algorithm of the memristive multilayer feedforward small-world neural network as below:

$$\begin{aligned} \Delta w_{li}^{s+2}(k) &= \alpha \Delta w_{li}^{s+2}(k-1) + \eta \delta_l^{s+2} O_i^{s+1}(k) \\ w_{li}^{s+2}(k+1) &= w_{li}^{s+2}(k) + \Delta w_{li}^{s+2}(k), \end{aligned} \tag{21}$$

where α is the inertial coefficient, whose scope ranges from 0 to 1, and $\eta \in (0, 1)$ is the learning rate.

5. Computer Simulations and Results

In this section, some numerical simulations of the memristive multilayer feedforward small-world neural network PID controller have been executed on MATLAB software. The mathematical model of the controlled plant is given as

$$y_{\mathrm{out}}(k) = \frac{a(k)\, y_{\mathrm{out}}(k-1)}{1 + y_{\mathrm{out}}^2(k-1)} + u(k-1), \tag{22}$$

where the $a(k)$ is slow time-variant and its expression is $a(k) = 1.2(1 - 0.8e^{0.1k})$.

The memristive neural network under investigation is constituted by seven layers with four neurons in the input layer, three neurons in the output layer, and five in each of the five hidden layers. The learning rate of the network $\eta = 0.4$, and the inertial coefficient $\alpha = 0.05$. The initial weighs as random values fall in $[-0.5\ 0.5]$, and the value of the rewiring probability is chosen as $P = 0$, $P = 0.08$, $P = 0.1$, and $P = 0.2$, respectively. The parameters are $R_{\mathrm{on}} = 100\,\Omega$, $R_{\mathrm{off}} = 20\,\mathrm{k}\Omega$, $M_0 = 10\,\mathrm{k}\Omega$, $D = 10\,\mathrm{nm}$, and $\mu_v \approx 10^{-14}\,\mathrm{m^2 s^{-1} V^{-1}}$, K_1 and K_3 are user-specified parameters whose value both are 20000, and the action time is $ts = 0.001$ s. When the system works steadily, the tracking results can be gotten as follows.

Figure 12(a) shows the input signal (step response curve $r_{\mathrm{in}}(k) = 1.0$) and the output curves under a different rewiring probability P. As can be seen from the figure, when the time $t = 0.5$ s, the whole system reaches the steady state. Making a further analysis, we can conclude that when the rewiring probability $P = 0$, the memristive neural network keeps regularly in architecture. Its respond speed is slower than that of network when the rewiring probability $P = 0.08$ and $P = 0.1$. Moreover, Figure 12(b) exhibits the error curves between the input signal and the output signal

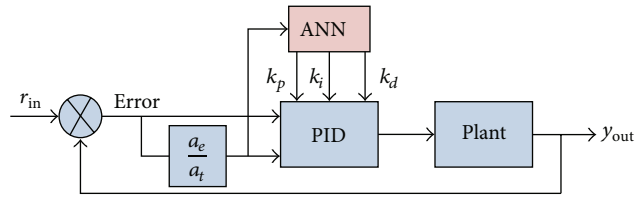

FIGURE 11: The structure diagram of the memristive neural network PID controller.

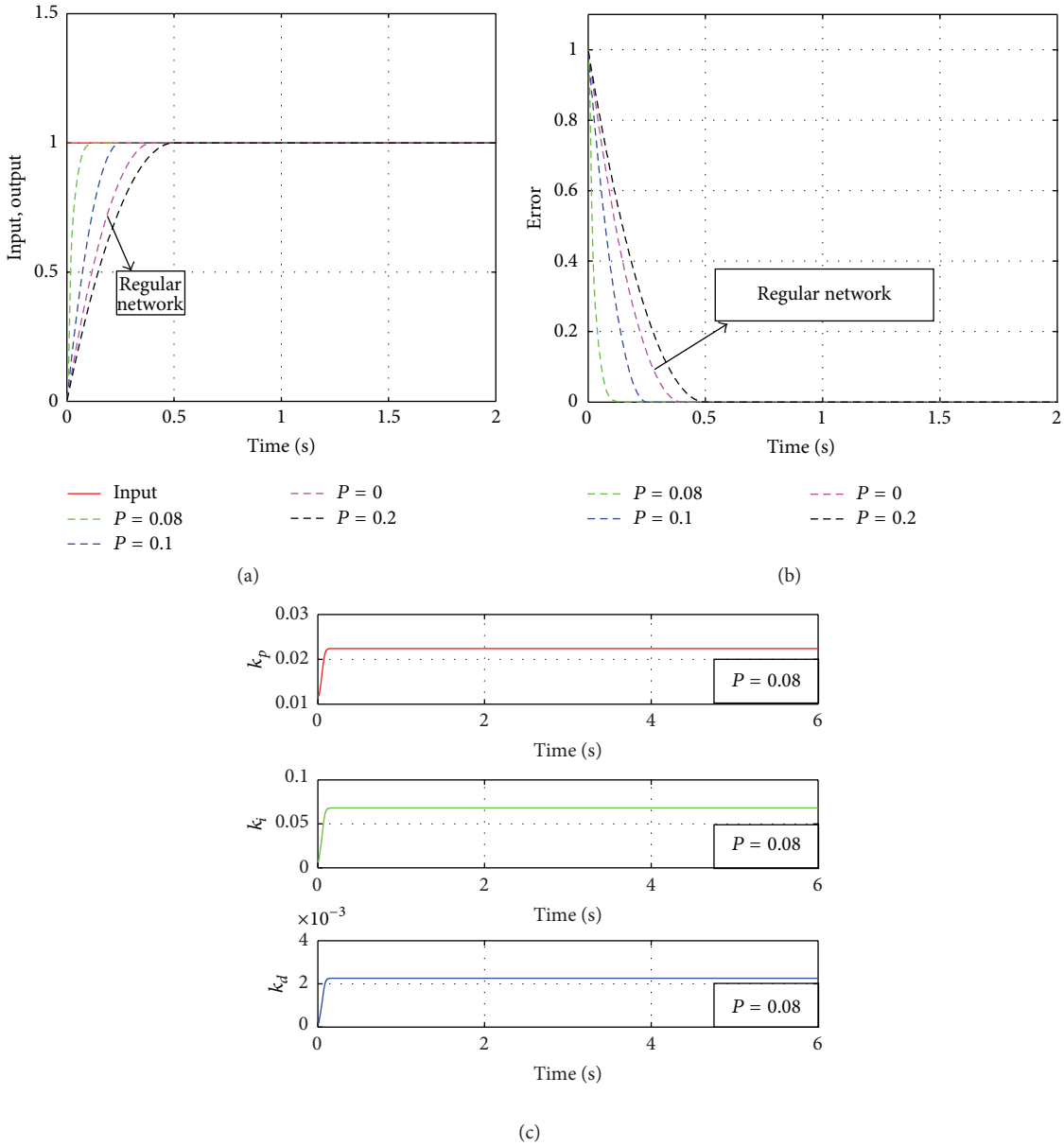

FIGURE 12: The simulation results of the memristive neural network PID controller ($r_{in}(k) = 1.0$) under a different rewiring probability P. (a) The step response curve. (b) The error curves. (c) The curves of the control parameters when the rewiring probability $P = 0.08$.

correspondingly. When the rewiring probability $P = 0.08$ and $P = 0.1$, the network spends less time on approaching the predefined approximation error than the regular network (when $P = 0$). Figure 12(c) shows the output variables of the memristive multilayer feedforward small-world neural network when $P = 0.08$ which are the control parameters k_p, k_i, and k_d, correspondingly.

In order to verify the superior performance of the memristive small-world neuronal networks and figure out the optimal structure, we conducted a series of simulations to

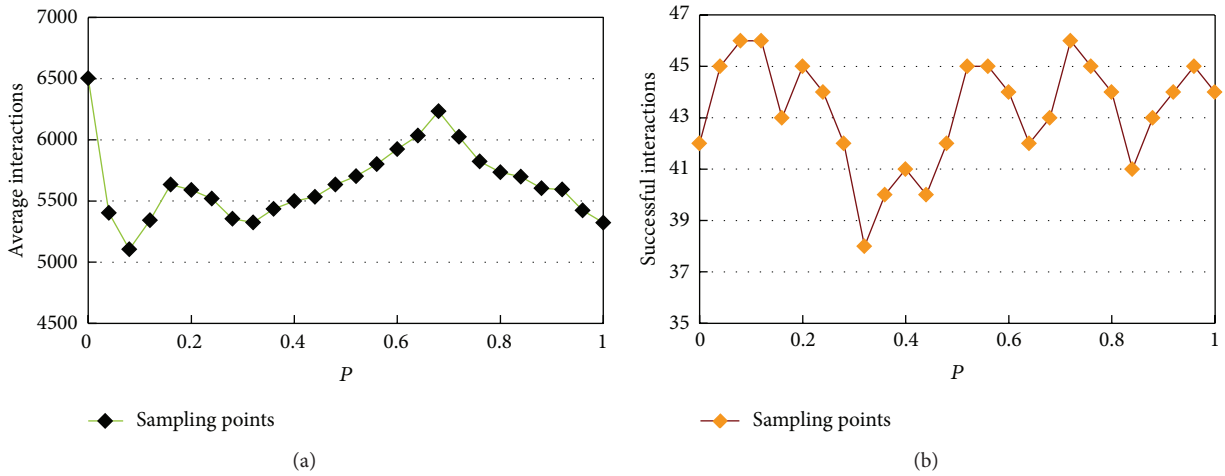

FIGURE 13: The convergence performance of the memristive neural network under different P. (a) The relationship between iteration and rewiring probability. (b) The effective approximation number in 50 times simulations under varying rewiring probability.

observe the convergence performance of the proposed network under different P. Figure 13(a) shows the approximation speed (iteration times) of different network structures, that is, the smallest iteration number for reaching the predefined approximation error $\varepsilon = 0.0001$. Each drawn point is the average value of 50 times runs. It can be observed that the small-world networks ($0 < P < 1$) need much less iteration times than the regular neural network (when $P = 0$), which demonstrates its advantage in processing speed. Furthermore, when $P = 0.08$, the network has the fast approximation speed.

Notably, the mathematical function of this system has the local minimum, for getting out of the local minimum, we define the maximum allowable iteration times to be 10000, as previously mentioned for each P, and we performed the simulation for 50 times, where the effective approximation times, that is, error < 0.0001 within 10000 iterations, are presented in Figure 13(b). It can be found that the small-world networks have higher accuracy rate than the regular network.

6. Conclusions

A mathematical closed-form charge-governed memristor model is recalled firstly and the corresponding Simulink model is presented. Using the change rule of memconductance, a memristive realization scheme for synaptic weight is proposed. Moreover, the activation functions in electric neurons are also implemented based on the single-input and double-output package of the memristor. Combining the proposed memristive synapse and activation functions, a memristor-based MFSNN is addressed. It exhibits advantages in computation speed and accuracy over the traditional multilayer neural networks by considering the small-world effect. Meanwhile, it has potential of hardware realization of the neural network because of the nanoscale size of the memristive synapse. These superior properties can further improve the application of the neural networks, such as in the intelligent controller design. Motivated by this, we apply the memristor-based MFSNN to classical PID control, and the proposed memristive PID controller may possess the following superiorities. (i) Its nanoscale physical implementation could promote the development of the microcontroller. (ii) Because of the participation of the memristive neural network, the proposed PID controller can realize the parameters self-adjustment. (iii) The control speed and accuracy are improved. Eventually, extensive numerical simulations justify the effectiveness and efficiency of the memristive PID controller over the regular neural network PID controller. This work may provide a theoretical reference to physically realize the small-world neural networks and further promote the development of modern intelligent control technology.

Conflict of Interests

The authors declare that there is no conflict of interests regarding the publication of this paper.

Acknowledgments

The work was supported by Program for New Century Excellent Talents in University (Grant nos. [2013] 47), National Natural Science Foundation of China (Grant nos. 61372139, 61101233, and 60972155), "Spring Sunshine Plan" Research Project of Ministry of Education of China (Grant no. z2011148), Technology Foundation for Selected Overseas Chinese Scholars, Ministry of Personnel in China (Grant no. 2012-186), University Excellent Talents Supporting Foundations in of Chongqing (Grant no. 2011-65), University Key Teacher Supporting Foundations of Chongqing (Grant no. 2011-65), Fundamental Research Funds for the Central Universities (Grant nos. XDJK2014A009, XDJK2013B011).

References

[1] L. O. Chua, "Memristors: the missing circuit element," *IEEE Transactions on Circuits and Systems*, vol. 18, pp. 507–519, 1971.

[2] J. M. Tour and H. Tao, "*Electronics*: the fourth element," *Nature*, vol. 453, no. 7191, pp. 42–43, 2008.

[3] D. B. Strukov, G. S. Snider, D. R. Stewart, and R. S. Williams, "The missing memristor found," *Nature*, vol. 453, pp. 80–83, 2008.

[4] R. S. Williams, "How we found the missing Memristor," *IEEE Spectrum*, vol. 45, no. 12, pp. 28–35, 2008.

[5] S. K. Duan, X. F. Hu, L. D. Wang, C. D. Li, and P. Mazumder, "Memristor-based RRAM with applications," *Science China Information Sciences*, vol. 55, no. 6, pp. 1446–1460, 2012.

[6] X. F. Hu, S. K. Duan, L. D. Wang, and C. D. Li, "Analog memory based on pulse controlled memristor," *Journal of the University of Electronic Science and Technology of China*, vol. 40, no. 5, pp. 642–647, 2011.

[7] S. Shin, K. Kim, and S. Kang, "Resistive computing: memristors-enabled signal multiplication," *IEEE Transactions on Circuits and Systems I: Regular Papers*, vol. 60, no. 5, pp. 1241–1249, 2013.

[8] S. P. Adhikari, C. Yang, H. Kim, and L. O. Chua, "Memristor bridge synapse-based neural network and its learning," *IEEE Transactions on Neural Networks and Learning Systems*, vol. 23, no. 9, pp. 1426–1435, 2012.

[9] S. H. Jo, T. Chang, I. Ebong, B. B. Bhadviya, P. Mazumder, and W. Lu, "Nanoscale memristor device as synapse in neuromorphic systems," *Nano Letters*, vol. 10, no. 4, pp. 1297–1301, 2010.

[10] Y. Dai, C. Li, and H. Wang, "Expanded HP memristor model and simulation in STDP learning," *Neural Computing and Applications*, vol. 24, no. 1, pp. 51–57, 2014.

[11] S. K. Duan, X. F. Hu, L. D. Wang, S. Y. Gao, and C. D. Li, "Hybrid memristor/RTD structure-based cellular neural networks with applications in image processing," *Neural Computing and Applications*, vol. 25, no. 2, pp. 291–296, 2014.

[12] L. Chen, C. D. Li, T. W. Huang, and Y. R. Chen, "Memristor crossbar-based unsupervised image learning," *Neural Computing and Applications*, vol. 25, no. 2, pp. 393–400, 2013.

[13] X. F. Hu, S. K. Duan, L. D. Wang, and X. F. Liao, "Memristive crossbar array with applications in image processing," *Science China Information Sciences*, vol. 41, pp. 500–512, 2011.

[14] B. Mouttet, "Proposal for memristors in signal processing," in *Nano-Net: 3rd International ICST Conference, NanoNet, Boston, MS, USA, September 14–16, 2008, Revised Selected Papers*, vol. 3 of *Lecture Notes of the Institute for Computer Sciences, Social Informatics and Telecommunications Engineering*, pp. 11–13, 2009.

[15] H. Abdalla and M. D. Pickett, "SPICE modeling of memristors," in *Proceedings of the 2011 IEEE International Symposium of Circuits and Systems (ISCAS '11)*, pp. 1832–1835, May 2011.

[16] X. B. Wang, Y. R. Chen, H. W. Xi, and D. Dimitrov, "Spintronic memristor through spin-thorque-induced magnetization motion," *IEEE Electron Device Letters*, vol. 30, no. 3, pp. 294–297, 2009.

[17] D. B. Strukov and R. S. Williams, "Exponential ionic drift: fast switching and low volatility of thin-film memristors," *Applied Physics A: Materials Science & Processing*, vol. 94, pp. 515–519, 2009.

[18] F. Corinto, A. Ascoli, and M. Gilli, "Mathematical models and circuit implementations of memristive systems," in *Proceedings of the 13th International Workshop on Cellular Nanoscale Networks and their Applications (CNNA '12)*, pp. 1–6, August 2012.

[19] S. Kvatinsky, E. G. Friedman, A. Kolodny, and U. C. Weiser, "TEAM: ThrEshold adaptive memristor model," *IEEE Transactions on Circuits and Systems. I: Regular Papers*, vol. 60, no. 1, pp. 211–221, 2013.

[20] O. Sporns and C. J. Honey, "Small worlds inside big brains," *Proceedings of the National Academy of Sciences of the United States of America*, vol. 103, no. 51, pp. 19219–19220, 2006.

[21] P. Tangkraingkij, C. Lursinsap, S. Sanguansintukul, and T. Desudchit, "Insider and outsider person authentication with minimum number of brain wave signals by neural and homogeneous identity filtering," *Neural Computing and Applications*, vol. 22, no. 1, pp. 463–476, 2013.

[22] D. S. Bassett and E. D. Bullmore, "Small-world brain networks," *Neuroscientist*, vol. 12, no. 6, pp. 512–523, 2006.

[23] D. J. Watts and S. H. Strogatz, "Collective dynamics of "small-world" networks," *Nature*, vol. 393, no. 6684, pp. 440–442, 1998.

[24] L. Douw, M. M. Schoonheim, D. Landi et al., "Cognition is related to resting-state small-world network topology: an magnetoencephalographic study," *Neuroscience*, vol. 175, pp. 169–177, 2011.

[25] T. Fekete, F. D. C. C. Beacher, J. Cha, D. Rubin, and L. R. Mujica-Parodi, "Small-world network properties in prefrontal cortex correlate with predictors of psychopathology risk in young children: a NIRS study," *NeuroImage*, vol. 85, part 1, pp. 345–353, 2014.

[26] N. R. Taylor, "Small world network strategies for studying protein structures and binding," *Computational and Structural Biotechnology Journal*, vol. 5, Article ID e201302006, 2013.

[27] D. Simard, L. Nadeau, and H. Kröger, "Fastest learning in small-world neural networks," *Physics Letters A: General, Atomic and Solid State Physics*, vol. 336, no. 1, pp. 8–15, 2005.

[28] Z. Biolek, D. Biolek, and V. Biolková, "SPICE model of memristor with nonlinear dopant drift," *Radioengineering*, vol. 18, no. 2, pp. 210–214, 2009.

[29] H. Kim, M. P. Sah, C. Yang, T. Roska, and L. O. Chua, "Memristor bridge synapses," *Proceedings of the IEEE*, vol. 100, no. 6, pp. 2061–2070, 2012.

[30] M. Esfandyari, M. A. Fanaei, and H. Zohreie, "Adaptive fuzzy tuning of PID controllers," *Neural Computing and Applications*, vol. 23, no. 1, pp. 19–28, 2013.

Hindawi Publishing Corporation
The Scientific World Journal
Volume 2014, Article ID 715963, 8 pages
http://dx.doi.org/10.1155/2014/715963

Research Article

Performance Analysis of Autonomous Microgrid Subsequent to Symmetrical and Unsymmetrical Fault Triggered Condition

Chitra Natesan,[1] Senthil Kumar Ajithan,[2] Shobana Mani,[1] Priyadharshini Palani,[1] and Prabaakaran Kandhasamy[3]

[1] *Department of Electrical & Electronics Engineering, SKP Engineering College, Anna University & Asso., Tiruvannamalai 606611, India*
[2] *Department of Electrical & Electronics Engineering, Velammal Engineering College, Chennai 600066, India*
[3] *Department of Electrical & Electronics Engineering, Sri Rangapoopathi College of Engineering, Gingee 604151, India*

Correspondence should be addressed to Chitra Natesan; psk_siva@hotmail.com

Received 6 May 2014; Revised 28 June 2014; Accepted 28 June 2014; Published 4 August 2014

Academic Editor: Guanghui Wen

Copyright © 2014 Chitra Natesan et al. This is an open access article distributed under the Creative Commons Attribution License, which permits unrestricted use, distribution, and reproduction in any medium, provided the original work is properly cited.

Hi-tech scenario and the ecological compression are the key point to drive the intervention of the renewable in the distribution system. In the perspective of complex power system planners, the transient performance of the microgrid is the main concern. For that purpose, various fault cases are explored in order to examine the microgrid transient performance when subjected to accidental events. In this work, the microgrid is modelled with two distributed generations (DGs) tied with a converter separately. With this intention, droop control strategy is adopted for the microsources to examine the microgrid performance during the symmetrical and unsymmetrical fault events. The ability of the control strategy adopted in this work and its effectiveness are evaluated through Matlab/Simulink platform.

1. Introduction

A new concept of microgrid (MG) was introduced with the help of power electronic devices and renewable energy sources. DG is considered to be a supplementary source of power in addition to the centralized power generation. Microsources and distributed generation combined with controllers, loads, and storage devices in order to compose a microgrid structure. Usually the microgrid sources are diesel generators, fuel cells, solar cells, and wind turbine. Distributed generations are usually combined with power electronic devices to get contact with the microgrid. DG interfaced with inverter can reduce oscillation throughout its fast control action [1].

Grid-tied mode and autonomous mode are the functions of microgrid system on the basis of static transfer switch position [2]. In case of any interruption, the microgrid should work on island mode to meet the demand in load. Also it should maintain power quality accordingly [3].

In case of real time, DG will breakdown accidentally or sometimes intentionally. So it has to provide uninterrupted supply; the microgrid has to sense mode of operation and switch to island mode in order to meet voltage supply for sensitive devices. This scenario is tough in real time for the power companies to provide reliable power supply [4]. But, in current industrial plot, it must detach DGs for the safety purpose. It also retards from switching to island mode to maintain protection constraints in distribution system.

Various research papers are discussed under the concept of transient stability subsequent to fault condition [5–11].

The author in [5] explores a new perspective by introducing different control strategies such as master slave approach and droop control approach for the transient stability analysis in a microgrid subsequent to fault triggered incident. In this work, diesel based generators and inverter based DG are composed. For inverter based DG, two control schemes such as real and reactive power (P and Q) control and current

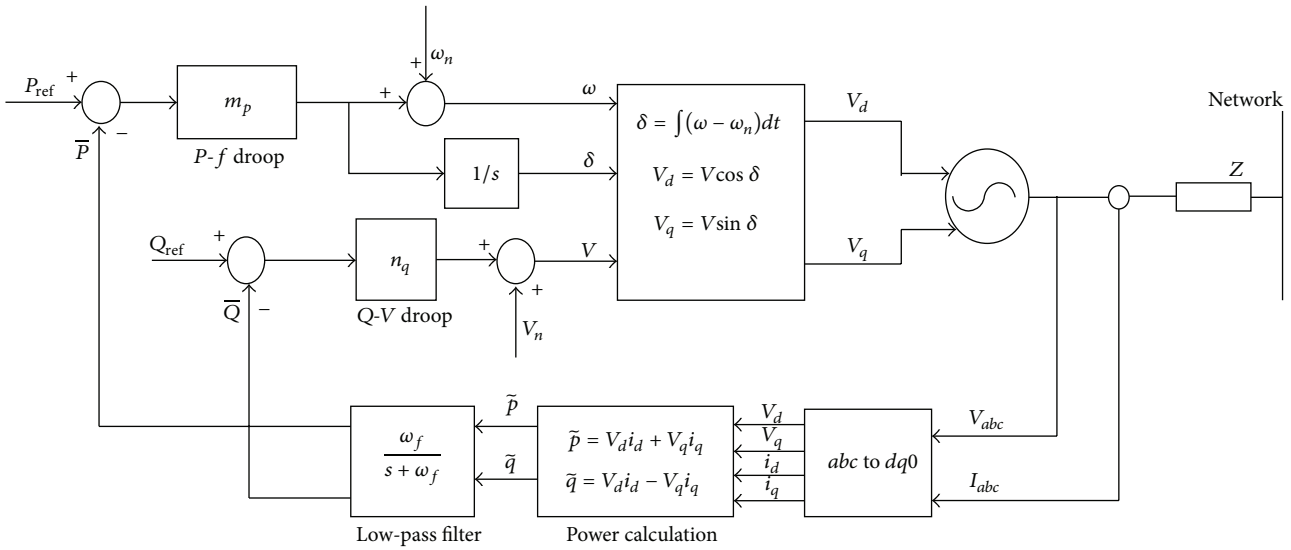

Figure 1: Droop control block diagram.

control scheme are introduced. Further, the author concluded that the droop control approach is best suited for subsequent transient incidents and P and Q control scheme holds good for inverter based DG.

Since the mechanism of microgrid operation differs from the traditional power grid, it is necessary to opt for the separate transient performance analysis [7]. So a dynamic model is projected for a microgrid to promote the difference among the microgrid and traditional grid transient analysis. In this work, differential algebraic equation is composed in order to model the dynamic system.

A new dimension of approach was conferred [8] about the transient stability in the course of network disruption in a wind farm when it is connected to a complex power system. To enhance the transient stability performance, superconducting magnetic energy storage (SMES) based controlled adaptive artificial neural network (ANN) was adopted. The SMES function on the basis of three criterions such as (i) voltage source converter (VSC), (ii) sinusoidal pulse width modulation (PWM), and (iii) an ANN controlled DC-DC converter using insulated gate bipolar transistors (IGBTs). Further, the ANN is compared with proportional integral (PI) on the basis of SMES control which is optimized by response surface methodology and genetic algorithm (RSM-GA) in view of both symmetrical and asymmetrical faults. Hence, in conclusion, the transient performance is better while adapting ANN controller than PI controller.

Another interesting technique was categorized in [9]; the effectiveness of two different models of doubly fed induction generator (DFIG) wind turbine is compared, that is, DFIG with dynamic voltage restorer (DVR) and DFIG with crowbar protection under different fault conditions. In the model of DFIG with crowbar protection, the reactive power production was found to be more complicated, whereas the model of DFIG with DVR helps to compensate the fault voltage so that the DFIG wind turbine provides an uninterruptable power supply as per the load demand without the need of any additional protection.

Another novel approach attempted in [10] is the enhancement of microgrid performance during fault conditions with the battery energy storage system controller (BESS). But it has the restrictions for the sustainable operation; that is, the remnant energy of BESS must be zero.

The author in [11] introduced a dynamic model for the general microgrid under different conditions such as island operation, emergency control function, and service restoration in case of block-out. Therefore, the author defined a new control procedure for microgrid operation and management in LV distribution networks. In addition, controllable loads are also modelled, which are in desperate need of load shedding.

When n number of inverter based DGs are connected in parallel to a microgrid system, there may raise problem in standalone operation, that is, less inertia which leads to either supply or consumption of energy during transient period. To resolve this problem, the author in [6] theoretically studied the small signal stability through Eigen value analysis.

It is compulsory to evaluate transient instability in order to prevent transient overloads. Highly dangerous transient overloads take part even though microsources are interconnected with power electronic devices [12]. Microgrid works parallel to main grid unless there is a fault in the system. It is hard to protect system from fault condition in case of grid connected mode. So the microgrid will operate separately after the fault event [13].

Concerning these common transient issues, a control strategy is developed to examine the performance of the microgrid. P-F and Q-V droop control are adopted to examine its impact during the transient stability period (Figure 1). Generally, the main use of the above method is to share appropriate power to DGs with the help of maintaining frequency and voltage [14, 15].

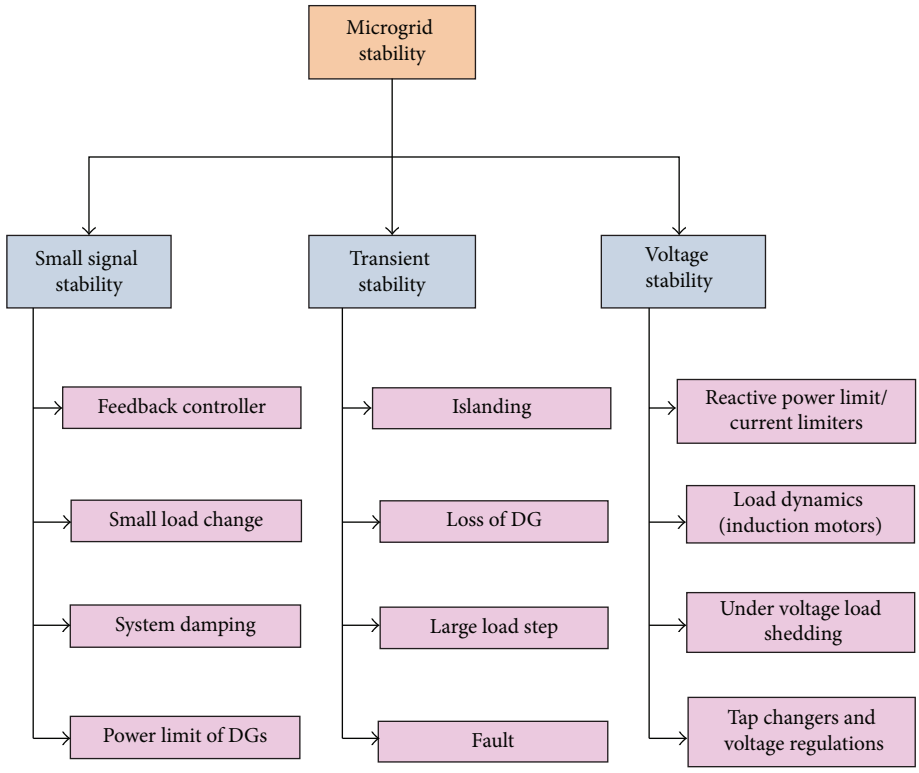

Figure 2: Different stability issues in microgrid.

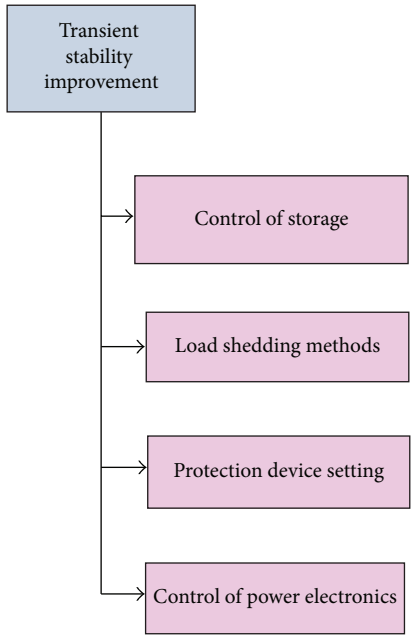

Figure 3: Different transient stability improvement methods.

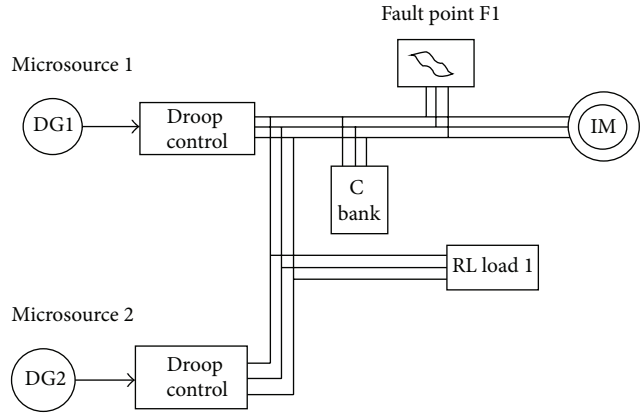

Figure 4: Single line layout of the utility and microgrid systems.

The impact of droop control technique and the stability of the DG based on inverter arrangement of microgrid consequent to fault-forced autonomous circumstances are examined in this work. Further, the microgrid stability performance is scrutinised with induction motor (IM) loads. MatLab/Simulink and its libraries (mainly the sim power systems toolbox) were employed in order to develop a simulation platform suitable for identifying MG control requirements and evaluating MG dynamic behaviour under several operating conditions.

2. Control Strategies

In microgrid, the system reliability and stability are achieved only by the voltage regulation when more microsources are interconnected. This voltage regulation damps the reactive power oscillations and voltage [16]. In a complex power

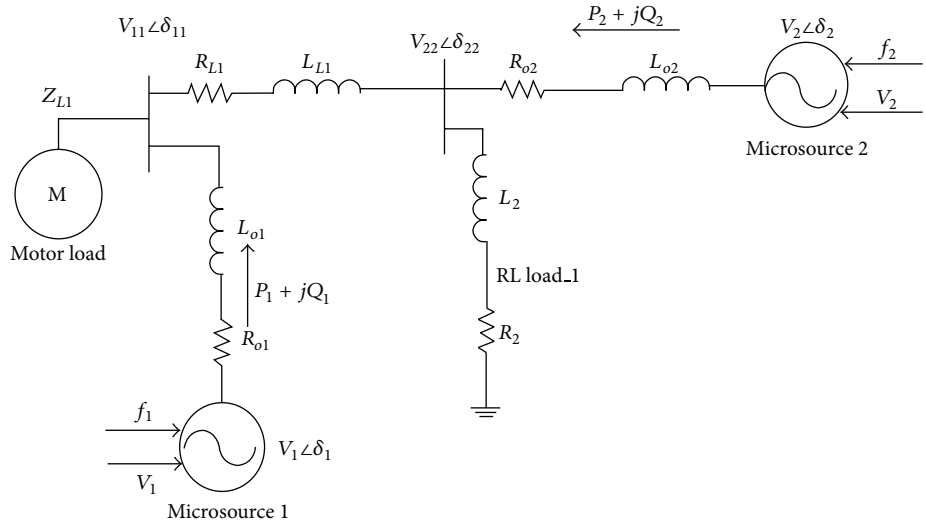

Figure 5: Equivalent model of the microgrid systems.

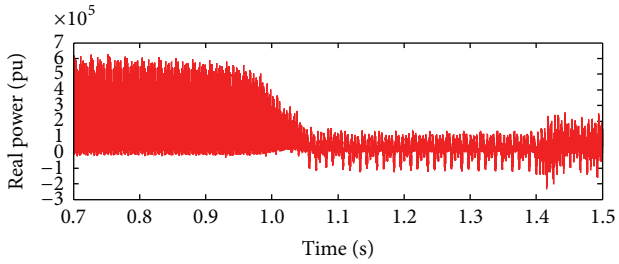

Figure 6: Real power during L-G fault.

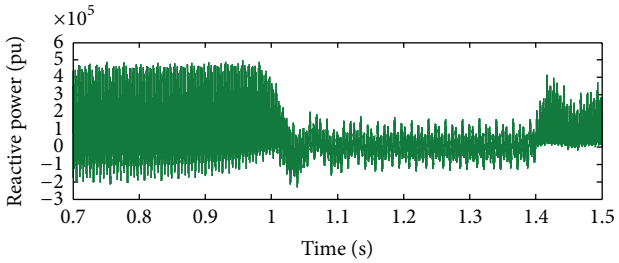

Figure 7: Reactive power during L-G fault.

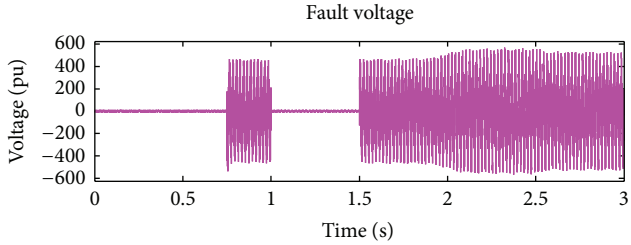

Figure 8: Load voltage during L-G fault.

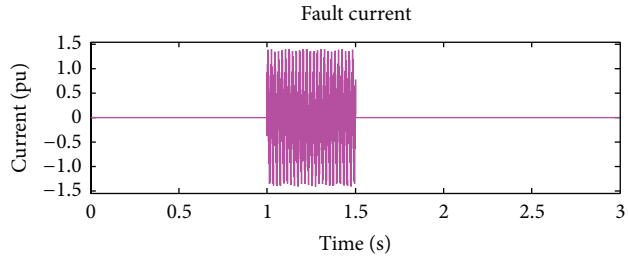

Figure 9: Load current during L-G fault.

system, when multiple DGs are attached to the microgrid, the power sharing among them is made properly with the help of a control strategy called droop control. Droop control also enables the system to disconnect smoothly and reconnect routinely to the complex power system [17].

The role of droop control in this work is that it controls the real power on the basis of frequency droop control and it controls the reactive power on the basis of voltage control [18, 19]. The voltage and frequency can be manipulated by regulating the real and reactive power of the system. This forms a droop control equation.

In a transmission line, the real and reactive power are designed as

$$P = \frac{V1V2}{X}\,\mathrm{Sin}\,\delta,$$
$$Q = \frac{V1^2}{X} - \frac{V1V2}{X}\,\mathrm{Cos}\,\delta. \quad (1)$$

In the abovementioned equation (1), resistance (R) is neglected for overhead transmission lines as it is much

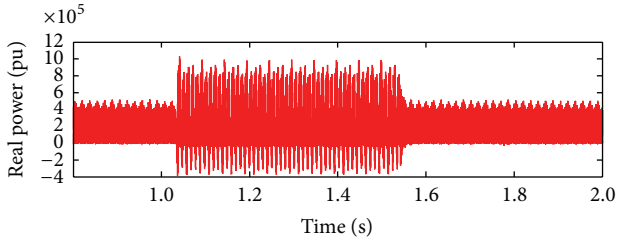

Figure 10: Real power during L-L fault.

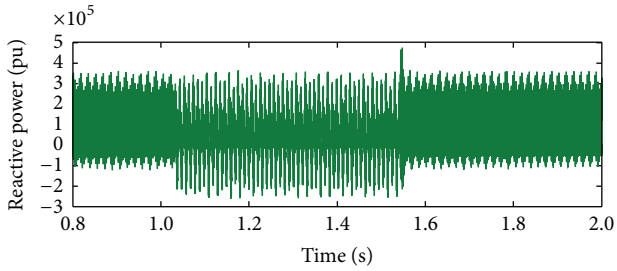

Figure 11: Reactive power during L-L fault.

lower than inductance (L). Also the power angle δ is lesser. Therefore, $\sin\delta = \delta$ and $\cos\delta = 1$.

$$\delta = \frac{XP}{V1V2},$$
$$V1 - V2 \cong \frac{XQ}{V1}. \tag{2}$$

Hence, from the above equation (2), it is clear that the power angle δ can be controlled by regulating real power P. Also, the voltage $V1$ can be controlled through reactive power Q. Dynamically, the frequency control leads to regulating the power angle and this in turn controls the real power flow [20]. Finally, the frequency and voltage amplitude of the microgrid are manipulated by adjusting the real and reactive power autonomously. As a result, the frequency and voltage droop regulation can be determined as

$$f - f_0 = K_p\left(P - P_0\right),$$
$$V - V_0 = K_q\left(Q - Q_0\right). \tag{3}$$

The relationship between real power, frequency, and reactive power, voltage, can be manipulated from (3):

$$f = f_0 + K_p\left(P - P_0\right),$$
$$V = V_0 + K_q\left(Q - Q_0\right), \tag{4}$$

where f, V = the frequency and voltage at a new operating point. P, Q = active and reactive power at a new operating point. f_0, V_0 = base frequency and voltage. P_0, Q_0 = temporary set points for the real and reactive power. K_p, K_q = droop constant.

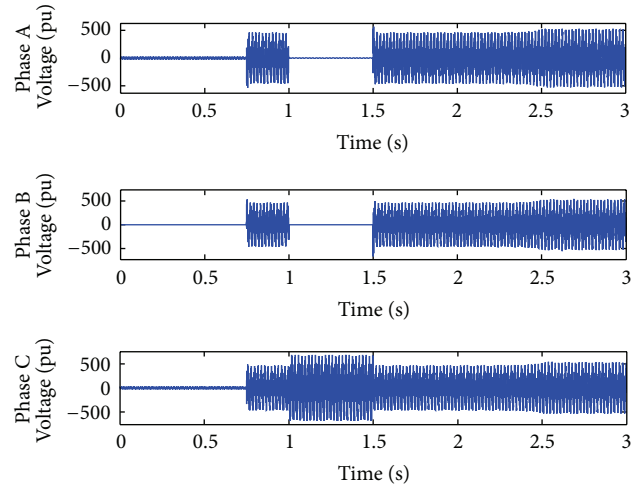

Figure 12: Load voltage during L-L fault.

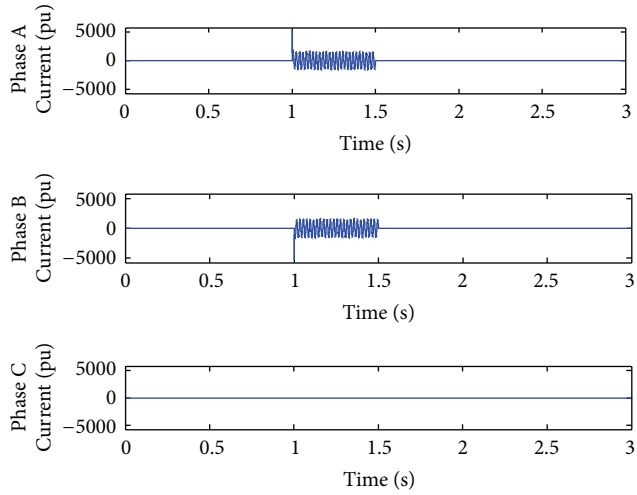

Figure 13: Load current during L-L fault.

3. Stability Analysis

In recent researches, the stability issue in the microgrid seems to be gaining its attention. The power system engineers chiefly focus the restructuring in the power system particularly when exposed to a severe disturbance. Typically, the system designers target the aspect of reliable and stable power supply as per their load demands [21, 22]. Among various stability issues of microgrid, transient stability alone is considered in this work. In course of islanding process, the transient effects depend on the criterions such as (i) working conditions before islanding and (ii) the events which cause islanding. Even though it may be planned or unplanned islanding, the microgrid is expected to stay in working condition. Therefore, it is necessary to enhance the dynamic response of the microgrid [23].

3.1. Transient Stability. Even at more disturbances, the microgrid can perform its action without any interventions. This

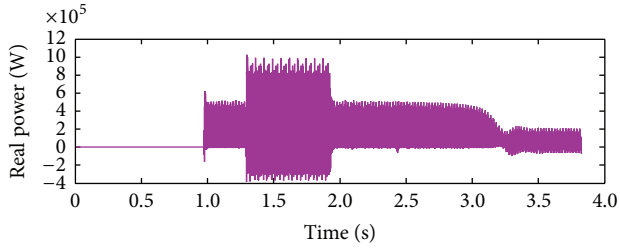

Figure 14: Real power during LLG fault.

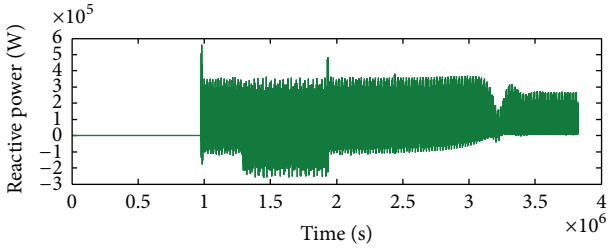

Figure 15: Reactive power during LLG fault.

function changes the microgrid mode from grid-tied mode to island mode. There is a possibility of occurrence of heavy disturbance in power system due to switching of heavy loads or transmission line fault. Hence, this disturbance will lead to synchronisation loss in the system. It is represented as transient stability [24]. In recent times, many system stability issues have been researched and some stability improvement methods have been developed which are shown in Figures 2 and 3. Control strategies, microsources, and type of microgrid are the main parameters of stability. All the microsources are connected to power electronic devices, that is, here voltage source inverter. So the control method of power electronic devices controls the stability [25, 26].

4. Simulation Model

The microgrid is modelled with two microsources which have a DC source as input and the P-F and Q-V droop control have been employed. At the time of starting, RL load is connected to the system as shown in Figure 4 and its equivalent model is shown in Figure 5. In order to highlight the performance difference of microgrid when connected with normal load and nonlinear load, induction motor is connected at 0.75 sec and disconnected at 2.5 sec. As a next, study about the activity of microgrid with RLload during fault triggered incident is analyzed. To perform this activity, a LG fault was introduced for a period of 1 to 1.5 secs. This microgrid system has been simulated under the Matlab/Simulink software environs.

5. Simulation Result

With the intention of authenticating the aforesaid control strategies, AC system was programmed to evaluate its performance when subjected to various faults. The symmetrical and unsymmetrical fault analysis was implemented in a Matlab/Simulink platform. The parameters such as real and reactive power, fault voltage, fault current, and the rotor speed waveforms are presented for all the faults in Figures 4 and 5.

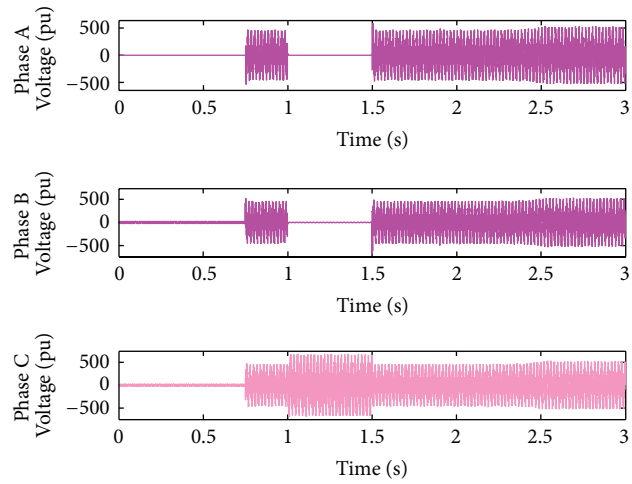

Figure 16: Fault voltage during LLG fault.

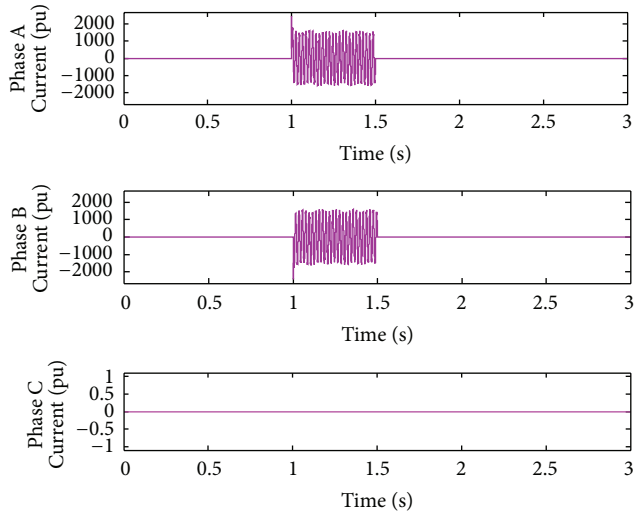

Figure 17: Fault current during LLG fault.

Case 1. LG fault occurs on phase A. The single line to ground fault occurs on phase A. The duration of the fault period is from 1 sec to 1.5 sec. After 1.5 sec, induction motor load will act, and this results in a gradual increase for a short duration and then it attains constant. The real and reactive power behaviour during faulty period is exposed in Figures 6 and 7. Initially, the voltage on the IM load side is zero as the IM load is included only at 0.75 sec. The IM load voltage is at 440 V as soon as the motor starts but it instantly drops to zero when the L-G fault occurs, that is, at 1 sec. So the load voltage remains at zero until the L-G fault is recovered, that is, till 1.5 sec. After 1.5 sec, the load voltage increases to 440 V. Similarly, during fault event, the fault current will increase to its maximum value of 1.5 mA from 1 sec to 1.5 sec. It will

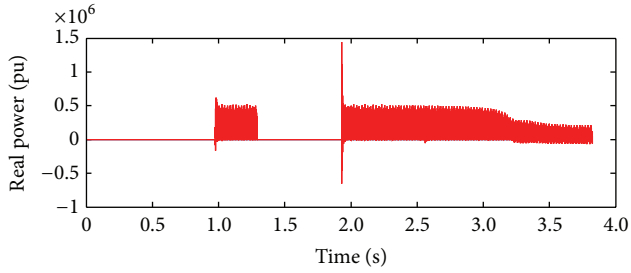

Figure 18: Real power during LLLG fault.

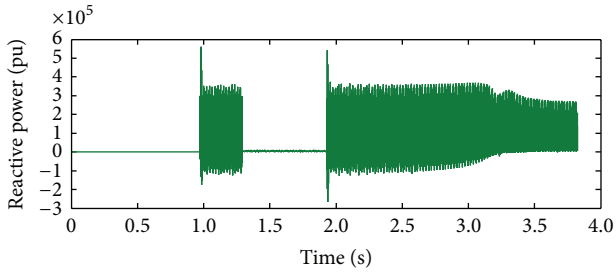

Figure 19: Reactive power during LLLG fault.

remain zero throughout the operating period as illustrated in Figures 8 and 9.

Case 2. LL fault occurs on phase A and phase B. The line to line fault occurs on phase A and phase B. The duration of the fault period is from 1 sec to 1.5 sec. As illustrated in Figures 10 and 11, initially the real power maintains a constant value till 1 sec. From 1 to 1.5 sec, the real power shoots up drastically about 10 pu. After the fault period, it regains its original value. Figure 12 illustrates the load voltage on the IM load side performance during fault on phase A and phase B. Voltage of phase A and phase B falls to zero, while voltage swell which exists in phase C can be seen during the faulty condition. In the same way, the current of phase A and phase B shoots up to its maximum value, while the current of phase C remains zero, Figure 13.

Case 3. LLG fault occurs on phase A and phase B to ground. From Figures 14 and 15, the behaviour of the real and reactive power on source side during faulty condition is clearly revealed. Since phase A and phase B were affected by the fault, phase C still continues to supply a maximum permissible power. At 1.5 sec, the circuit breaker connects the system and the IM load is included. As per Figures 16 and 17, the fault voltage and fault current fluctuate accordingly.

Case 4. LLLG fault—symmetrical fault. For the stability analysis, 3LG fault is also considered along with the asymmetrical fault. The fault occurs at the fault position F1 on the load side as shown in Figure 4. The real and reactive power on the source side and the voltage and current at the time of fault are projected. The real power and reactive power are controlled to the sufficient level during the fault period by means of the proposed droop control strategy. Figures 18 and 19 show the response of real and reactive power. The voltage and current

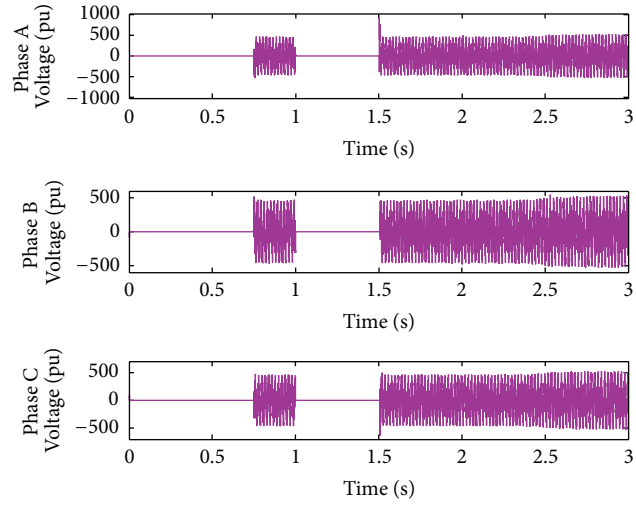

Figure 20: Fault voltage during LLLG fault.

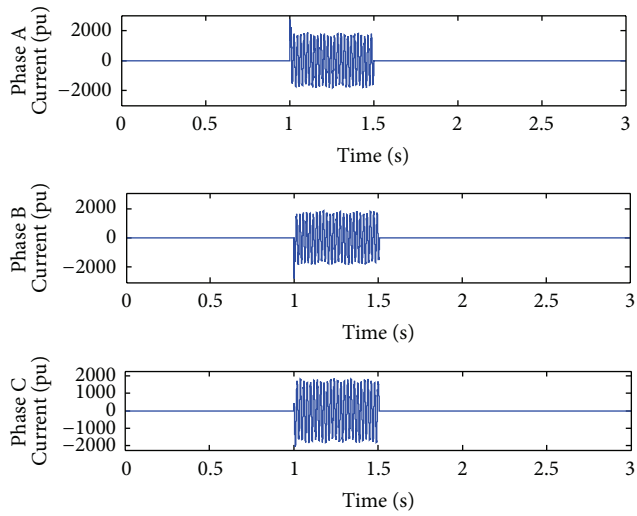

Figure 21: Fault current during LLLG fault.

behaviour on the faulty condition are presented in Figures 20 and 21.

6. Conclusion

This paper explores the microgrid system behaviour when it is exposed to the consequent faults like symmetrical fault (LLLG) and asymmetrical fault (L-G, LL, and LLG). With this intention to enhance the system performance, droop control technique is adopted. Particularly *P-F* droop control technique is enabled for the inverter based DGs. For the simulation results, it is evidence that the droop control strategy enhances the performance of DGs during the various faults conditions and also when the DGs are connected to the IM load and RL load. The simulation results evidenced that the proposed power controller proffers an exceptional response in regulating the microgrid voltage and

frequency with an allowable level of harmonic content during autonomous mode.

Conflict of Interests

The authors declare that there is no conflict of interests regarding the publication of this paper.

References

[1] Z.-x. Xiao and H.-w. Fang, "Impacts of P-f & Q-V droop control on microgrids transient stability," *Physics Procedia*, vol. 24, pp. 276–282, 2012.

[2] S. M. Ashabani and Y. A. I. Mohamed, "A flexible control strategy for grid-connected and islanded microgrids with enhanced stability using nonlinear microgrid stabilizer," *IEEE Transactions on Smart Grid*, vol. 3, no. 3, pp. 1291–1301, 2012.

[3] C. X. Dou and B. Liu, "Transient control for micro-grid with multiple distributed generations based on hybrid system theory," *International Journal of Electrical Power and Energy Systems*, vol. 42, no. 1, pp. 408–417, 2012.

[4] I. J. Balaguer, Q. Lei, S. Yang, U. Supatti, and F. Z. Peng, "Control for grid-connected and intentional islanding operations of distributed power generation," *IEEE Transactions on Industrial Electronics*, vol. 58, no. 1, pp. 147–157, 2011.

[5] A. H. Kasem Alaboudy, H. H. Zeineldin, and J. Kirtley, "Microgrid stability characterization subsequent to fault-triggered islanding incidents," *IEEE Transactions on Power Delivery*, vol. 27, no. 2, pp. 658–669, 2012.

[6] M. Illindala and G. Venkataramanan, "Small signal stability of a microgrid with parallel connected distributed generation," *Intelligent Automation and Soft Computing*, vol. 16, no. 2, pp. 235–254, 2010.

[7] X. Xiong and J. Ouyang, "Modeling and transient behavior analysis of an inverter-based microgrid," *Electric Power Components and Systems*, vol. 40, no. 1, pp. 112–130, 2011.

[8] S. M. Muyeen, H. M. Hasanien, and A. Al-Durra, "Transient stability enhancement of wind farms connected to a multimachine power system by using an adaptive ANN-controlled SMES," *Energy Conversion and Management*, vol. 78, pp. 412–420, 2014.

[9] C. Wessels, F. Gebhardt, and F. W. Fuchs, "Fault ride-through of a DFIG wind turbine using a dynamic voltage restorer during symmetrical and asymmetrical grid faults," *IEEE Transactions on Power Electronics*, vol. 26, no. 3, pp. 807–815, 2011.

[10] M. Jain, S. Gupta, D. Masand, and G. Agnihotri, "Analysis of a microgrid under transient conditions using voltage and frequency controller," *Advances in Power Electronics*, vol. 2012, Article ID 208231, 15 pages, 2012.

[11] C. L. Moreira and J. A. Peças Lopes, "Microgrids operation and control under emergency conditions," *Intelligent Automation and Soft Computing*, vol. 16, no. 2, pp. 255–272, 2010.

[12] R. M. Kamel, "Effect of wind generation system types on Micro-Grid (MG) fault performance during both standalone and grid connected modes," *Energy Conversion and Management*, vol. 79, pp. 232–245, 2014.

[13] T.-C. Ou, "A novel unsymmetrical faults analysis for microgrid distribution systems," *International Journal of Electrical Power & Energy Systems*, vol. 43, no. 1, pp. 1017–1024, 2012.

[14] H. Liang, B. J. Choi, W. Zhuang, and X. Shen, "Decentralized inverter control in microgrids based on power sharing information through wireless communications," in *Proceedings of the IEEE Global Communications Conference (GLOBECOM '12)*, pp. 5148–5153, IEEE, December 2012.

[15] P. Rodriguez, A. V. Timbus, R. Teodorescu, M. Liserre, and F. Blaabjerg, "Flexible active power control of distributed power generation systems during grid faults," *IEEE Transactions on Industrial Electronics*, vol. 54, no. 5, pp. 2583–2592, 2007.

[16] J. A. P. Lopes, C. L. Moreira, and A. G. Madureira, "Defining control strategies for microgrids islanded operation," *IEEE Transactions on Power Systems*, vol. 21, no. 2, pp. 916–924, 2006.

[17] J. He and Y. W. Li, "An enhanced microgrid load demand sharing strategy," *IEEE Transactions on Power Electronics*, vol. 27, no. 9, pp. 3984–3995, 2012.

[18] R. Majumder, B. Chaudhuri, A. Ghosh, R. Majumder, G. Ledwich, and F. Zare, "Improvement of stability and load sharing in an autonomous microgrid using supplementary droop control loop," *IEEE Transactions on Power Systems*, vol. 25, no. 2, pp. 796–808, 2010.

[19] F. Razavi, R. Torani, I. Askarian, A. Asgharizadeh, and N. Masoomi, "Optimal design of islanded microgrid using genetic algorithm," in *International Conference on Genetic and Evolutionary Methods (GEM '12)*, 2012.

[20] F. Shahnia, R. Majumder, A. Ghosh, G. Ledwich, and F. Zare, "Operation and control of a hybrid microgrid containing unbalanced and nonlinear loads," *Electric Power Systems Research*, vol. 80, no. 8, pp. 954–965, 2010.

[21] W. S. Lee and S. H. Kang, "Protection for distributed generations in the DC micro-grid," in *Proceedings of the 2nd IEEE PES International Conference and Exhibition on Innovative Smart Grid Technologies (ISGT Europe '11)*, pp. 1–5, December 2011.

[22] R. Majumder, "Some aspects of stability in microgrids," *IEEE Transactions on Power Systems*, vol. 28, no. 3, pp. 3243–3252, 2013.

[23] S. Sanchez, M. Molinas, M. Degano, and P. Zanchetta, "Stability evaluation of a DC micro-grid and future interconnection to an AC system," *Renewable Energy*, vol. 62, pp. 649–656, 2014.

[24] M. B. Delghavi and A. Yazdani, "An adaptive feedforward compensation for stability enhancement in droop-controlled inverter-based microgrids," *IEEE Transactions on Power Delivery*, vol. 26, no. 3, pp. 1764–1773, 2011.

[25] X. Chen, W. Pei, and X. Tang, "Transient stability analyses of micro-grids with multiple distributed generations," in *Proceeding of the International Conference on Power System Technology (POWERCON '10)*, pp. 1–8, Hangzhou, China, October 2010.

[26] J. V. Milanovic, M. T. Aung, and S. C. Vegunta, "The influence of induction motors on voltage sag propagation - Part I: Accounting for the change in sag characteristics," *IEEE Transactions on Power Delivery*, vol. 23, no. 2, pp. 1063–1071, 2008.

Hindawi Publishing Corporation
The Scientific World Journal
Volume 2014, Article ID 476912, 8 pages
http://dx.doi.org/10.1155/2014/476912

Research Article

Observer Design for a Core Circadian Rhythm Network

Yuhuan Zhang

School of Mathematics and Information Sciences, Henan University, Kaifeng 475004, China

Correspondence should be addressed to Yuhuan Zhang; baiyigecun@163.com

Received 8 June 2014; Accepted 15 June 2014; Published 8 July 2014

Academic Editor: Guanghui Wen

Copyright © 2014 Yuhuan Zhang. This is an open access article distributed under the Creative Commons Attribution License, which permits unrestricted use, distribution, and reproduction in any medium, provided the original work is properly cited.

The paper investigates the observer design for a core circadian rhythm network in *Drosophila* and *Neurospora*. Based on the constructed highly nonlinear differential equation model and the recently proposed graphical approach, we design a rather simple observer for the circadian rhythm oscillator, which can well track the state of the original system for various input signals. Numerical simulations show the effectiveness of the designed observer. Potential applications of the related investigations include the real-world control and experimental design of the related biological networks.

1. Introduction

Controllability, observability, and stability are typical problems of dynamical systems [1, 2]. Suppose we have a dynamical system with the following form:

$$\frac{dx}{dt} = f(t, x(t), u(t)), \tag{1}$$

where $x(t) \in R^N$ is the state vector of the system and $u(t) \in R^M$ is the input vector. System (1) is said to be observable, if we can find a function

$$y(t) = h(t, x(t), u(t)), \tag{2}$$

from which one can determine all the state variables of system (1). Here, $y(t) \in R^P$ depends on t, a set of the system's state $x(t)$ and the external input $u(t)$ [1–6].

For $f(t, x(t), u(t))$ with polynomial or rational expressions, existing results have reported that system (1) is observable if the Jacobian matrix $J = [J_{ij}]_{NP\times N}$ has full rank [3, 4], where J_{ij} is the Lie derivative of the output function $h(t, x(t), u(t))$.

Recently, Liu et al. [4] proposed a graphical approach to reduce the observability problem to a property of the inference diagram of a system. The inference diagram is based on the dynamical equation of the system. If x_j appears in x_i's differential equation, then there is a link from x_i to x_j in the inference diagram. The inference diagram can be decomposed into some strongly connected component (SCC). Those SCCs without incoming edges are called root SCCs. Liu et al. [4] reported that the number of the root SCCs provides the lower bound of the monitored state variables in $y(t)$. Furthermore, for many nonlinear systems, they declared that the number of the root SCCs provides not only necessary but also sufficient numbers of state variables to realize observability. That is, if the inference diagram of a system has k root SCCs, then one may only need to select k state variables from different root SCCs, and the system will be observable through monitoring these k state variables.

Biological systems are typical nonlinear systems [7–23]. Observer design for biological systems has important real-world implications. For example, through monitoring a few state variables of a complex biological system, if we can infer the state of the whole system, then lots of resources can be saved [4]. Circadian rhythms are typical biological phenomenon, which display endogenous, entrainable oscillations with a period that lasts approximately 24 hours. Circadian rhythms are widely in existence in various plants and animals [12], which are controlled by biomolecular networks. Circadian rhythms have been extensively investigated during the last decades [18–23]. For example, in 1995, Goldbeter established a mathematical model for the circadian rhythms in the *Drosophila* [11]. In 1999, Leloup et al. established a model for the circadian rhythms in the *Drosophila* and *Neurospora* [13]. In 2002, Gonze and coauthors [7] investigated the deterministic and stochastic dynamics in a core circadian

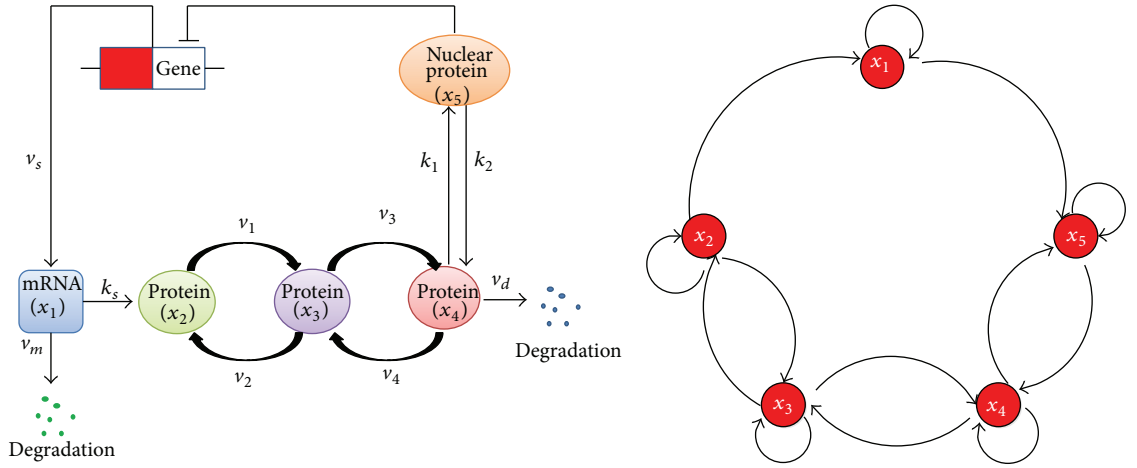

Figure 1: (a) A core model for circadian rhythms [7]. Parameters marked on the directed edges denote reaction rates. x_1 denotes the concentration of the mRNA; x_2, x_3, x_4, and x_5 are the concentrations of four forms of the protein expressed by the gene; x_2, x_3, and x_4 are cytosolic proteins; x_5 is nuclear protein. The circadian gene transcripts mRNA x_1 and then translates protein x_2. Proteins x_2, x_3, and x_4 can be reversibly phosphorylated successively. x_4 can be transported into the nucleus; the nucleus protein x_5 can negatively regulate the expression of the circadian gene. The mRNA and protein x_4 suffer from degradations. (b) The inference diagram [4] for the circadian rhythm model (3). If x_i appears in x_j's differential equation, then there will be a directed edge from x_j to x_i.

rhythm network. They found that the core network can display roughly the same circadian oscillations under both deterministic and stochastic descriptions.

In this paper, based on the graphical approach introduced by Liu et al. [4], for the core circadian rhythm network [7] in *Drosophila* and *Neurospora*, we design some simple observers for the network. Based on the Lyapunov stability theory, we theoretically verify the correctness of the designed observers. Finally, numerical simulations show the effectiveness of the designed observers for various input signals. The rest of the paper is organized as follows. In Section 2, we briefly introduce the mathematical model for the core circadian rhythm network. Observers will be designed in Section 3. We perform numerical simulations in Section 4. Discussions and some concluding remarks will be in Section 5.

2. The Core Circadian Rhythm Model

The core circadian rhythm network is reported by Gonze et al. [7]; the detailed biochemical processes are shown in Figure 1(a). Figure 1(a) represents a prototype for the molecular mechanism of circadian oscillations based on negative autoregulation of gene expression. Real-world circuits corresponding to Figure 1(a) include the *per* mRNA and *PER* protein in *Drosophila* [11, 12] and *frq* mRNA and *FRQ* protein in *Neurospora* [13].

The core model involves gene transcription and transport of mRNA x_1 into the cytosol where it is translated into protein x_2 and degraded. Protein x_2 can be reversibly phosphorylated from the form x_2 into the forms x_3 and x_4, successively. The phosphorylated protein x_4 is degraded or transported into the nucleus, and the nucleus protein x_5 can negatively regulate the expression of its gene. Based on the work from Gonze et al. [7] in 2002, the modified mathematical model

Table 1: Parameter values.

Parameter	Value
v_s	0.5 nMh^{-1}
n	4
K_m	0.2 nM
v_1	6.0 nMh^{-1}
v_2	3.0 nMh^{-1}
v_3	6.0 nMh^{-1}
v_4	3.0 nMh^{-1}
v_d	1.5 nMh^{-1}
k_1	2.0 h^{-1}
K_I	2 nM
v_m	0.3 nMh^{-1}
k_s	2.0 h^{-1}
K_1	1.5 nM
K_2	2.0 nM
K_3	1.5 nM
K_4	2.0 nM
K_d	0.1 nM
k_2	1.0 h^{-1}

for the core circadian model can be established as follows. Consider

$$\frac{dx_1}{dt} = v_s \frac{K_I^n}{K_I^n + x_5^n} - v_m \frac{x_1}{K_m + x_1} + u(t),$$

$$\frac{dx_2}{dt} = k_s x_1 - v_1 \frac{x_2}{K_1 + x_2} + v_2 \frac{x_3}{K_2 + x_3},$$

$$\begin{aligned}
\frac{dx_3}{dt} &= v_1\frac{x_2}{K_1+x_2} - v_2\frac{x_3}{K_2+x_3} - v_3\frac{x_3}{K_3+x_3} + v_4\frac{x_4}{K_4+x_4},\\
\frac{dx_4}{dt} &= v_3\frac{x_3}{K_3+x_3} - v_4\frac{x_4}{K_4+x_4} - v_d\frac{x_4}{K_d+x_4} - k_1x_4 + k_2x_5,\\
\frac{dx_5}{dt} &= k_1x_4 - k_2x_5,
\end{aligned} \tag{3}$$

where x_i $(i = 1, \ldots, 5)$ are state variables, which correspond to species concentrations of the mRNA, the four forms of proteins. $u(t)$ represents the external input, which can be seen as the effect of the environment on the system. K_i $(i = I, m, 1, 2, 3, 4, d)$, k_j $(j = 1, 2, s)$, and v_k $(k = s, m, 1, 2, 3, 4, d)$ are Michaelis constants, first-order reaction rate constants, and maximum rates of protein degradation, transcription, and phosphorylation. It is noted that if we set $u(t) = 0$, then system (3) degenerates into the model investigated in [7]. A typical set of parameter values for system (3) are shown in Table 1. Under the parameter values as shown in Table 1 and for $u(t) = 0$, dynamical system (3) can display circadian rhythms with a period close to 24 hours.

3. Observer Design for the Circadian Rhythm Model

For simplicity, in the following, we rewrite system (3) as the following form:

$$\begin{aligned}
\frac{dx}{dt} &= Ax(t) + f(x(t), u(t)),\\
y(t) &= Cx(t),
\end{aligned} \tag{4}$$

where $x(t) = (x_1(t), \ldots, x_5(t))^T$ and $f(x(t), u(t)) \in R^5$ denotes the nonlinear term. $y(t)$ denotes the monitored output. C is a constant matrix. $Ax(t)$ denotes the linear term, with

$$A = \begin{bmatrix} 0 & 0 & 0 & 0 & 0\\ k_s & 0 & 0 & 0 & 0\\ 0 & 0 & 0 & 0 & 0\\ 0 & -k_1 & 0 & 0 & k_2\\ 0 & k_1 & 0 & 0 & -k_2 \end{bmatrix}. \tag{5}$$

For system (4), similar to the works in [4–6], our objective is to design the following observer, which can track the states of system (4):

$$\frac{dz}{dt} = Az(t) + f(z(t), u(t)) + K(y(t) - Cz(t)), \tag{6}$$

where K is a gain matrix, which is to be determined. The estimation error dynamics are then given by

$$\frac{de}{dt} = (A - KC)e(t) + [f(x(t), u(t)) - f(z(t), u(t))], \tag{7}$$

where $e(t) = x(t) - z(t)$.

From Liu et al. [4], the observability of a dynamical system can be revealed by its inference diagram. The inference diagram of system (3) is shown in Figure 1(b), where the five nodes are strongly connected and consist of the single root SCC. From the conclusion in [4], system (3) is observable, and one should only monitor any one of the five nodes in Figure 1(b). In the following, for simplicity, we assume that only $x_1(t)$ is monitored. The designed observer of system (3) is described as

$$\begin{aligned}
\frac{dz_1}{dt} &= v_s\frac{K_I^n}{K_I^n + z_5^n} - v_m\frac{z_1}{K_m + z_1} + u(t) + kc(x_1 - z_1),\\
\frac{dz_2}{dt} &= k_sz_1 - v_1\frac{z_2}{K_1 + z_2} + v_2\frac{z_3}{K_2 + z_3},\\
\frac{dz_3}{dt} &= v_1\frac{z_2}{K_1 + z_2} - v_2\frac{z_3}{K_2 + z_3} - v_3\frac{z_3}{K_3 + z_3} + v_4\frac{z_4}{K_4 + z_4},\\
\frac{dz_4}{dt} &= v_3\frac{z_3}{K_3 + z_3} - v_4\frac{z_4}{K_4 + z_4} - v_d\frac{z_4}{K_d + z_4} - k_1z_4 + k_2z_5,\\
\frac{dx_5}{dt} &= k_1z_4 - k_2z_5,
\end{aligned} \tag{8}$$

where k, c are the nonzero elements in matrix K and C of (6). For simplicity, we denote

$$g(K_j, x_i) = \frac{x_i}{K_j + x_i}. \tag{9}$$

Then,

$$\frac{K_I^n}{K_I^n + x_5^n} = 1 - g(K_I^n, x_5^n). \tag{10}$$

The corresponding error dynamics are described as

$$\begin{aligned}
\frac{de_1}{dt} &= v_s[g(K_I^n, z_5^n) - g(K_I^n, x_5^n)]\\
&\quad - v_m[g(K_m, x_1) - g(K_m, z_1)] - kce_1,\\
\frac{de_2}{dt} &= k_se_1 - v_1[g(K_1, x_2) - g(K_1, z_2)]\\
&\quad + v_2[g(K_2, x_3) - g(K_2, z_3)],\\
\frac{de_3}{dt} &= v_1[g(K_1, x_2) - g(K_1, z_2)]\\
&\quad - v_2[g(K_2, x_3) - g(K_2, z_3)]\\
&\quad - v_3[g(K_3, x_3) - g(K_3, z_3)]\\
&\quad + v_4[g(K_4, x_4) - g(K_4, z_4)],\\
\frac{de_4}{dt} &= v_3[g(K_3, x_3) - g(K_3, z_3)]\\
&\quad - v_4[g(K_4, x_4) - g(K_4, z_4)]\\
&\quad - v_d[g(K_d, x_4) - g(K_d, z_4)] - k_1e_4 + k_2e_5,\\
\frac{de_5}{dt} &= k_1e_4 - k_2e_5.
\end{aligned} \tag{11}$$

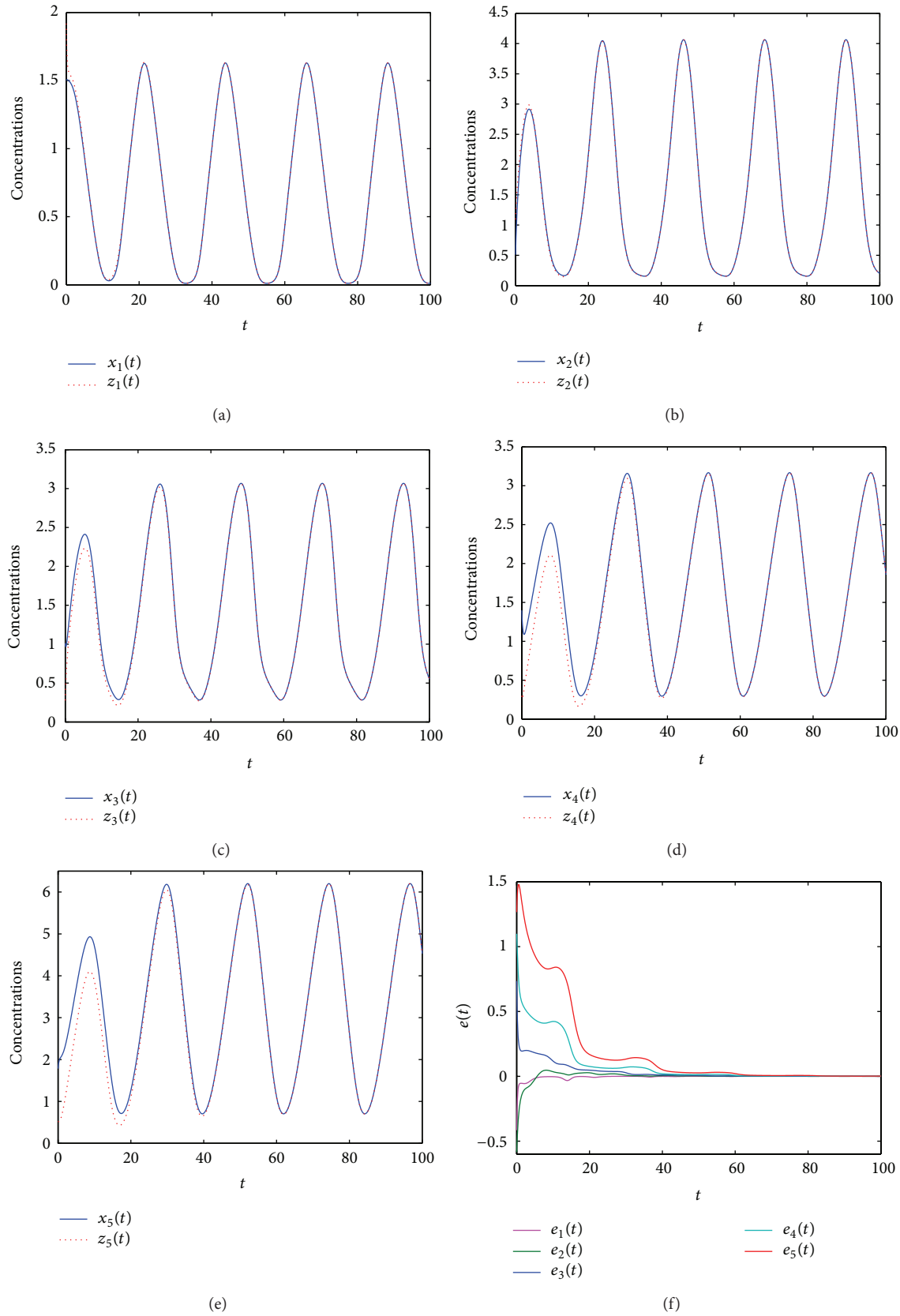

FIGURE 2: (a)–(e) State trajectories of systems (3) and (8). (f) The error dynamics of system (11). Here, $u(t) = 0$, $y(t) = x_1(t)$, and $k = 5$. Initial values are randomly chosen.

Before we analyze the stability of system (11), we note that since x_i, z_i represent species concentrations, they must be nonnegative and bounded [24]. Furthermore, since $g(K_j, x_i)$ is continuous and differentiable, by the mean value theorem, there must exist ξ_i between x_i and z_i, satisfying

$$g\left(K_j, x_i\right) - g\left(K_j, z_i\right) = g'\left(K_j, \xi\right)\left(x_i - z_i\right) = \frac{K_j}{\left(K_j + \xi_i\right)^2}\left(x_i - z_i\right). \tag{12}$$

For system (11), we construct the following Lyapunov function:

$$V(t) = \frac{1}{2}\sum_{i=1}^{5} e_i(t)^2. \tag{13}$$

Based on (12), the derivative of (13) along system (11) is

$$\begin{aligned}\dot{V}(t) &= \sum_{i=1}^{5} e_i(t)\,\dot{e}_i(t)\\ &= -\left[kc + \frac{V_m K_m}{\left(K_m + \xi_1\right)^2}\right]e_1^2 - \frac{V_1 K_1}{\left(K_1 + \xi_2\right)^2}e_2^2\\ &\quad - \left[\frac{V_2 K_2}{\left(K_2 + \xi_3\right)^2} + \frac{V_3 K_3}{\left(K_3 + \xi_3'\right)^2}\right]e_3^2\\ &\quad - \left[\frac{V_4 K_4}{\left(K_4 + \xi_4\right)^2} + \frac{V_d K_d}{\left(K_d + \xi_4'\right)^2} + k_1\right]e_4^2\\ &\quad - k_2 e_5^2 + k_s e_1 e_2 + \left[\frac{V_2 K_2}{\left(K_2 + \xi_3\right)^2} + \frac{V_1 K_1}{\left(K_1 + \xi_2\right)^2}\right]e_2 e_3\\ &\quad + \left(k_1 + k_2\right)e_4 e_5\\ &\quad + \left[\frac{V_4 K_4}{\left(K_4 + \xi_4\right)^2} + \frac{V_3 K_3}{\left(K_3 + \xi_3'\right)^2}\right]e_3 e_4 - \frac{n V_s K_I^n \xi_5^{n-1}}{\left(K_I^n + \xi_5^n\right)^2}e_1 e_5\\ &= e^T Q e.\end{aligned} \tag{14}$$

Here,

$$Q = \begin{bmatrix} \frac{-V_m K_m}{\left(K_m + \xi_1\right)^2} - kc & \frac{k_s}{2} & 0 & 0 & \frac{-n V_s K_I^n \xi_5^{n-1}}{2\left(K_I^n + \xi_5^n\right)^2}\\ * & \frac{-V_1 K_1}{\left(K_1 + \xi_2\right)^2} & \frac{0.5 V_2 K_2}{\left(K_2 + \xi_3\right)^2} + \frac{0.5 V_1 K_1}{\left(K_1 + \xi_2\right)^2} & 0 & 0\\ 0 & * & \frac{-V_2 K_2}{\left(K_2 + \xi_3\right)^2} - \frac{V_3 K_3}{\left(K_3 + \xi_3'\right)^2} & \frac{0.5 V_4 K_4}{\left(K_4 + \xi_4\right)^2} + \frac{0.5 V_3 K_3}{\left(K_3 + \xi_3'\right)^2} & 0\\ 0 & 0 & * & \frac{-V_4 K_4}{\left(K_4 + \xi_4\right)^2} - \frac{V_d K_d}{\left(K_d + \xi_4'\right)^2} - k_1 & \frac{k_1 + k_2}{2}\\ * & 0 & 0 & * & -k_2 \end{bmatrix}, \tag{15}$$

which is a symmetrical matrix. ξ_i, ξ_i' are values between x_i and z_i. For appropriate gain k, if $Q < 0$, $\dot{V}(t) < 0$. System (11) will be globally asymptotically stable. In other words, system (3) can be observed through the observer (8).

Remark 1. If any one of the other variables is used to track the state of the original system (3), one should only slightly revise the observer (8). If more than one variable is measured to track the original system, the observer can be similarly designed. For example, if $y(t)$ in (4) is $y(t) = (c_1 x_1, c_2 x_2)^T$, the control gain matrix K is chosen as

$$K = \begin{bmatrix} \alpha & 0\\ 0 & \beta\\ 0 & 0\\ 0 & 0\\ 0 & 0 \end{bmatrix}. \tag{16}$$

Then, the observer is designed as

$$\begin{aligned}\frac{dz_1}{dt} &= v_s\frac{K_I^n}{K_I^n + z_5^n} - v_m\frac{z_1}{K_m + z_1} + u(t) + \alpha c_1\left(x_1 - z_1\right),\\ \frac{dz_2}{dt} &= k_s z_1 - v_1\frac{z_2}{K_1 + z_2} + v_2\frac{z_3}{K_2 + z_3} + \beta c_2\left(x_2 - z_2\right),\\ \frac{dz_3}{dt} &= v_1\frac{z_2}{K_1 + z_2} - v_2\frac{z_3}{K_2 + z_3} - v_3\frac{z_3}{K_3 + z_3} + v_4\frac{z_4}{K_4 + z_4},\\ \frac{dz_4}{dt} &= v_3\frac{z_3}{K_3 + z_3} - v_4\frac{z_4}{K_4 + z_4} - v_d\frac{z_4}{K_d + z_4} - k_1 z_4 + k_2 z_5,\\ \frac{dx_5}{dt} &= k_1 z_4 - k_2 z_5.\end{aligned} \tag{17}$$

For appropriate parameters α, β, one can easily prove that the original system is also observable from the observer (17).

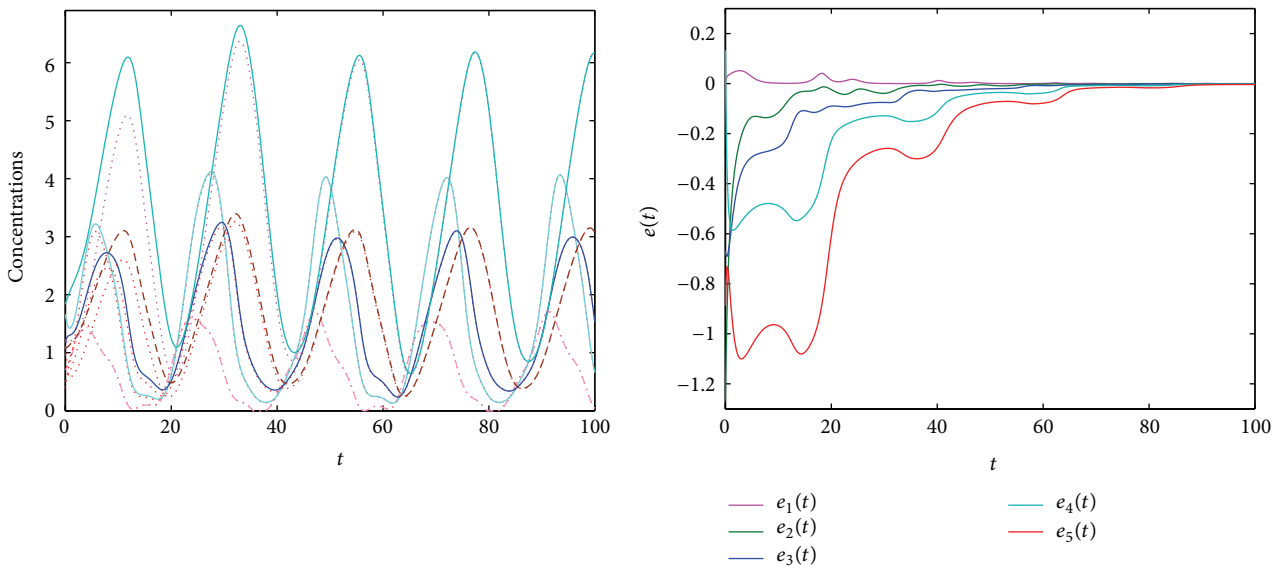

(a) (b)

Figure 3: (a) State trajectories of systems (3) and (8) with $u(t) = \epsilon \sin(t)$. (b) The error dynamics of system (11). Here, $y(t) = cx_1(t)$, $k = 2.5$, $c = 2$, and $\epsilon = 0.1$.

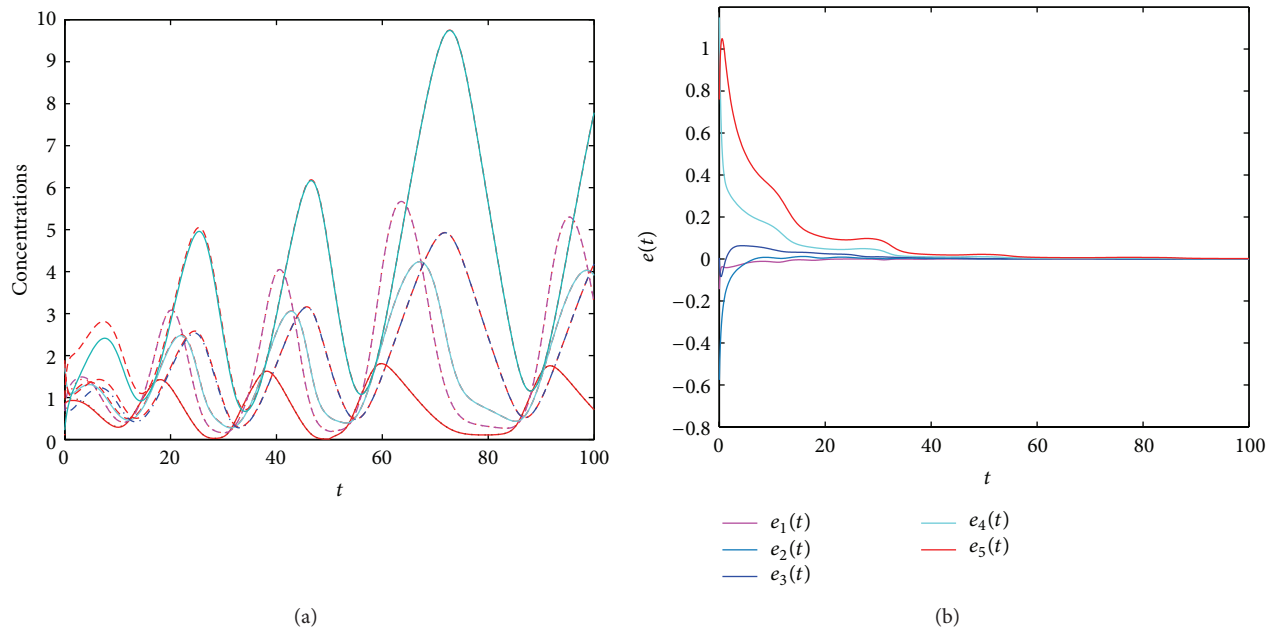

(a) (b)

Figure 4: (a) State trajectories of systems (3) and (8) with step input signal $u(t)$. (b) The error dynamics of system (11). Here, $y(t) = cx_1(t)$, $k = 2.5, c = 2$, and $u(t) = 0$ for $t \leq 50$ and $u(t) = 0.1$ for $t > 50$.

Obviously, the corresponding observer (17) is more complex than the observer (11).

Remark 2. There are many methods to prove the stability of a dynamical system. One can easily prove that the nonlinear terms on the right-hand side of system (11) are Lipschitz. For Lipschitz nonlinear systems, Rajamani [5] proposed a general theorem for the observer design. However, due to the complexity of the biological model, the theorem obtained in [5] fails to work for the error system (11). Therefore, we have used the mean value theorem to simplify the error system (11) and obtained a sufficient condition for the observer design. The matrix Q relies on the bound of system (3).

4. Numerical Simulations

Hereinafter, we numerically verify the effectiveness of the designed observers. Firstly, we assume $u(t) = 0$; the output

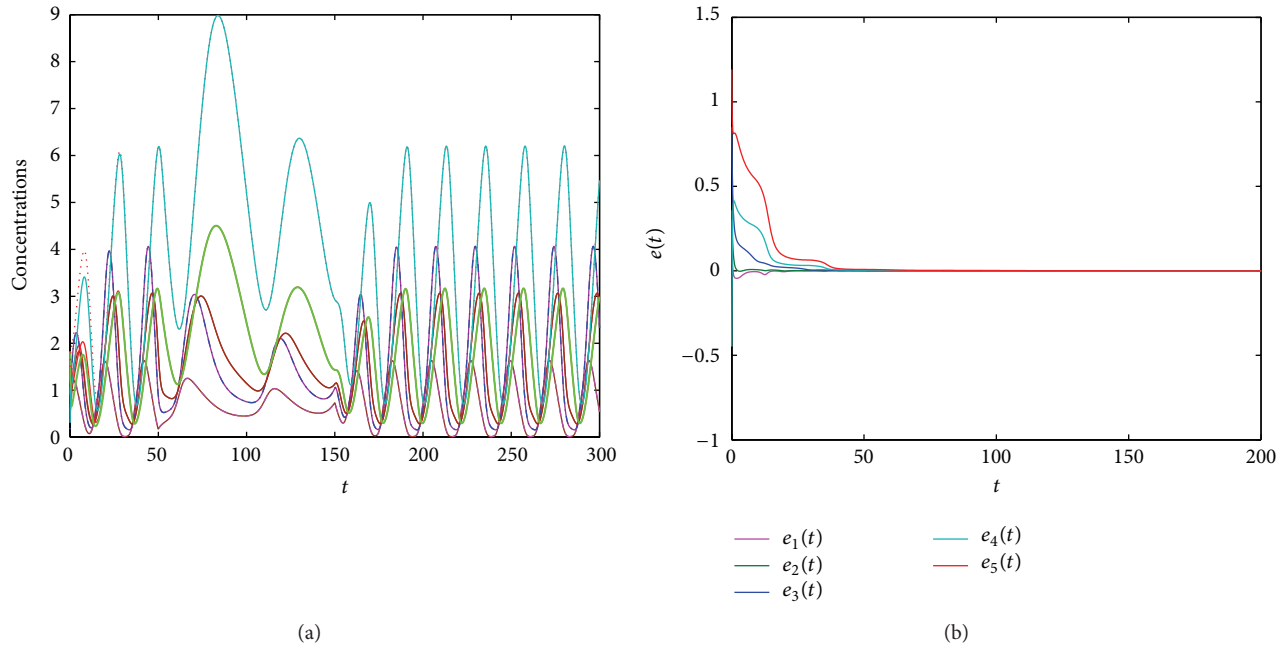

(a) (b)

FIGURE 5: (a) State trajectories of systems (3) and (17) with step input signal $u(t)$ in (19). (b) The error dynamics between systems (3) and (17). Here $y(t) = (c_1x_1(t), c_2x_2(t))^T$, $\alpha = 2$, $\beta = 3$, $c_1 = 2.2$, and $c_2 = 1$.

function $y(t) = x_1(t)$. For $k = 5$, all the state variables in the original system (3) can be tracked by the observer (8). Under randomly initial values, Figure 2 shows the state trajectories of systems (3) and (8), as well as the error dynamics of system (11). From Figure 2, one can see that the state variables of (3) oscillate with a period close to 24 hours. The observer system (8) can track the states of the original system. The error between the observer system and the original system quickly approximates to zero.

For different input signals and under appropriate gain k, system (8) can always track the states of system (3). For example, when $u(t) = \epsilon \sin(t)$, $y(t) = cx_1(t)$, $k = 2.5$, $c = 2$, and $\epsilon = 0.1$, Figure 3 shows the state trajectories of systems (3) and (8) as well as the error dynamics of system (11). From Figure 3, we can see that the states of system (3) can be observed by the observer (8). The error system (11) converges to zero quickly. When $u(t)$ is a step signal, the observer (11) can also well monitor the states of the original (3). Figure 4 shows the case for $y(t) = cx_1(t)$, $k = 2.5$, and $c = 2$, and the step input signal

$$u(t) = \begin{cases} 0, & t \le 50, \\ 0.1, & t > 50. \end{cases} \tag{18}$$

For the cases discussed in Remark 1, when we choose $\alpha = 2$, $\beta = 3$, $c_1 = 2.2$, $c_2 = 1$, and the following input signal,

$$u(t) = \begin{cases} 0, & t \le 50, \\ 0.2, & 50 < t < 150, \\ 0, & t \ge 150, \end{cases} \tag{19}$$

Figure 5 shows the numerical simulation results for such case. From Figure 5, we see that the observer (17) can also well track the states of system (3). Additionally, combined with the simulation results as shown in Figures 2–5, we can conclude that the designed observers have good performance under various kinds of inputs, and the input signal $u(t)$ can affect the period of the circadian oscillator.

5. Discussions and Conclusions

Biological systems are typical complex dynamical systems. To efficiently infer the state of a biological system, it is necessary to develop some simple observers via monitoring a few system variables. Based on the recently proposed graphical approach, we have designed some rather simple observers for a core circadian rhythm network. For various input signals and under appropriate control gains, the designed observer can well infer the states of the original system. The investigations in this paper further support the conclusions in [4]. Real-world applications of the related investigations on biological networks include the experimental design and control of the related biological systems.

We have considered three types of inputs, and it is intriguing to investigate the observer design problems for stochastic systems, since biological systems are inherent stochastic and perturbed by environment [14–16]. Another question that deserves to be further investigated is to develop some general theorems to guarantee the observability of the biological systems [25–28]. Finally, it is also intriguing to investigate the observability of large-scale biological networks [17], such as the yeast cell cycle network with boolean dynamical model or differential equation models [18–23]. These topics will be discussed in our future works.

Conflict of Interests

The authors declare that there is no conflict of interests regarding the publication of this paper.

Acknowledgments

This work was supported by the National Natural Science Foundation of China under Grant no. 61304151 and the Science Foundation of Henan University under Grants nos. 2012YBZR007 and 2013YBRW005.

References

[1] B. C. Moore, "Principal component analysis in linear systems: controllability, observability, and model reduction," *IEEE Transactions on Automatic Control*, vol. 26, no. 1, pp. 17–32, 1981.

[2] J. P. Gauthier and I. Kupka, *Deterministic Observation Theory and Applications*, Cambridge University Press, 2001.

[3] S. Diop and M. Fliess, "Nonlinear observability, identifiability, and persistent trajectories," in *Proceedings of the 30th IEEE Conference on Decision and Control*, vol. 1, pp. 714–719, December 1991.

[4] Y.-Y. Liu, J.-J. Slotine, and A.-L. Barabási, "Observability of complex systems," *Proceedings of the National Academy of Sciences of the United States of America*, vol. 110, no. 7, pp. 2460–2465, 2013.

[5] R. Rajamani, "Observers for Lipschitz nonlinear systems," *IEEE Transactions on Automatic Control*, vol. 43, no. 3, pp. 397–401, 1998.

[6] J. Tsinias, "Observer design for nonlinear systems," *Systems and Control Letters*, vol. 13, no. 2, pp. 135–142, 1989.

[7] D. Gonze, J. Halloy, and A. Goldbeter, "Deterministic versus stochastic models for circadian rhythms," *Journal of Biological Physics*, vol. 28, no. 4, pp. 637–653, 2002.

[8] P. Wang, X. Yu, and J. Lü, "Identification and evolution of structurally dominant nodes in protein protein interaction networks," *IEEE Transactions on Biomedical Circuits and Systems*, vol. 8, no. 1, pp. 87–97, 2014.

[9] P. Wang and J. Lü, "Control of genetic regulatory networks: opportunities and challenges," *Acta Automatica Sinica*, vol. 39, no. 12, pp. 1969–1979, 2013.

[10] P. Wang, J. Lü, and M. J. Ogorzalek, "Global relative parameter sensitivities of the feed-forward loops in genetic networks," *Neurocomputing*, vol. 78, no. 1, pp. 155–165, 2012.

[11] A. Goldbeter, "A model for circadian oscillations in the Drosophila period protein (PER)," *Proceedings of the Royal Society B: Biological Sciences*, vol. 261, no. 1362, pp. 319–324, 1995.

[12] A. Goldbeter, *Biochemical Oscillations and Cellular Rhythms. The Molecular Bases of Periodic and Chaotic Behaviour*, Cambridge University Press, Cambridge, UK, 1996.

[13] J. Leloup, D. Gonze, and A. Goldbeter, "Limit cycle models for circadian rhythms based on transcriptional regulation in *Drosophila* and *Neurospora*," *Journal of Biological Rhythms*, vol. 14, no. 6, pp. 433–448, 1999.

[14] L. Wan, Q. Zhou, Z. Zhou, and P. Wang, "Dynamical behaviors of the stochastic Hopfield neural networks with mixed time delays," *Abstract and Applied Analysis*, vol. 2013, Article ID 384981, 8 pages, 2013.

[15] S. Wang, Y. Shen, C. Shi, T. Wang, Z. Wei, and H. Li, "Defining biological networks for noise buffering and signaling sensitivity using approximate Bayesian computation," *The Scientific World Journal*, vol. 2014, Article ID 625754, 12 pages, 2014.

[16] P. Wang, J. Lü, L. Wan, and Y. Chen, "A stochastic simulation algorithm for biochemical reactions with delays," in *Proceedings of the IEEE International Conference on Systems Biology*, pp. 109–114, Huangshan, China, August 2013.

[17] P. Wang, R. Lu, Y. Chen, and X. Wu, "Hybrid modelling of the general middle-sized genetic regulatory networks," in *Proceedings of the IEEE International Symposium on Circuits and Systems (ISCAS '13)*, pp. 2103–2106, Beijing, China, May 2013.

[18] B. Novak and J. J. Tyson, "Modeling the control of DNA replication in fission yeast," *Proceedings of the National Academy of Sciences of the United States of America*, vol. 94, no. 17, pp. 9147–9152, 1997.

[19] A. Sveiczer, J. J. Tyson, and B. Novak, "Modelling the fission yeast cell cycle," *Briefings in Functional Genomics and Proteomics*, vol. 2, no. 4, pp. 298–307, 2004.

[20] F. Li, T. Long, Y. Lu, Q. Ouyang, and C. Tang, "The yeast cell-cycle network is robustly designed," *Proceedings of the National Academy of Sciences of the United States of America*, vol. 101, no. 14, pp. 4781–4786, 2004.

[21] B. Novak, Z. Pataki, A. Ciliberto, and J. J. Tyson, "Mathematical model of the cell division cycle of fission yeast," *Chaos*, vol. 11, no. 1, pp. 277–286, 2001.

[22] B. Novak and J. J. Tyson, "Quantitative analysis of a molecular model of mitotic control in fission yeast," *Journal of Theoretical Biology*, vol. 173, no. 3, pp. 283–305, 1995.

[23] B. Novak, K. C. Chen, and J. J. Tyson, "Systems biology of the yeast cell cycle engine," in *Systems Biology: Definitions and Perspectives*, L. Alberghina and H. V. Westerhoff, Eds., vol. 13 of *Topics in Current Genetics*, pp. 305–324, Springer, Berlin, Germany, 2005.

[24] P. Wang, D. Li, X. Wu, and J. Lü, "Ultimate bound estimation of a class of high dimensional quadratic autonomous dynamical systems," *International Journal of Bifurcation and Chaos*, vol. 21, no. 9, pp. 2679–2694, 2011.

[25] G. Wen, Z. Duan, G. Chen, and W. Yu, "Consensus tracking of multi-agent systems with Lipschitz-type node dynamics and switching topologies," *IEEE Transactions on Circuits and Systems I: Regular Papers*, vol. 61, no. 2, pp. 499–511, 2014.

[26] J. Qiu and J. Cao, "Global synchronization of delay-coupled genetic oscillators," *Neurocomputing*, vol. 72, no. 16–18, pp. 3845–3850, 2009.

[27] T. Zhou, J. Zhang, Z. Yuan, and L. Chen, "Synchronization of genetic oscillators," *Chaos*, vol. 18, no. 3, Article ID 037126, 2008.

[28] G. Wen, W. Yu, Y. Zhao, and J. Cao, "Pinning synchronisation in fixed and switching directed networks of Lorenz-type nodes," *IET Control Theory & Applications*, vol. 7, no. 10, pp. 1387–1397, 2013.

Hindawi Publishing Corporation
The Scientific World Journal
Volume 2014, Article ID 840185, 10 pages
http://dx.doi.org/10.1155/2014/840185

Research Article

Synchronization Control for Stochastic Neural Networks with Mixed Time-Varying Delays

Qing Zhu,[1,2] Aiguo Song,[1] Shumin Fei,[3] Yuequan Yang,[2] and Zhiqiang Cao[4]

[1] *School of Instrument Science, Southeast University, Nanjing 210096, China*
[2] *College of Information Engineering, Yangzhou University, Yangzhou 225009, China*
[3] *School of Automation, Southeast University, Nanjing 210096, China*
[4] *Institute of Automation, Chinese Academy of Science, Beijing 100190, China*

Correspondence should be addressed to Aiguo Song; a.g.song@seu.edu.cn

Received 18 May 2014; Accepted 7 June 2014; Published 2 July 2014

Academic Editor: Guanghui Wen

Copyright © 2014 Qing Zhu et al. This is an open access article distributed under the Creative Commons Attribution License, which permits unrestricted use, distribution, and reproduction in any medium, provided the original work is properly cited.

Synchronization control of stochastic neural networks with time-varying discrete and continuous delays has been investigated. A novel control scheme is proposed using the Lyapunov functional method and linear matrix inequality (LMI) approach. Sufficient conditions have been derived to ensure the global asymptotical mean-square stability for the error system, and thus the drive system synchronizes with the response system. Also, the control gain matrix can be obtained. With these effective methods, synchronization can be achieved. Simulation results are presented to show the effectiveness of the theoretical results.

1. Introduction

In recent years, stochastic neural networks (NNs) have gained particular research interests. These systems represent a class of stochastic systems that is popular in modeling practical systems which may experience random disturbances and parameters varying. Such a system can be found in biology systems, social systems, and wireless communication networks. Numerous results on stochastic neural network have been reported in the literature [1–5]. As one of the mostly investigated dynamical behaviors, the synchronization in stochastic NNs with or without time delays has drawn significant research interest; see, for example, [6–10] and the references therein.

On the other hand, time delays are frequently encountered in many practical control systems, such as aircraft, chemical, or process control systems. The existence of the time delays may be the source of instability of serious deterioration in the performance of the closed-loop systems. Thus, stability of delayed NNs has been a focal subject for research [11–15]. Most recently, significant and substantial progresses have been achieved in the synchronization of stochastic NNs. These include synchronization of randomly coupled neural networks with Markovian jumping and time-delay [15], adaptive synchronization for stochastic NNs with time-varying delays and distributed delays [16], passivity analysis for discrete time stochastic Markovian jump NNs with mixed time delays [17], adaptive synchronization for stochastic T-S fuzzy NNs with time-delay and Markovian jumping parameters [18], nonfragile synchronization of NNs with time-varying delay and randomly occurring controller gain fluctuation synchronization of biological NN systems with stochastic perturbations and time delays [19], global exponential adaptive synchronization of complex dynamical networks with neutral-type NN nodes and stochastic disturbances [20], adaptive synchronization for uncertain chaotic neural networks with mixed time delays using fuzzy disturbance observer [21], the effects of time delay on the stochastic resonance in feed-forward-loop NN motifs [22], state estimation for wireless network control system with stochastic uncertainty and time delay based on sliding mode observer [23], pinning synchronization in fixed and switching directed networks of Lorenz-type nodes [24], consensus tracking for higher-order multiagent systems with switching directed

topologies and occasionally missing control inputs [25], and consensus tracking of multiagent systems with Lipschitz-type node dynamics and switching topologies [26].

Although substantial progresses have been made in the synchronization control of delayed stochastic neural network systems [16–32], there are still some problems which have not been fully studied. For example, many control schemes of time-varying delayed NNs assume that the derivative of the time-delay function is less than one. Also, few works have been done on the synchronization of mixed delayed stochastic NNs. In this paper, we propose sufficient conditions of the synchronization of the stochastic NN system, as well as the state feedback control design. At first, sufficient conditions are proposed in terms of LMIs to guarantee the stochastic asymptotical stability of the error system. The assumption that the derivative of the time-delay function is less than one is eliminated. Then, we give some corollaries to solve the problem in some special cases.

This paper is organized as follows. After the introduction in Section 1, the problem statement and preliminaries are presented in Section 2. Next, some sufficient conditions are presented for the synchronization of the delayed drive and response system. Also, some corollaries and remarks are given to show the advantages of this paper in Section 3. Then, the numerical simulation result is given in Section 4. A conclusion is drawn in Section 5.

2. Problem Statement and Preliminaries

Before proceeding, we introduce some notations which will be used later for derivations and discussions. $\|\cdot\|$ denotes the Euclidean norm of a vector or the Frobenius norm of a matrix. $M > 0$ (<0) denotes that matrix M is a positive (negative) definite matrix. $E\cdot$ denotes the mathematical expectation.

The recurrent network under investigation is

$$dx(t) = \left[-Cx(t) + Af(x(t)) + Bf(x(t-\tau(t))) + D\int_{t-\sigma(t)}^{t} f(x(s))\,ds \right] dt, \tag{1}$$

where $x(t) = [x_1(t), x_2(t), \ldots, x_n(t)]^T$ is the system state associated with the neurons, n denotes the number of neurons in the network, $f(x(t)) = [f_1(x_1(t)), f_2(x_2(t)), \ldots, f_n(x_n(t))]$ corresponds to the activation functions of neurons, and $\tau(t)$ and $\sigma(t)$ are the time-varying discrete delay and continuous delay, respectively; the initial conditions are given by $x(t) = \phi(t) \in \ell([-\overline{\tau}, 0], R^n)$, where $\phi(t) \in \ell([-\overline{\tau}, 0], R^n)$ denotes the set of all continuous functions from $[-\overline{\tau}, 0]$ to R. $C = \mathrm{diag}(c_1, c_2, \ldots, c_n)$ is a diagonal matrix, $A = (a_{ij})_{n\times n}$, $B = (b_{ij})_{n\times n}$, and $D = (d_{ij})_{n\times n}$ are the connection weight matrix, discrete time-delay, and continuous time-delay connection weight matrices, respectively.

In this paper, we consider model (1) as the master system. The response system is

$$dy(t) = \left[-Cy(t) + Af(y(t)) + Bf(y(t-\tau(t))) + D\int_{t-\sigma(t)}^{t} f(y(s))\,ds + u(t) \right] dt + \sigma(t, e(t), e(t-\tau(t)))\,d\omega(t), \tag{2}$$

where A, B, C, and D are matrices which are the same as (1) and $u(t)$ is the controller. It has the same structure as the drive system. $e(t) = y(t) - x(t)$ is the error state. $\omega(t) = [\omega_1(t), \omega_2(t), \ldots, \omega_n(t)]^T$ is a n dimension Brownian motion defined on a complete probability space (Ω, F, P).

To propose our main results, it is necessary to make the following assumptions.

(A1) Each function f_i is nondecreasing and globally Lipschitz with a constant $k_i > 0$:

$$|f_i(x) - f_i(y)| \le k_i |x - y| \quad \forall x, y \in R,\ i = 1, 2, \ldots, n, \qquad K = \mathrm{diag}(k_1, k_2, \ldots, k_n). \tag{3}$$

(A2) Matrix function $\sigma(t, e(t), e(t-\tau(t)))$ satisfies

$$\mathrm{trace}\left[\sigma^T(t, e(t), e(t-\tau(t)))\,\sigma(t, e(t), e(t-\tau(t)))\right] \le \|M_1 e(t)\|^2 + \|M_2 e(t-\tau(t))\|^2, \tag{4}$$

where M_1 and M_2 are matrices with appropriate dimensions.

(A3) Discrete delay $\tau(t)$ and continuous delay $\sigma(t)$ are both differential functions of time, and the following conditions hold:

$$0 \le \tau(t) \le \overline{\tau}, \qquad \dot{\tau}(t) \le \overline{\tau}_1, \qquad 0 \le \sigma(t) \le \overline{\sigma}, \tag{5}$$

where $\overline{\tau}, \overline{\tau}_1$, and σ are positive constants. It is worth to emphasis that the constraint, the derivative of time-delay function is less than one [1], is eliminated in this paper, while a more general upper boundary constraint is utilized instead of it. This improvement makes our results applicable for a wide range of time-delayed stochastic neural networks.

Let error state be $e(t) = y(t) - x(t)$; subtracting (1) from (2) yields the synchronization error dynamical system as follows:

$$de(t) = \left[-Ce(t) + Ag(t) + Bg(t-\tau(t)) + D\int_{t-\sigma(t)}^{t} g(s)\,ds + u(t) \right] dt + \sigma(t, e(t), e(t-\tau(t)))\,d\omega, \tag{6}$$

where $g(t) = f(y(t)) - f(x(t))$.

In this paper, we design a memoryless state feedback controller:

$$u(t) = Ge(t), \tag{7}$$

where $G \in R^{n\times n}$ is a constant gain matrix.

Substituting the controller into the error system (6), we get

$$de(t) = \Big[(-C+G)\, e(t) + Ag(t) + Bg(t-\tau(t)) + D\int_{t-\sigma(t)}^{t} g(s)\, ds \Big] dt + \sigma(t, e(t), e(t-\tau(t)))\, d\omega. \tag{8}$$

It is well known that system (8) has a unique solution [33].

Definition 1. The system (8) is called globally asymptotically mean-square stable, if the following holds:

$$\lim_{t\to\infty} E\|e(t)\|^2 = 0, \quad \text{for any } e(t_0), \tag{9}$$

where $E\cdot$ is the mathematical expectation. The following Lemma is given.

Lemma 2 (Schur complement lemma). *For matrices A, B, and C with compatible dimensions, the following three conditions are equivalent:*

$$(a)\quad \begin{bmatrix} A & C \\ C^T & B \end{bmatrix} < 0; \tag{10}$$

$$(b)\quad A - CB^{-1}C^T < 0, \quad B < 0, \quad \text{if } B \text{ is invertible}; \tag{11}$$

$$(c)\quad B - C^TA^{-1}C < 0, \quad A < 0, \quad \text{if } A \text{ is invertible}. \tag{12}$$

Lemma 3. *For vector function $f(t) \in R^n$ and symmetric matrix $P > 0$, the following holds:*

$$\int_a^b f^T(t)\, dt\, P \int_a^b f(t)\, dt \le (b-a)\int_a^b f^T(t)\, Pf(t)\, dt. \tag{13}$$

3. Criteria of Synchronization

In this section, new criteria are presented for the global asymptotical stability of the equilibrium point of the neural network defined by (8), and thus the drive system (1) synchronizes with the response system (2). Its proof is based on a new Lyapunov functional method and linear matrix inequality (LMI) approach.

Theorem 4. *Under the assumptions A1–A3, the equilibrium point of model* (8) *is called globally asymptotically stable in mean-square, if there exist symmetric positive-definite matrices P_j ($j = 1, \ldots, 4$), diagonal matrices D_1, D_2, and general matrix Q_1 such that the following inequalities hold:*

$$\Pi = \begin{bmatrix} \Pi_{11} & Q_1 & \Pi_{13} & \Pi_{14} & 0 & P_1D + \overline{\tau}^2 D & \overline{\tau}(-C+G)^T P_1 \\ * & \Pi_{22} & 0 & K^T D_2 & -Q_1 & 0 & 0 \\ * & * & \Pi_{33} & \overline{\tau}^2 A^T P_1 B & 0 & \overline{\tau}^2 A^T P_1 D & 0 \\ * & * & * & \Pi_{44} & 0 & \overline{\tau}^2 B^T P_1 D & 0 \\ * & * & * & * & -P_1 & 0 & 0 \\ * & * & * & * & * & -P_4 + \overline{\tau}^2 D^T P_1 D & 0 \\ * & * & * & * & * & * & -P_1 \end{bmatrix} < 0, \tag{14}$$

$$P_1 < \rho I, \tag{15}$$

where

$$\begin{aligned} \Pi_{11} &= P_1(-C+G) + (-C+G)^T P_1 + P_2 + \rho M_1^T M_1, \\ \Pi_{13} &= P_1A + K^T D_1 + \overline{\tau}^2 (-C+G)^T P_1 A, \\ \Pi_{14} &= P_1B + \overline{\tau}^2 (-C+G)^T P_1 B, \\ \Pi_{22} &= -(1-\overline{\tau}_1) P_2 - Q_1 - Q_1^T + \rho M_2^T M_2, \\ \Pi_{33} &= P_3 - 2D_1 + \overline{\sigma}^2 P_4 + \overline{\tau}^2 A^T P_1 A, \\ \Pi_{44} &= -(1-\overline{\tau}_1) P_3 - 2D_2 + \overline{\tau}^2 B^T P_1 B. \end{aligned} \tag{16}$$

Proof. The Lyapunov function candidate is given as

$$V(t) = \sum_{i=1}^{5} V_i(t), \tag{17}$$

where

$$V_1(t) = e^T(t) P_1 e(t),$$
$$V_2(t) = \int_{t-\tau(t)}^{t} e^T(s) P_2 e(s)\, ds,$$
$$V_3(t) = \int_{t-\tau(t)}^{t} g^T(s) P_3 g(s)\, ds,$$
$$V_4(t) = \overline{\tau} \int_0^{\overline{\tau}} \int_{t-s}^{t} \dot{e}^T(\theta) P_1 \dot{e}(\theta)\, d\theta\, ds,$$
$$V_5(t) = \overline{\sigma} \int_{-\overline{\sigma}}^{0} \int_{t+s}^{t} g^T(\theta) P_4 g(\theta)\, d\theta\, ds. \tag{18}$$

The weak infinitesimal operator L of the process $\{x_t = x(t+s), t \geq 0, -\overline{\tau} \leq t \leq 0\}$ is given by

$$\begin{aligned} LV_1 = {} & 2e^T(t) P_1 \Big[(-C+G) e(t) + Ag(t) \\ & + Bg(t-\tau(t)) + D \int_{t-\sigma(t)}^{t} g(s)\, ds \Big] \\ & + \operatorname{trace}\Big[\sigma^T(t, e(t), e(t-\tau(t))) \\ & \times P_1 \sigma(t, e(t), e(t-\tau(t)))\Big]. \end{aligned} \tag{19}$$

By (5) and (14), we have

$$\begin{aligned} & \operatorname{trace}\Big[\sigma^T(t, e(t), e(t-\tau(t))) \\ & \quad \times P_1 \sigma(t, e(t), e(t-\tau(t)))\Big] \\ & \leq \rho \operatorname{trace}\Big[\sigma^T(t, e(t), e(t-\tau(t))) \\ & \quad \times \sigma(t, e(t), e(t-\tau(t)))\Big] \\ & = \rho \Big[e^T(t) M_1^T M_1 e(t) \\ & \quad + e^T(t-\tau(t)) M_2^T M_2 e(t-\tau(t))\Big], \end{aligned} \tag{20}$$

$$\begin{aligned} LV_2(t) = {} & e^T(t) P_2 e(t) - (1-\dot{\tau}(t)) e^T \\ & \times (t-\tau(t)) P_2 e(t-\tau(t)), \end{aligned} \tag{21}$$

$$\begin{aligned} LV_3(t) = {} & g^T(t) P_3 g(t) - (1-\dot{\tau}(t)) g^T \\ & \times (t-\tau(t)) P_3 g(t-\tau(t)), \end{aligned} \tag{22}$$

$$LV_4(t) = \overline{\tau}^2 \dot{e}^T(t) P_1 \dot{e}(t) - \overline{\tau} \int_{t-\overline{\tau}}^{t} \dot{e}^T(s) P_1 \dot{e}(s)\, ds, \tag{23}$$

$$LV_5(t) = \overline{\sigma}^2 g^T(t) P_4 g(t) - \overline{\sigma} \int_{t-\overline{\sigma}}^{t} g^T(s) P_4 g(s)\, ds. \tag{24}$$

By Lemma 3, we obtain

$$\begin{aligned} & -\overline{\tau} \int_{t-\overline{\tau}}^{t} \dot{e}^T(s) P_1 \dot{e}(s)\, ds \\ & \quad \leq -\tau(t) \int_{t-\tau(t)}^{t} \dot{e}^T(s) P_1 \dot{e}(s)\, ds \\ & \quad \leq -\int_{t-\tau(t)}^{t} \dot{e}^T(s)\, ds\, P_1 \int_{t-\tau(t)}^{t} \dot{e}(s)\, ds, \end{aligned} \tag{25}$$

$$\begin{aligned} & -\overline{\sigma} \int_{t-\overline{\sigma}}^{t} g^T(s) P_4 g(s)\, ds \\ & \quad \leq -\sigma(t) \int_{t-\sigma(t)}^{t} g^T(s) P_4 g(s)\, ds \\ & \quad \leq -\int_{t-\sigma(t)}^{t} g^T(s)\, ds\, P_4 \int_{t-\sigma(t)}^{t} g(s)\, ds. \end{aligned} \tag{26}$$

By Newton-Leibniz formula, we have

$$e(t) - e(t-\tau(t)) = \int_{t-\tau(t)}^{t} \dot{e}(s)\, ds. \tag{27}$$

From assumption A1, we get

$$\begin{aligned} & g^T(t) D_1 g(t) \leq g^T(t) D_1 K e(t), \\ & g^T(t-\tau(t)) D_2 g(t-\tau(t)) \leq g^T(t-\tau(t)) D_2 K e(t-\tau(t)), \end{aligned} \tag{28}$$

where K, D_1, and D_2 are positive-definite diagonal matrices. By (27) and (28), we define several nonnegative expressions as follows:

$$\begin{aligned} L1 = {} & 2e(t-\tau(t)) Q_1 \Big[e(t) - e(t-\tau(t)) - \int_{t-\tau(t)}^{t} \dot{e}(s)\, ds \Big] \\ = {} & 0, \end{aligned} \tag{29}$$

$$L2 = 2\left[g^T(t) D_1 K e(t) - g^T(t) D_1 g(t)\right] \geq 0, \tag{30}$$

$$\begin{aligned} L3 = {} & 2\Big[g^T(t-\tau(t)) D_2 K e(t-\tau(t)) - g^T(t-\tau(t)) \\ & \times D_2 g(t-\tau(t))\Big] \geq 0. \end{aligned} \tag{31}$$

Then expressions $L1, L2$, and $L3$ are to be added to the inequality of $LV(t)$ to facilitate the proof.

Therefore, combining (19)–(29) we have

$$\begin{aligned} LV(t) \leq {} & \sum_{i=1}^{5} LV_i(t) + L1 + L2 + L3 \\ \leq {} & e^T(t) \left[2P_1(-C+G) + \rho M_1^T M_1 + P_2\right] e(t) \\ & + e^T(t-\tau(t)) \left[-(1-\overline{\tau}_1) P_2 + \rho M_2^T M_2 - 2Q_1\right] \\ & \times e(t-\tau(t)) \end{aligned}$$

$$
\begin{aligned}
&+ g^T(t)\left[P_3 - 2D_1 + \overline{\sigma}^2 P_4\right] g(t) \\
&+ g^T(t-\tau(t))\left[-\left(1-\overline{\tau}_1\right)P_3 - 2D_2\right] g(t-\tau(t)) \\
&- \int_{t-\overline{\tau}}^{t} \dot{e}^T(s)\,ds\, P_1 \int_{t-\overline{\tau}}^{t} \dot{e}(s)\,ds \\
&- \int_{t-\overline{\sigma}}^{t} g^T(\theta)\,d\theta\, P_4 \int_{t-\overline{\sigma}}^{t} g(\theta)\,d\theta \\
&+ 2e^T(t) Q_1 e(t-\tau(t)) \\
&+ e^T(t)\left[2P_1 A + 2K^T D_1\right] g(t) \\
&+ 2e^T(t)\left[P_1 B\right] g(t-\tau(t)) \\
&+ 2e^T(t)\left[P_1 D\right] \int_{t-\sigma(t)}^{t} g(\theta)\,d\theta \\
&+ 2e^T(t-\tau(t))\left[K^T D_2\right] g(t-\tau(t)) \\
&+ 2e^T(t-\tau(t))\left[Q_1\right] \int_{t-\overline{\tau}}^{t} \dot{e}(s)\,ds \\
&+ \left[(-C+G)e(t) + Ag(t) + Bg(t-\tau(t)) \right.\\
&\qquad \left. + D\int_{t-\sigma(t)}^{t} g(s)\,ds\right]^T \\
&\times \overline{\tau}^2 P_1 \left[(-C+G)e(t) + Ag(t) \right.\\
&\qquad \left. + Bg(t-\tau(t)) + D\int_{t-\sigma(t)}^{t} g(s)\,ds\right] \\
&\le \xi^T N \xi,
\end{aligned}
\tag{32}
$$

where

$$
\begin{aligned}
\xi = &\left[e^T(t), e^T(t-\tau(t)), g^T(t), g^T(t-\tau(t)),\right. \\
&\left.\int_{t-\tau(t)}^{t} \dot{e}^T(s)\,ds, \int_{t-\sigma(t)}^{t} g^T(s)\,ds\right]^T,
\end{aligned}
$$

$$
N = \begin{bmatrix}
N_{11} & Q_1 & \Pi_{13} & \Pi_{14} & 0 & P_1 D + \overline{\tau}^2 D \\
* & \Pi_{22} & 0 & K^T D_2 & -Q_1 & 0 \\
* & * & \Pi_{33} & \overline{\tau}^2 A^T P_1 B & 0 & \overline{\tau}^2 A^T P_1 D \\
* & * & * & \Pi_{44} & 0 & \overline{\tau}^2 B^T P_1 D \\
* & * & * & * & -P_1 & 0 \\
* & * & * & * & * & -P_4 + \overline{\tau}^2 D^T P_1 D
\end{bmatrix},
$$

$$
\begin{aligned}
N_{11} = {} & P_1(-C+G) + (-C+G)^T P_1 + P_2 \\
& + \rho M_1^T M_1 + \overline{\tau}^2 (-C+G)^T P_1 (-C+G).
\end{aligned}
\tag{33}
$$

We introduce matrices M and H which satisfy

$$
\Pi = \begin{bmatrix} M & H \\ H^T & -P_1 \end{bmatrix}, \qquad N = M - H\left(-P_1\right)^{-1} H^T, \tag{34}
$$

where

$$
M = \begin{bmatrix}
\Pi_{11} & Q_1 & \Pi_{13} & \Pi_{14} & 0 & P_1 D + \overline{\tau}^2 D \\
* & \Pi_{22} & 0 & K^T D_2 & -Q_1 & 0 \\
* & * & \Pi_{33} & \overline{\tau}^2 A^T P_1 B & 0 & \overline{\tau}^2 A^T P_1 D \\
* & * & * & \Pi_{44} & 0 & \overline{\tau}^2 B^T P_1 D \\
* & * & * & * & -P_1 & 0 \\
* & * & * & * & * & -P_4 + \overline{\tau}^2 D^T P_1 D
\end{bmatrix},
$$

$$
H = \begin{bmatrix}
\overline{\tau}(-C+G)^T P_1 \\ 0 \\ 0 \\ 0 \\ 0 \\ 0
\end{bmatrix}.
\tag{35}
$$

By Lemma 2, we get that $\Pi < 0 \Leftrightarrow N < 0, -P_1 < 0$. Thus $LV < 0$. From (24) and the Ito formula, it is obvious that

$$
EV(t) - EV\left(t_0\right) = E\int_{t_0}^{t} LV(s)\,ds. \tag{36}
$$

From the definition of $V(t)$ in (15), there exists positive constant λ_1 such that

$$
\begin{aligned}
\lambda_1 E\|e(t)\|^2 &\le EV(t) \le EV\left(t_0\right) + E\int_{t_0}^{t} LV(s)\,ds \\
&\le EV\left(t_0\right) + \lambda_{\max} E\int_{t_0}^{t} \|e(s)\|^2 ds,
\end{aligned}
\tag{37}
$$

where $\lambda_{\max}$ is the maximal eigenvalue of N and it is negative.

Therefore, from (26) and the discussion in [34], we know that the equilibrium of (11) is globally asymptotically stable in mean-square. This completes the proof. □

Corollary 5. *Under the assumptions A1–A3, the equilibrium point of model* (8) *is called globally asymptotically stable in mean-square, if there exist symmetric positive-definite matrices* P_j $(j = 1, \ldots, 4)$, *diagonal matrices* D_1, D_2, *and general matrices* Q_1 *and* W, *such that the following inequalities hold:*

$$\Pi = \begin{bmatrix} \Pi_{11} & Q_1 & \Pi_{13} & \Pi_{14} & 0 & P_1D + \overline{\tau}^2 D & \overline{\tau}\left(-C^T P_1 + W^T\right) \\ * & \Pi_{22} & 0 & K^T D_2 & -Q_1 & 0 & 0 \\ * & * & \Pi_{33} & \overline{\tau}^2 A^T P_1 B & 0 & \overline{\tau}^2 A^T P_1 D & 0 \\ * & * & * & \Pi_{44} & 0 & \overline{\tau}^2 B^T P_1 D & 0 \\ * & * & * & * & -P_1 & 0 & 0 \\ * & * & * & * & * & -P_4 + \overline{\tau}^2 D^T P_1 D & 0 \\ * & * & * & * & * & * & -P_1 \end{bmatrix} < 0, \tag{38}$$

$$P_1 < \rho I,$$

where

$$\begin{aligned} \Pi_{11} &= -P_1 C - C^T P_1 + W + W^T + P_2 + \rho M_1^T M_1, \\ \Pi_{13} &= P_1 A + K^T D_1 + \overline{\tau}^2 \left(-C^T P_1 + W^T\right) A, \\ \Pi_{14} &= P_1 B + \overline{\tau}^2 \left(-C^T P_1 + W^T\right) B, \\ \Pi_{22} &= -\left(1 - \overline{\tau}_1\right) P_2 - Q_1 - Q_1^T + \rho M_2^T M_2, \\ \Pi_{33} &= P_3 - 2D_1 + \overline{\sigma}^2 P_4 + \overline{\tau}^2 A^T P_1 A, \\ \Pi_{44} &= -\left(1 - \overline{\tau}_1\right) P_3 - 2D_2 + \overline{\tau}^2 B^T P_1 B. \end{aligned} \tag{39}$$

Furthermore, the control gain matrix G is given as

$$G = P_1^{-1} W. \tag{40}$$

Proof. Let $W = P_1 G$ in Theorem 4; it is easy to get the result. □

Corollary 6. *If the systems* (1) *and* (2) *have no integral time-delay items (e.g., $D = 0$), the result can be simplified as follows. Under assumptions A1–A3 and $D = 0$, the equilibrium point of model* (8) *is called globally asymptotically stable in mean-square, if there exist symmetric positive-definite matrices P_j $(j = 1, \ldots, 4)$, diagonal matrices D_1, D_2, and general matrices Q_1 and W, such that the following inequalities hold:*

$$\Pi = \begin{bmatrix} \Pi_{11} & Q_1 & \Pi_{13} & \Pi_{14} & 0 & \overline{\tau}\left(-C^T P_1 + W^T\right) \\ * & \Pi_{22} & 0 & K^T D_2 & -Q_1 & 0 \\ * & * & \Pi_{33} & \overline{\tau}^2 A^T P_1 B & 0 & 0 \\ * & * & * & \Pi_{44} & 0 & 0 \\ * & * & * & * & -P_1 & 0 \\ * & * & * & * & * & 0 \\ * & * & * & * & * & -P_1 \end{bmatrix} < 0, \tag{41}$$

$$P_1 < \rho I,$$

where

$$\begin{aligned} \Pi_{11} &= -P_1 C - C^T P_1 + W + W^T + P_2 + \rho M_1^T M_1, \\ \Pi_{13} &= P_1 A + K^T D_1 + \overline{\tau}^2 \left(-C^T P_1 + W^T\right) A, \\ \Pi_{14} &= P_1 B + \overline{\tau}^2 \left(-C^T P_1 + W^T\right) B, \\ \Pi_{22} &= -\left(1 - \overline{\tau}_1\right) P_2 - Q_1 - Q_1^T + \rho M_2^T M_2, \\ \Pi_{33} &= P_3 - 2D_1 + \overline{\sigma}^2 P_4 + \overline{\tau}^2 A^T P_1 A, \\ \Pi_{44} &= -\left(1 - \overline{\tau}_1\right) P_3 - 2D_2 + \overline{\tau}^2 B^T P_1 B. \end{aligned} \tag{42}$$

Furthermore, the control gain matrix G is given as

$$G = P_1^{-1} W. \tag{43}$$

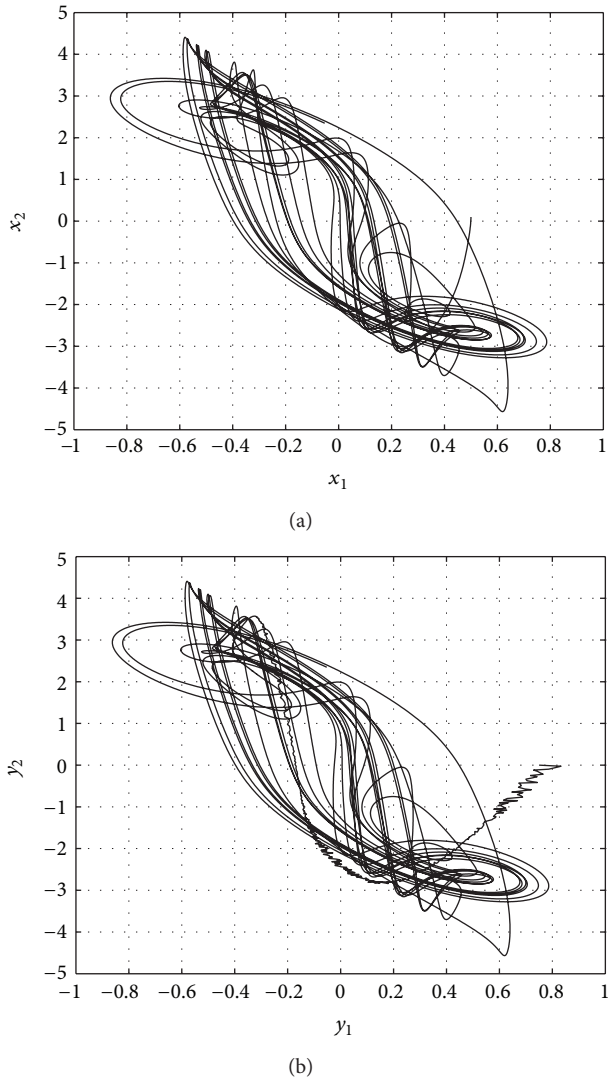

Figure 1: Phase trajectories of drive (a) and response (b) system.

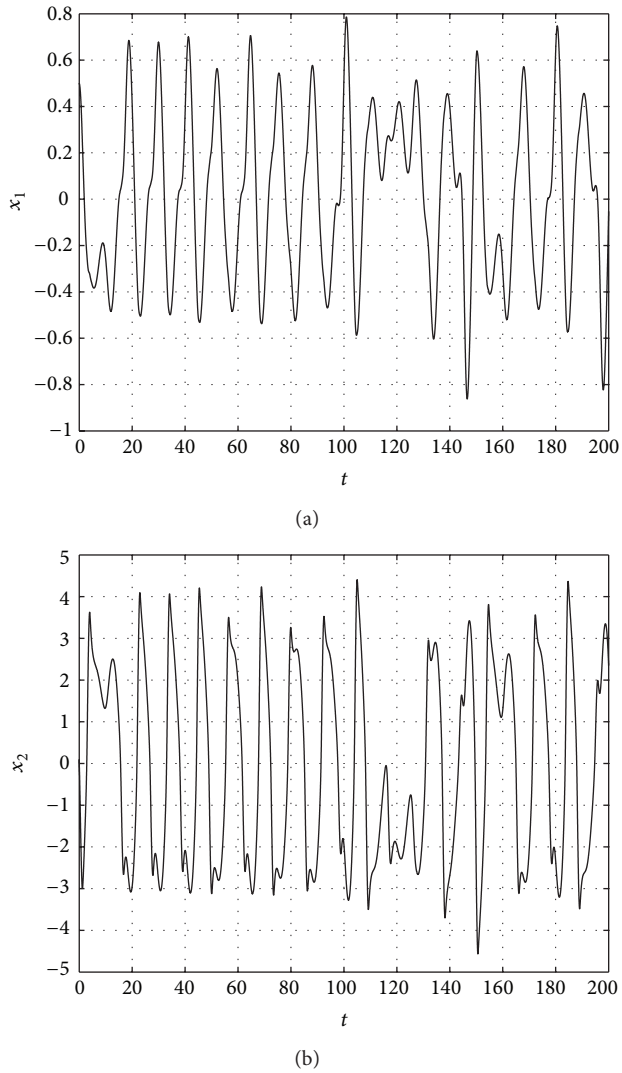

Figure 2: State trajectories of drive system.

Proof. Let $D = 0$ in system (8). It is much similar to the proof of Theorem 4 and is then omitted. □

Remark 7. In this paper, we use a memoryless state feedback control to achieve the synchronization of the stochastic delayed neural network system. Compared with the delayed feedback control [1], it is easy to implement. The biggest advantage of this approach is that we only need to know the boundaries of time delays, instead of exact values of time delays.

Remark 8. In Corollary 5, we give an approach to choose the control gain matrix G and it is helpful for the design of the controller to let the drive system synchronize with the response system.

4. Numerical Simulations

In this section, we present numerical simulations to show the effectiveness of the theoretical results.

Consider the drive system (1) of a delayed Hopfield neural network with coefficient matrices as

$$A = \begin{bmatrix} 1 & -0.5 \\ -0.2 & 1 \end{bmatrix}, \qquad B = \begin{bmatrix} -0.5 & -0.1 \\ -0.3 & -0.6 \end{bmatrix},$$
$$C = \begin{bmatrix} 1 & 0 \\ 0 & 1 \end{bmatrix}, \qquad D = \begin{bmatrix} 1 & 0 \\ 0 & 1 \end{bmatrix},$$
$$\tau(t) = 0.3 + 0.3\sin(4t), \qquad \sigma(t) = 0.4 - 0.2\sin(t), \tag{44}$$
$$f(t) = \begin{bmatrix} \tanh(x_1) \\ \tanh(x_2) \end{bmatrix}.$$

The corresponding response system refers to (2), where

$$\sigma(t, e(t), e(t - \tau(t))) = \begin{bmatrix} \|e(t)\| & 0 \\ 0 & 0.6\|e(t - \tau(t))\| \end{bmatrix}. \tag{45}$$

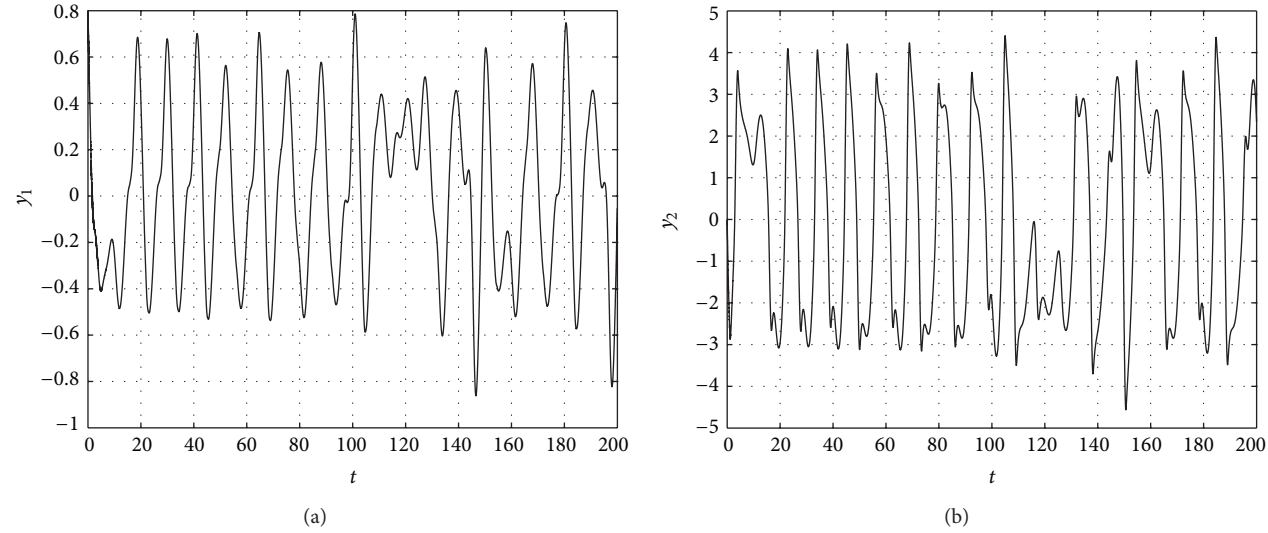

(a) (b)

Figure 3: State trajectories of response system.

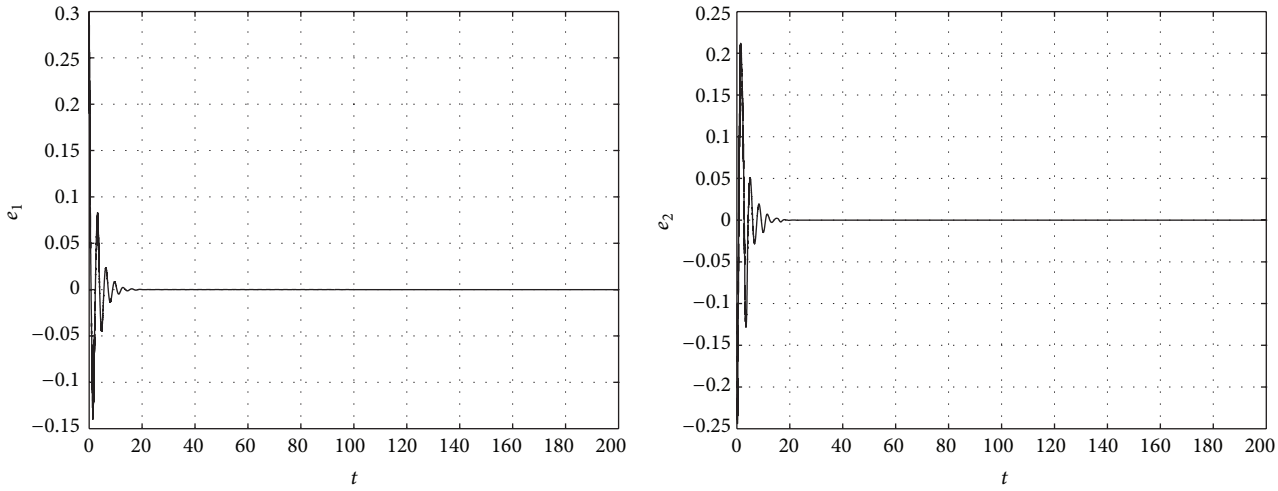

(a) (b)

Figure 4: State trajectories of error system.

It is easy to see that $K = M = M_1 = I$, where I is the identity matrix. By Theorem 4 and Corollary 5, we can get the following feasible solutions:

$$W = \begin{bmatrix} -1918.2 & 12.4 \\ 77.5 & -1984.4 \end{bmatrix},$$

$$Q_1 = \begin{bmatrix} 545.5568 & 3.6943 \\ 17.0650 & 557.7364 \end{bmatrix},$$

$$D_1 = \begin{bmatrix} 1046.5 & 0 \\ 0 & 1207.4 \end{bmatrix},$$

$$D_2 = \begin{bmatrix} 226.3259 & 0 \\ 0 & 242.7899 \end{bmatrix},$$

$$\rho = 1084.8, \qquad G = \begin{bmatrix} -1.8352 & 0.0425 \\ 0.1038 & -1.9002 \end{bmatrix},$$

$$P_1 = \begin{bmatrix} 1.046.2 & 0.016.9 \\ 0.016.9 & 1.044.7 \end{bmatrix}, \qquad P_2 = \begin{bmatrix} 52.1765 & -18.3810 \\ -18.3810 & 48.2007 \end{bmatrix},$$

$$P_3 = \begin{bmatrix} 94.2132 & -39.7350 \\ -39.7350 & 86.2442 \end{bmatrix}, \qquad P_4 = \begin{bmatrix} 2626.1 & 148.4 \\ 148.4 & 2760.3 \end{bmatrix}. \tag{46}$$

The initial states of drive system and response system are $x(0) = [0.75\ 0]^T$ and $y(0) = [0.5\ 0.1]^T$.

The results are shown in Figures 1, 2, 3, and 4.

5. Conclusion

In this paper, we considered synchronization control of stochastic neural networks with time-varying delays. We use Lyapunov functional method and linear matrix inequality (LMI) technique to solve this problem. Several sufficient

conditions have been derived to ensure the global asymptotical stability for the error system, and thus the drive system synchronizes with the response system. Also, the control gain can be obtained. The results are novel since there are few works about the synchronization of mixed delayed system and the constraint of the derivative of the time-delay function is relaxed. It is easy to apply these sufficient conditions to the real networks. Finally, a numerical simulation is presented to verify the theoretical results.

Conflict of Interests

The authors declare that there is no conflict of interests regarding the publication of this paper.

Acknowledgments

The authors would like to thank the editor and the reviewers for their helpful and valuable comments and suggestions, which have improved the presentation. This work is supported by National Natural Science Foundation of China under Grant nos. 61273352, 61175111, 61174046, 60904030, 60874045, and 60874030, Natural Science Foundation of the Jiangsu Higher Education Institutions (nos. 10KJB510027 and 09KJB510019), Postdoctoral Science Research Project of Jiangsu Province (no. 1102167C).

References

[1] W. Yu and J. Cao, "Synchronization control of stochastic delayed neural networks," *Physica A: Statistical Mechanics & Its Applications*, vol. 373, no. 1, pp. 252–260, 2007.

[2] Z. G. Wu, P. Shi, H. Su, and J. Chu, "Stochastic synchronization of Markovian jump neural networks with time-varying delay using sampled data," *IEEE Transactions on Cybernetics*, vol. 43, no. 6, pp. 1796–1806, 2013.

[3] Z. Wang, Y. Wang, and Y. Liu, "Global synchronization for discrete-time stochastic complex networks with randomly occurred nonlinearities and mixed time delays," *IEEE Transactions on Neural Networks*, vol. 21, no. 1, pp. 11–25, 2010.

[4] M. J. Park, O. M. Kwon, J. H. Park, S. M. Lee, and E. J. Cha, "Synchronization criteria for coupled stochastic neural networks with time-varying delays and leakage delay," *Journal of the Franklin Institute*, vol. 349, no. 5, pp. 1699–1720, 2012.

[5] Z. Wu, J. H. Park, H. Su, and J. Chu, "Discontinuous lyapunov functional approach to synchronization of time-delay neural networks using sampled-data," *Nonlinear Dynamics*, vol. 69, no. 4, pp. 2021–2030, 2012.

[6] B. Shen, Z. Wang, and X. Liu, "Bounded H∞ synchronization and state estimation for discrete time-varying stochastic complex networks over a finite horizon," *IEEE Transactions on Neural Networks*, vol. 22, no. 1, pp. 145–157, 2011.

[7] H. R. Karimi and H. Gao, "New delay-dependent exponential H∞ synchronization for uncertain neural networks with mixed time delays," *IEEE Transactions on Systems, Man, and Cybernetics B: Cybernetics*, vol. 40, no. 1, pp. 173–185, 2010.

[8] C. Li, W. Yu, and T. Huang, "Impulsive synchronization schemes of stochastic complex networks with switching topology: average time approach," *Neural Networks*, vol. 54, pp. 85–94, 2014.

[9] C. Li, C. Li, X. Liao, and T. Huang, "Impulsive effects on stability of high-order BAM neural networks with time delays," *Neurocomputing*, vol. 74, no. 10, pp. 1541–1550, 2011.

[10] Q. Zhu, S. Fei, T. Zhang, and T. Li, "Adaptive RBF neural-networks control for a class of time-delay nonlinear systems," *Neurocomputing*, vol. 71, no. 16–18, pp. 3617–3624, 2008.

[11] W. Zhou, D. Tong, Y. Gao, C. Ji, and H. Su, "Mode and delay-dependent adaptive exponential synchronization in pth moment for stochastic delayed neural networks with markovian switching," *IEEE Transactions on Neural Networks & Learning Systems*, vol. 23, no. 4, pp. 662–668, 2012.

[12] J. Cao, Z. Wang, and Y. Sun, "Synchronization in an array of linearly stochastically coupled networks with time delays," *Physica A: Statistical Mechanics and its Applications*, vol. 385, no. 2, pp. 718–728, 2007.

[13] J. Cao and Y. Wan, "Matrix measure strategies for stability and synchronization of inertial BAM neural network with time delays," *Neural Networks*, vol. 53, no. 5, pp. 165–172, 2014.

[14] G. Wen, Z. Duan, Z. Li, and G. Chen, "Stochastic consensus in directed networks of agents with non-linear dynamics and repairable actuator failures," *IET Control Theory & Applications*, vol. 6, no. 11, pp. 1583–1593, 2012.

[15] X. Yang, J. Cao, and J. Lu, "Synchronization of randomly coupled neural networks with markovian jumping and time-delay," *IEEE Transactions on Circuits and Systems I: Regular Papers*, vol. 60, no. 2, pp. 363–376, 2013.

[16] Q. Zhu and J. Cao, "Adaptive synchronization under almost every initial data for stochastic neural networks with time-varying delays and distributed delays," *Communications in Nonlinear Science & Numerical Simulation*, vol. 16, no. 4, pp. 2139–2159, 2011.

[17] Z. Wu, P. Shi, H. Su, and J. Chu, "Passivity analysis for discrete-time stochastic markovian jump neural networks with mixed time delays," *IEEE Transactions on Neural Networks*, vol. 22, no. 10, pp. 1566–1575, 2011.

[18] D. Tong, Q. Zhu, W. Zhou, Y. Xu, and J. A. Fang, "Adaptive synchronization for stochastic T-S fuzzy neural networks with time-delay and Markovian jumping parameters," *Neurocomputing*, vol. 117, pp. 91–97, 2013.

[19] M. Fang and J. H. Park, "Non-fragile synchronization of neural networks with time-varying delay and randomly occurring controller gain fluctuation," *Applied Mathematics and Computation*, vol. 219, no. 15, pp. 8009–8017, 2013.

[20] Y. Zhang, D. W. Gu, and S. Xu, "Global exponential adaptive synchronization of complex dynamical networks with neutral-type neural network nodes and stochastic disturbances," *IEEE Transactions on Circuits & Systems I: Regular Papers*, vol. 60, no. 10, pp. 2709–2718, 2013.

[21] S. C. Jeong, D. H. Ji, J. H. Park, and S. C. Won, "Adaptive synchronization for uncertain chaotic neural networks with mixed time delays using fuzzy disturbance observer," *Applied Mathematics and Computation*, vol. 219, no. 11, pp. 5984–5995, 2013.

[22] C. Liu, J. Wang, H. Yu et al., "The effects of time delay on the stochastic resonance in feed-forward-loop neuronal network motifs," *Communications in Nonlinear Science and Numerical Simulation*, vol. 19, no. 4, pp. 1088–1096, 2014.

[23] P. Guo, J. Zhang, H. R. Karimi, Y. Liu, M. Lyu, and Y. Bo, "State estimation for wireless network control system with stochastic uncertainty and time delay based on sliding mode observer," *Abstract and Applied Analysis*, vol. 2014, Article ID 303840, 8 pages, 2014.

[24] G. Wen, W. Yu, Y. Zhao, and J. Cao, "Pinning synchronisation in fixed and switching directed networks of Lorenz-type nodes," *IET Control Theory & Applications*, vol. 7, no. 10, pp. 1387–1397, 2013.

[25] G. Wen, G. Hu, W. Yu, J. Cao, and G. Chen, "Consensus tracking for higher-order multi-agent systems with switching directed topologies and occasionally missing control inputs," *Systems & Control Letters*, vol. 62, no. 12, pp. 1151–1158, 2013.

[26] G. Wen, Z. Duan, G. Chen, and W. Yu, "Consensus tracking of multi-agent systems with Lipschitz-type node dynamics and switching topologies," *IEEE Transactions on Circuits and Systems I: Regular Papers*, vol. 61, no. 2, pp. 499–511, 2014.

[27] W. H. Chen, J. X. Xu, and Z. H. Guan, "Guaranteed cost control for uncertain Markovian jump systems with mode-dependent time-delays," *IEEE Transactions on Automatic Control*, vol. 48, no. 12, pp. 2270–2277, 2003.

[28] S. Xu, J. Lam, and X. Mao, "Delay-dependent H_∞ control and filtering for uncertain Markovian jump systems with time-varying delays," *IEEE Transactions on Circuits and Systems I: Regular Papers*, vol. 54, no. 9, pp. 2070–2077, 2007.

[29] S. Xu, T. Chen, and J. Lam, "Robust H^∞ filtering for uncertain Markovian jump systems with mode-dependent time delays," *IEEE Transactions on Automatic Control*, vol. 48, no. 5, pp. 900–907, 2003.

[30] Z. Wang, Y. Liu, L. Yu, and X. Liu, "Exponential stability of delayed recurrent neural networks with Markovian jumping parameters," *Physics Letters A*, vol. 356, no. 4-5, pp. 346–352, 2006.

[31] X. Mao, "Exponential stability of stochastic delay interval systems with Markovian switching," *IEEE Transactions on Automatic Control*, vol. 47, no. 10, pp. 1604–1612, 2002.

[32] X. Zeng, Q. Hui, W. M. Haddad, T. Hayakawa, J. M. Bailey, and X. Zeng, "Synchronization of biological neural network systems with stochastic perturbations and time delays," *Journal of the Franklin Institute*, vol. 351, no. 3, pp. 1205–1225, 2013.

[33] V. B. Kolmanovskii and A. D. Myshkis, *Introduction to the theory and applications of functional-differential equations*, Kluwer Academic Publishers, Dordrecht, The Netherlands, 1999.

[34] Z. Schuss, *Theory and Applications of Stochastic Differential Equations*, Wiley, New York, NY, USA, 1980.